

N71-17669  
NASA CR-72813  
PWA-4055



EVALUATION OF ADVANCED SUPERALLOY PROTECTION SYSTEMS

by

F. P. Talboom, R. C. Elam, and L. W. Wilson

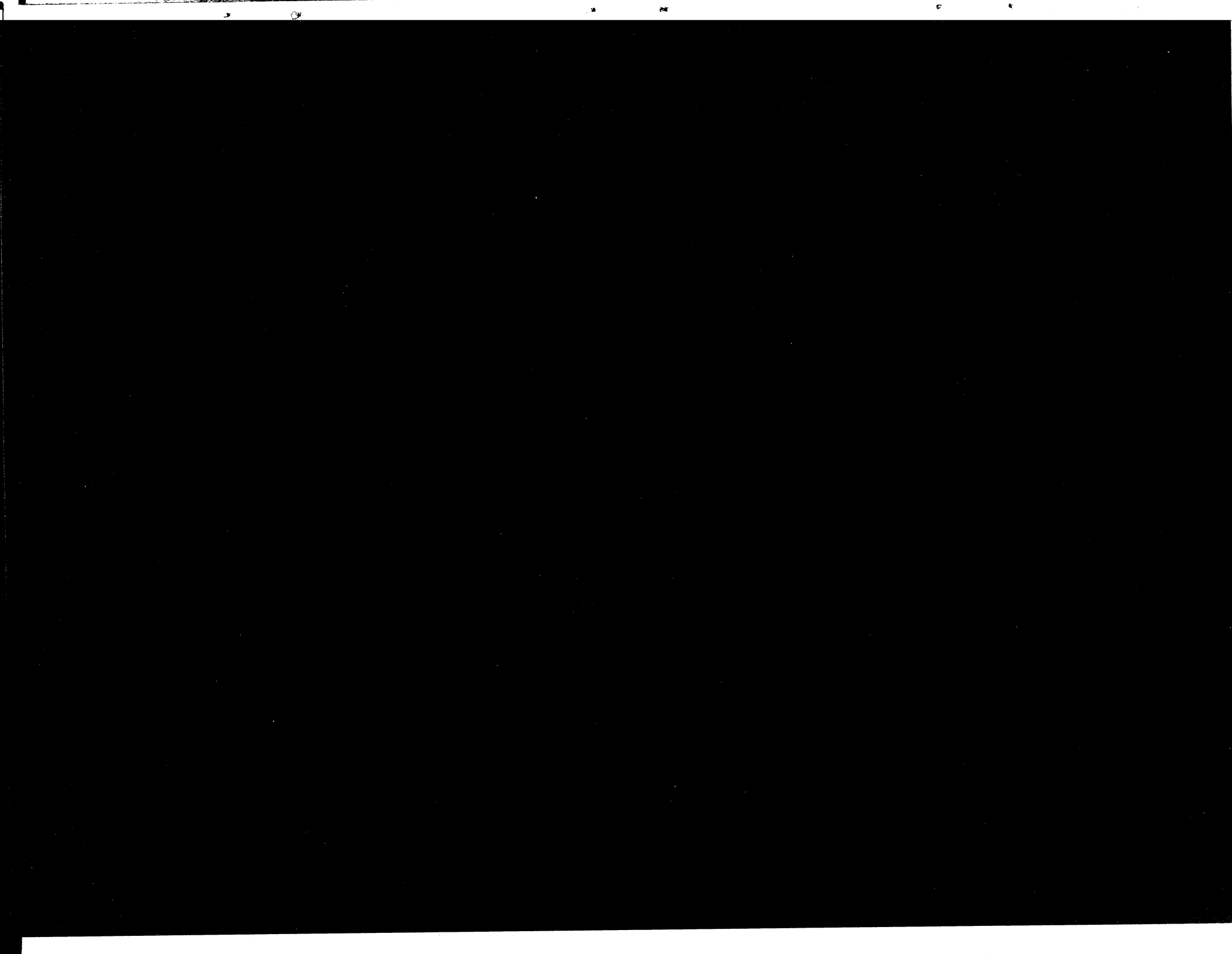
PRATT & WHITNEY AIRCRAFT  
DIVISION OF UNITED AIRCRAFT CORPORATION  
EAST HARTFORD, CONNECTICUT

prepared for

NATIONAL AERONAUTICS AND SPACE ADMINISTRATION

NASA LEWIS RESEARCH CENTER  
Contract NAS3-12415  
Fredric H. Harf, Project Manager  
Salvatore J. Grisaffe, Research Advisor

CASE FILE  
COPY



FINAL REPORT

EVALUATION OF ADVANCED SUPERALLOY PROTECTION SYSTEMS

by

F. P. Talboom, R. C. Elam, and L. W. Wilson

PRATT & WHITNEY AIRCRAFT  
DIVISION OF UNITED AIRCRAFT CORPORATION  
400 Main Street  
East Hartford, Connecticut 06108

prepared for

NATIONAL AERONAUTICS AND SPACE ADMINISTRATION

December 2, 1970

CONTRACT NAS3-12415

NASA LEWIS RESEARCH CENTER  
Cleveland, Ohio  
Fredric H. Harf, Project Manager  
Salvatore J. Grisaffe, Research Advisor  
Materials and Structures Division



## FOREWORD

This is the final report of the work performed at the Materials Development Laboratory of Pratt & Whitney Aircraft Division of United Aircraft Corporation, East Hartford, Connecticut on contract NAS3-12415, Evaluation of Advanced Superalloy Protection Systems, during the period July 2, 1969 to November 2, 1970.

National Aeronautics and Space Administration, Lewis Research Center personnel assigned to the contract are:

Mr. Leonard W. Schopen, Contracting Officer  
Mr. Fredric H. Harf, Project Manager  
Mr. Salvatore J. Grisaffe, Research Advisor  
Mr. Reginald J. Paginton, Contract Administrator

The following Pratt & Whitney Aircraft personnel were the prime contributors to the experimental program and are the authors of this report:

Mr. Frank P. Talboom, Program Manager  
Mr. Richard C. Elam, Responsible Engineer  
Mr. Lloyd W. Wilson, Metallurgist

Special recognition is given to the following P&W Materials Development Laboratory personnel: Mr. N. E. Union, who performed the coating operations; Mr. N. P. Anderson, who performed the microprobe analyses; and Messrs. R. L. Farrington and A. E. Simmons, who performed the x-ray analyses.

**TABLE OF CONTENTS**

Section	Title	Page
	Foreword	iii
	Abstract	v
I	Summary	1
II	Introduction	2
III	Furnace Oxidation Evaluation	3
	A. Optimization of Coating Deposition Process	3
	B. Ballistic Impact and Furnace Oxidation Testing	8
	C. Discussion of Test Results and Selection of Alloy Modifications for Burner Rig Test	16
IV	1100-Hour Burner Rig Test	22
	A. Coating of Test Specimens	22
	B. Burner Rig Test	28
	C. Discussion of Test Results and Selection of Compositions for Characterization by Tensile and Stress-to-Rupture Tests	40
V	Tensile and Stress-to-Rupture Tests	41
	A. Program	41
	B. Specimen Coating and Heat Treatment	41
	C. Results and Conclusions	42
VI	Analytical Characterization of Coatings	45
	A. X-Ray Diffraction Analysis	45
	B. Electron Microprobe Analysis	46
VII	Summary of Results	69

## ABSTRACT

Eleven coating compositions based on the Co-Cr-Al-Y system were applied to nickel-base alloy test specimens by electron beam vapor deposition. Coating composition was optimized through ballistic impact, furnace oxidation, and long-term burner rig oxidation tests. Appropriate metallographic, x-ray diffraction, and electron beam microprobe analyses were conducted. Two coating compositions capable of protecting the nickel-base alloy NASA-TRW VI-A from excessive oxidation at a temperature of 2000°F (1366°K) were additionally characterized by tensile and stress-to-rupture tests. Four compositions demonstrated oxidation resistance more than three times that of comparison aluminide coatings in burner rig tests. The two coating compositions produced no adverse effect on the mechanical properties of the VI-A base metal.

## NOTICE

Certain developments relating to the coating systems herein disclosed are the subject of background patent rights of United Aircraft Corporation.



## I. SUMMARY

An oxidation-resistant cobalt-chromium-aluminum composition containing small amounts of yttrium was optimized as a coating to protect the nickel-base alloy NASA-TRW VI-A from excessive oxidation. The coatings were applied by electron beam vapor deposition in vacuum. Four of the coatings completed 1100 hours of burner rig oxidation testing in the combustion products of JP-5 fuel and air at 2000°F (1366°K) without failure. The unique feature of the coating application process is that the process deposits a protective surface alloy layer which does not depend upon reaction with the substrate to form aluminides as in conventional coating.

Five variations of the Co-Cr-Al-Y system were originally selected for evaluation. Initial efforts were concerned with adjustment of the coating parameters to provide coatings of uniform thickness in the range of 0.003 to 0.005 inch (76 to 127  $\mu\text{m}$ ). Coatings meeting these criteria were tested by ballistic impact and by oxidation in a static air furnace for 200 hours at 2000°F (1366°K). From the results of these tests, six compositional variations were selected for further evaluation.

Burner rig testing was performed on the original five compositions and the six modifications at 2000°F (1366°K) in the combustion products of JP-5 fuel. Test time for the 11 compositions was 1100 hours or until failure of the coating, whichever occurred first. Appropriate metallographic, x-ray diffraction, and electron beam microprobe analyses were conducted to characterize all compositions in the as-coated condition and after burner rig testing.

Four coating compositions completed 1100 hours of burner rig testing without failure. These four compositions performed in excess of three times better than the comparative aluminide coated specimens.

The two most promising compositions of the four were additionally characterized by tensile and stress-to-rupture tests. Tensile and stress-to-rupture test results showed that the two selected compositions exhibited no adverse effects on base metal properties.

## II. INTRODUCTION

Design trends for advanced gas turbine engines are toward ever-increasing turbine inlet temperatures, and the demands on turbine materials have increased to the extent where contemporary aluminide coating systems are the life limiting component of alloy-coating composites. Furthermore, the protective character of an aluminide coating depends to a large extent upon the constituents of the basis alloy acquired through the formative diffusion processes. This coating-basis alloy interdependency inhibits design for advanced capability in turbine structural alloys.

The inadequacies of present day coatings as metal temperatures approach 2000°F (1366°K) have been related to excessive interdiffusion of coating and substrate at temperature, insufficient oxidation and sulfidation resistance, and excessive gas and particulate erosion. Other factors which can limit the utility of an aluminide coating are modification of the coating by substrate constituents and substrate morphological features, such as primary carbides, which may appear in the microstructure of a diffusion coating.

This program was directed toward the evaluation of a new coating system not dependent upon reaction with the substrate to form aluminides which would protect superalloys for extended times in the 1900° to 2000°F (1311° to 1366°K) metal temperature range.

An electron beam vapor deposition process was employed for the application of 11 cobalt-base coating compositions that were evaluated under this contract. The optimization of coating composition through the use of ballistic impact, furnace oxidation, and long-term burner rig oxidation tests form the basis for this report. Details and results of this testing, with appropriate metallographic, x-ray diffraction, and electron beam microprobe analyses, are presented in the ensuing sections. Finally, two compositions were additionally characterized by means of tensile and stress-to-rupture tests.

### III. FURNACE OXIDATION EVALUATION

#### A. OPTIMIZATION OF COATING DEPOSITION PROCESS

Initial efforts were directed toward the application and evaluation of five compositional variations of a cobalt-chromium-aluminum-yttrium oxidation-resistant coating on nickel-base alloy NASA-TRW VI-A. The coating alloy systems were selected in factorial fashion to permit a determination of the effect and value of variations of chemistry in the Co-Cr-Al-Y system. The five target compositions listed below are presented graphically in Figure 1.

Coating Composition Number	Target Coating Composition
1	Co – 20Cr – 12 Al – 0.5Y
2	Co – 20Cr – 20 Al – 0.5Y
3	Co – 30Cr – 16 Al – 0.5Y
4	Co – 40Cr – 12 Al – 0.5Y
5	Co – 40Cr – 20 Al – 0.5Y

Each of the coating systems was applied by the electron beam vapor deposition process. The technique depends upon a continuous feeding of ingot stock at a rate consistent with the evaporation rate of the liquid in order to control thickness and composition.

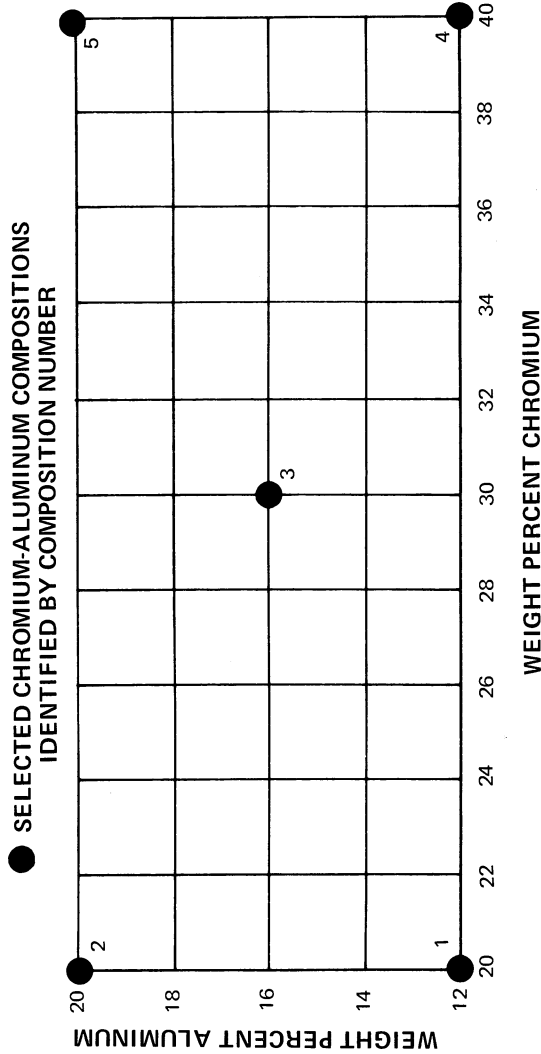


Figure 1 Chromium-Aluminum Content of the Five Initial Co-Cr-Al-Y Coating Compositions.  
Yttrium is constant at 0.5 percent and cobalt is balance.

An alloy ingot of composition X is fed upward through a water-cooled crucible (Figure 2). As the ingot emerges at the top of the crucible, a high-powered, focused electron beam is played on the emerging end, causing local melting and forming a liquid pool contained by the walls of the crucible and solid ingot below. Elements of higher vapor pressures begin to evaporate immediately, while those with lower vapor pressures are accumulated in the liquid pool and become more concentrated with time, leading to increased amounts of these elements in the vapor phase. Under constant conditions, the liquid inventory of composition Y will approach equilibrium with a gaseous phase of composition X. Normally, with a finite supply of alloy for the molten pool, the compositions X and Y would exist only momentarily. In this case, more ingot material of composition X is fed into the molten pool and at precisely the same rate as vapors of composition X leave the pool. The result is a condition in which all three phases are in equilibrium with each other and the composition of the resulting coating can be kept constant, provided that the process is maintained under constant conditions. Thus, control of composition was accomplished mainly in the casting process used to produce the ingot feed stock. Actual compositions of the ingot feed stock, which was formed by an investment casting technique, are listed below.

Composition Number	Analysis by X-ray Fluorescence
1	Co - 20.35 Cr - 11.52 Al - 0.42Y
2	Co - 19.56 Cr - 19.69 Al - 0.48Y
3	Co - 31.02 Cr - 15.01 Al - 0.57Y
4	Co - 41.24 Cr - 11.70 Al - 0.34Y
5	Co - 39.95 Cr - 22.62 Al - 0.36Y

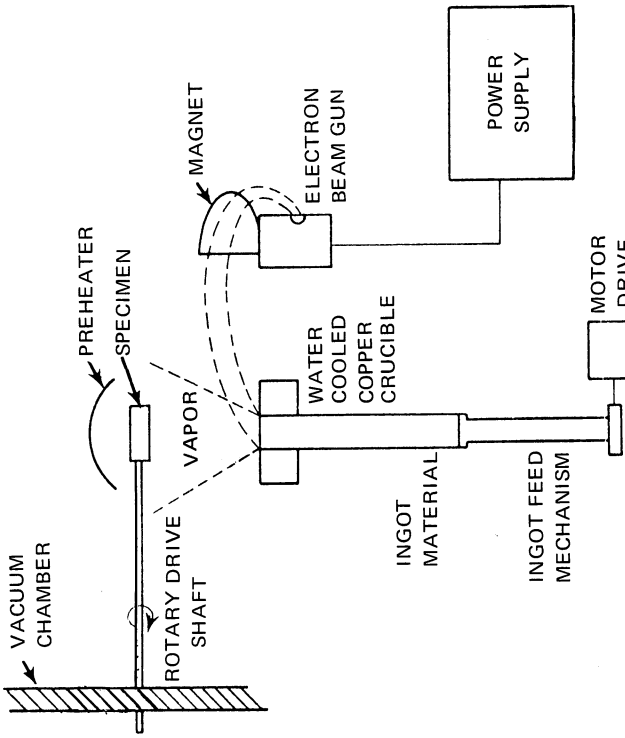


Figure 2 Electron Beam Evaporation Apparatus

Following casting, the ingots were machined by centerless grinding in preparation for evaporation. Machinability of the ingot was considered an important criterion in establishing the utility of a composition for this process. Compositions 2 and 5 were extremely difficult to machine and were marginally acceptable for this program, while compositions 1, 3, and 4 were acceptable. The poor machinability of 2 and 5 could preclude their use in a production process due to the brittle nature of the castings.

Trial evaporation runs were conducted for each new composition introduced to determine coating weight versus thickness relationships and time to reach vapor equilibrium. The relationship between weight deposited and the coating thickness for a given substrate geometry and coating composition, as determined in the trial runs, permitted the calculation of coating thickness for subsequent coatings with each composition.

Following trial deposition runs, the coating of test coupons measuring  $2 \times 1 \times 0.10$  inch ( $50 \times 25 \times 2.5$  mm) for metallographic analyses, ballistic impact testing, and furnace oxidation testing was completed. In addition, two bow paddle specimens (Figure 3) were coated for each composition to establish the parameters for coating of further specimens of this type. All coatings deposited were subsequently analyzed by means of x-ray fluorescence performed on sample plates simultaneously coated with each specimen. Table I presents these values and the calculated coating thickness for each specimen. An actual coating thickness (determined metallographically) is given in the table for each specimen subsequently tested in furnace oxidation and ballistic impact.

The coatings which were analyzed did not meet the goal that composition be within 10 percent of absolute value on major constituents and within 20 percent on the additive elements of the sample ingot. However, the compositions provided a meaningful test format. The systematic nature of the deviations permitted control of the coating chemistry, and the desired compositional spread for a factorial study was achieved (Figure 4).

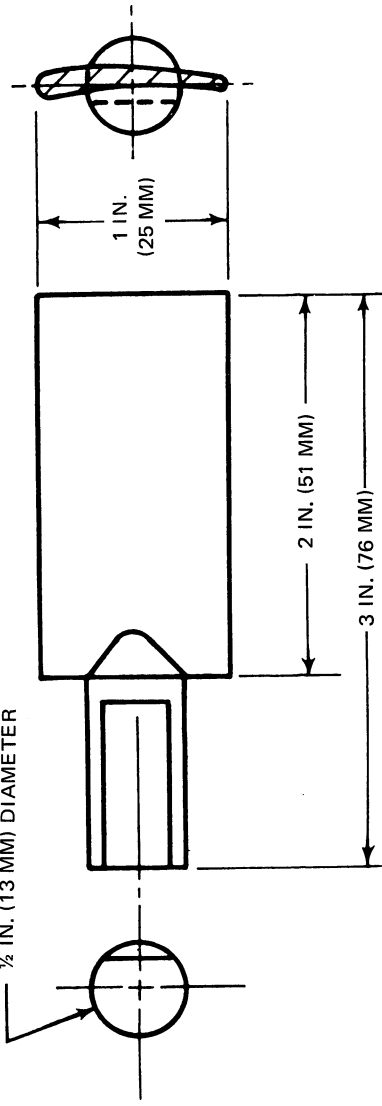


Figure 3 Bow Paddle Specimen

**TABLE I**  
**CHEMICAL ANALYSIS OF STARTING INGOTS**  
**AND VAPOR DEPOSITED COATINGS**

Compo- sition No.	Specimen No.	Composition (Weight %)			Calculated Thickness (mils)	Calculated Thickness (μm)	Actual Thickness (mils)	Actual Thickness (μm)	Where Measured	Where Measured
		Co	Cr	Al						
1	V6277	66.04	20.59	11.12	0.48	INGOT	—	—	—	—
	259	70.22	18.27	10.85	0.07	4.82	122	—	—	—
	267	71.21	18.11	10.64	0.09	4.97	126	—	—	—
	268	70.72	18.35	10.84	0.12	4.76	121	4.2	107	107
	269	70.14	19.02	10.52	0.12	5.02	128	4.2	107	107
	270	70.06	19.17	11.05	0.15	4.75	121	4.2	107	107
	271	69.68	19.35	10.81	0.15	4.83	123	4.2	107	107
	G4162K	70.28	18.68	10.92	0.16	4.79	122	—	—	—
	G4092D	70.59	17.95	10.90	0.16	4.77	121	4.5	114	114
2	V6267	61.95	19.61	19.01	0.78	INGOT	—	—	—	—
	272	Bal.	18.30	16.20	0.11	4.79	122	—	—	—
	273	Bal.	17.56	16.80	0.15	5.40	137	5.0	127	127
	274	66.93	17.95	16.76	0.15	5.62	143	—	—	—
	276	67.72	17.59	16.03	0.16	5.19	132	—	—	—
	277	66.88	18.68	16.14	0.15	5.28	134	4.8	122	122
	278	67.14	17.96	16.44	0.18	4.98	126	4.8	122	122
	280	67.14	17.96	16.44	0.18	5.16	131	4.8	122	122
	G4162O	66.76	18.39	16.62	0.21	4.92	125	—	—	—
	G4162L	Bal.	18.15	16.68	0.20	4.88	124	4.9	124	124
3	V6278	53.83	31.16	14.97	0.48	INGOT	—	—	—	—
	281	59.39	27.63	14.20	0.20	5.13	130	—	—	—
	282	58.32	28.72	14.38	0.20	5.25	133	5.1	130	130
	283	59.78	26.77	14.34	0.14	4.78	121	—	—	—
	284	59.64	27.04	14.48	0.15	4.96	126	—	—	—
	285	60.08	26.89	13.80	0.17	4.85	123	4.8	122	122
	287	59.40	27.48	14.01	0.17	5.15	131	5.0	127	127
	288	59.47	26.67	15.19	0.19	4.83	123	4.5	114	114
	290	60.23	26.43	14.53	0.22	5.11	130	—	—	—
	G4162T	59.36	27.18	14.49	0.22	4.84	123	5.0	127	127
	G4162S	59.86	26.84	14.55	0.22	5.03	128	—	—	—
4	V6265	47.52	41.24	11.70	0.34	INGOT	—	—	—	—
	291	52.95	36.59	11.72	0.02	4.14	105	—	—	—
	292	54.11	35.96	11.54	0.02	4.82	122	—	—	—
	293	53.96	36.21	11.45	0.02	5.35	136	—	—	—
	V6279	47.74	41.04	11.32	0.25	INGOT	—	—	—	—
	294	52.62	37.28	11.51	0.05	5.08	129	—	—	—
	295	52.97	37.51	11.43	0.06	5.50	140	5.3	135	135
	296	53.45	36.23	11.60	0.05	4.63	118	5.0	127	127
	298	53.53	36.60	11.67	0.05	5.07	129	—	—	—
	G4162U	53.77	35.28	11.41	0.05	*	*	—	—	—
	G4162V	53.25	36.23	11.50	0.07	5.19	132	5.0	127	127
	310 & 312 Bal.		33.42	11.42	0.09	4.30 & 4.50	109 & 114	5.0	127	127
5	V6266	Bal.	39.95	22.62	0.36	INGOT	—	—	—	—
	299	Bal.	34.32	17.49	0.14	4.89	124	—	—	—
	300	Bal.	36.76	18.31	0.11	5.02	128	5.0	127	127
	301	Bal.	36.73	17.97	0.11	5.44	138	—	—	—
	303	Bal.	35.66	17.79	0.13	4.70	119	4.5	114	114
	304	Bal.	34.86	17.49	0.13	5.08	129	—	—	—
	305	Bal.	35.10	17.75	0.15	5.09	129	4.5	114	114
	306	Bal.	35.55	17.87	0.15	5.57	141	5.0	127	127
	G4162W	Bal.	35.80	17.89	0.18	5.27	134	—	—	—
	G4162X	Bal.	36.19	17.84	0.18	5.29	134	5.6	142	142

\* Did not rotate.

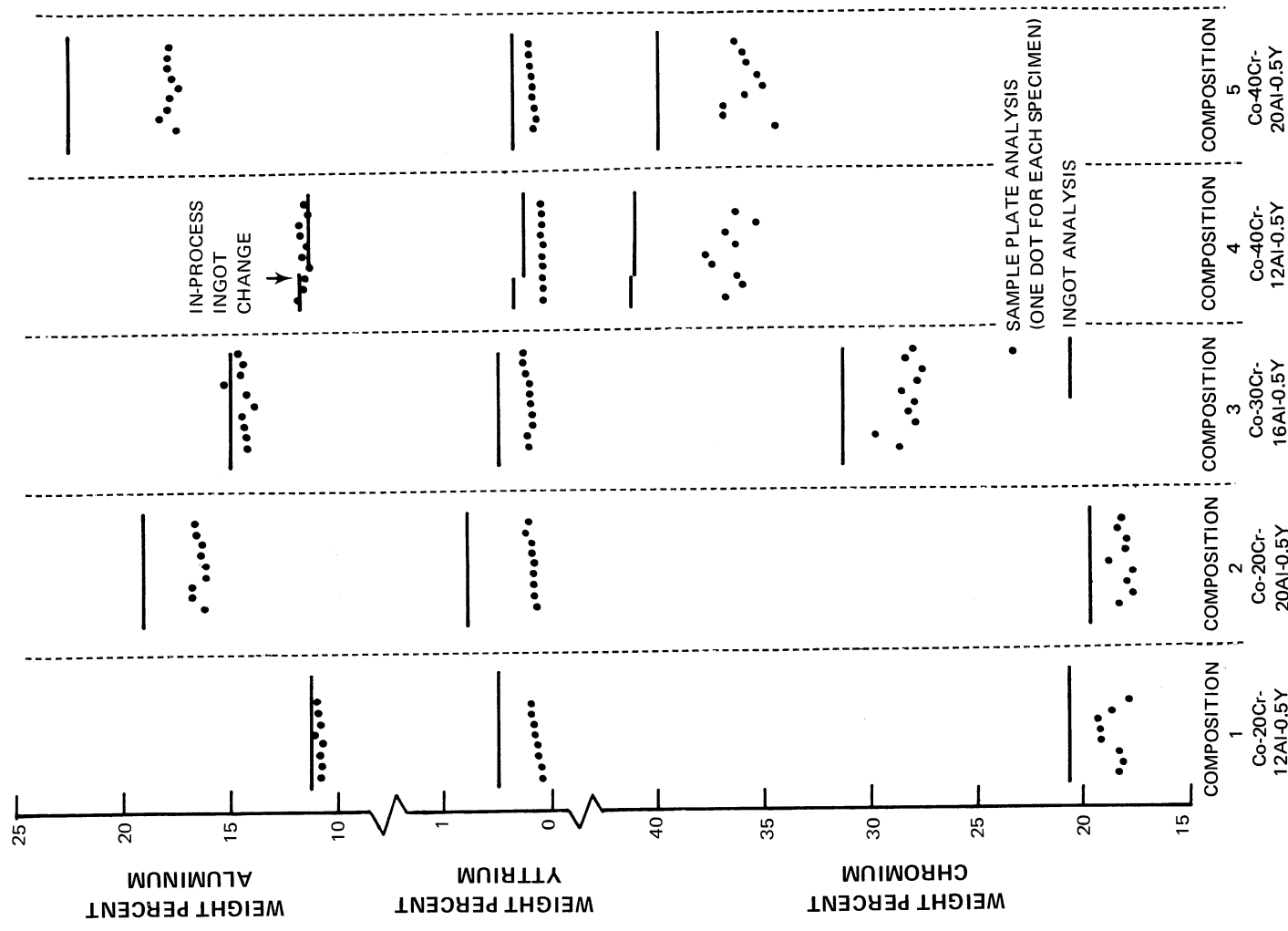


Figure 4

Analysis of Sample Plate Aluminum, Yttrium, and Chromium Compared With the Ingots

Approximately 1/4 inch (6.4 mm) was cut from the end of each coated test coupon to ensure that all specimen coated areas were of equal size. This cut removed the uncoated portion which was masked by the specimen holder during coating. The sectioning included approximately 1/8 inch (3.2 mm) of the fully coated portion of each specimen in order to provide a sample for metallography for each test specimen. The sectioning also left each test specimen with one uncoated cut end in common. Representative photomicrographs are shown for each composition tested in Figures 5 through 7.

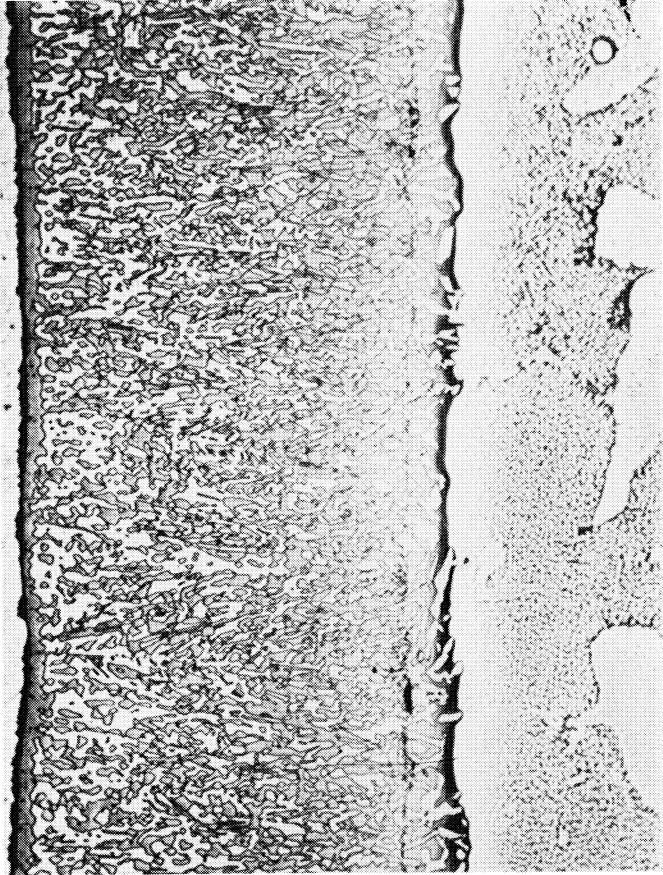
Following coating application and prior to heat treatment, trial processing runs involving glass bead peening were made on representative coated test specimens from each composition to minimize the grain boundaries typical of vapor deposited structures. (The as-deposited structure obtained from electron beam processing is very similar to that obtained from chemical vapor deposition.) This process was successful on composition 1 (Co-20Cr-12Al-0.5Y) and was applied to the furnace oxidation test specimens of this composition, but the remaining compositions could not be processed without mechanical damage to the coatings. All specimens were given a 1975°F (1353°K) 4-hour heat treatment in hydrogen.

#### B. BALLISTIC IMPACT AND FURNACE OXIDATION TESTING

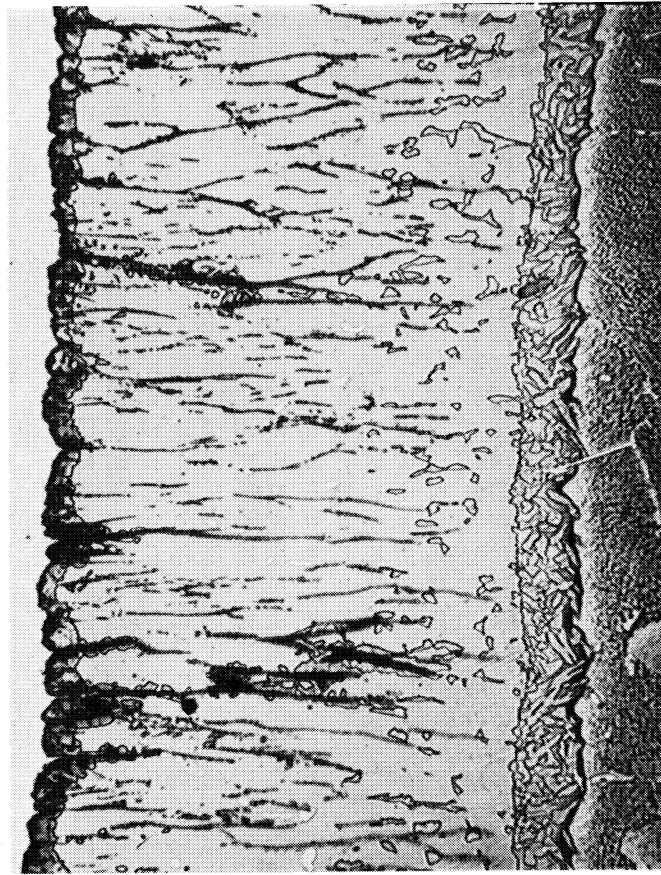
Two test coupons of each coating composition were impacted twice each at the nominal velocities of 400 and 600 feet per second (122 and 183 meters per second). Steel-tipped lead pellets 0.125 inch (3.175 millimeter) in diameter and weighing 0.70 gram were fired from a modified air rifle in order to obtain cracks or severe plastic deformation of the coating. The ballistic impact specimens were cleaned with a solution of two volume parts acetic acid and one volume part hydrogen peroxide for the purpose of removing lead splatter. The results of ballistic impact testing are summarized in Table II, and the appearance of each composition after impact is typified in Figure 8.

Following ballistic impact testing, four test coupons coated with each coating composition (two coupons impacted and two not impacted) were weighed and placed in a static air furnace at 2000°F (1366°K) for a 200-hour cyclic oxidation test. The first 24 hours of testing consisted of 2-hour cycles at temperature followed by ambient air cooling to room temperature and subsequent weighing. Thereafter, specimens were subjected to three exposure cycles of 2 hours each followed by air cooling, one 16-hour exposure followed by air cooling, and one weighing for each 22 hours of exposure per day.

The results of screening by furnace oxidation are presented graphically in Figures 9 and 10. Composition 1 lost weight from the outset of the test. There was nothing to distinguish compositions 2 through 5 from one another on a weight-change basis. No distinction could be made between impacted and nonimpacted specimens, based on weight changes, for compositions 1 and 2. Impacted specimens of compositions 3 and 5 gained slightly more weight than nonimpacted specimens; the reverse was true of composition 4. The appearance of representative samples of each composition is shown in Figure 11.

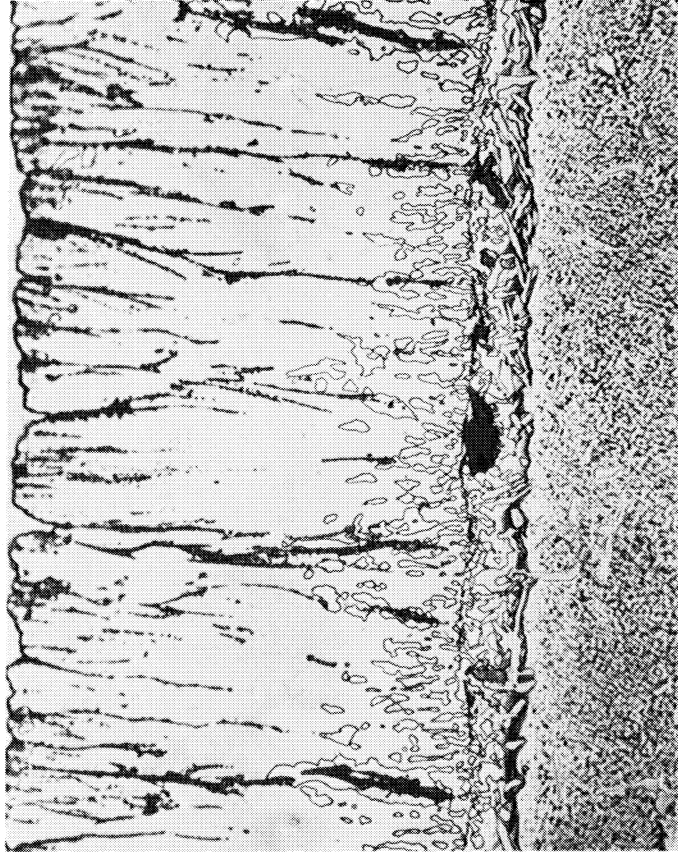


COMPOSITION 1 (Co-20Cr-12Al-0.5Y), SPECIMEN 268, SHOWING A 2-PHASE STRUCTURE

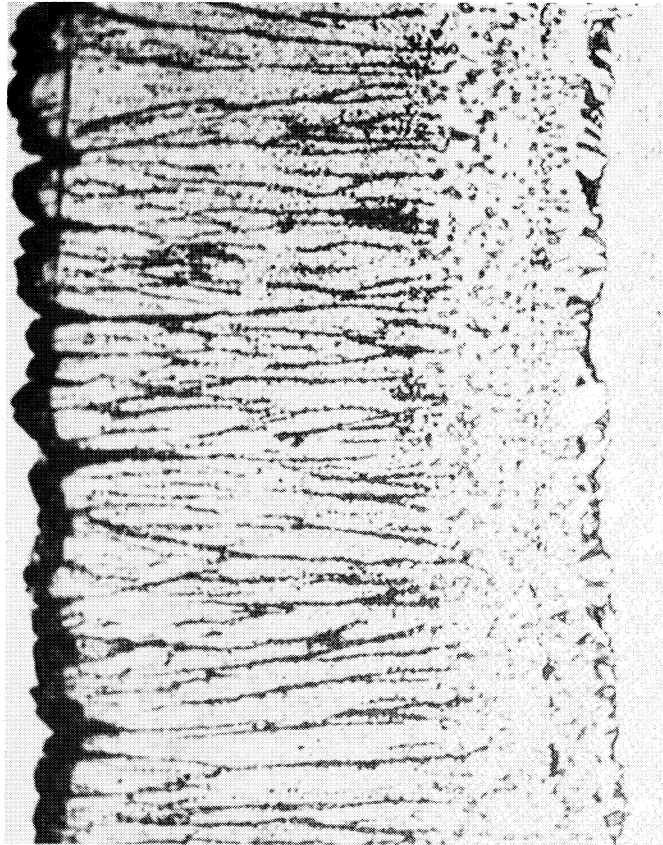


COMPOSITION 2 (Co-20Cr-20Al-0.5Y), SPECIMEN 280, SHOWING MAINLY A 1-PHASE COLUMNAR STRUCTURE WITH A SMALL AMOUNT OF A SECOND PHASE PRESENT

Figure 5      Representative Microstructures of Compositions 1 and 2 Coatings (500X Magnification)



COMPOSITION 3 (Co-30Cr-16Al-0.5Y), SPECIMEN 285, WITH MICROSTRUCTURE SIMILAR TO COMPOSITION 2, SPECIMEN 280 (SEE FIGURE 5), WITH INCREASED AMOUNT OF SECOND PHASE



COMPOSITION 4 (Co-40Cr-12Al-0.5Y), SPECIMEN 296

Figure 6 Representative Microstructures of Compositions 3 and 4 Coatings (500X Magnification)

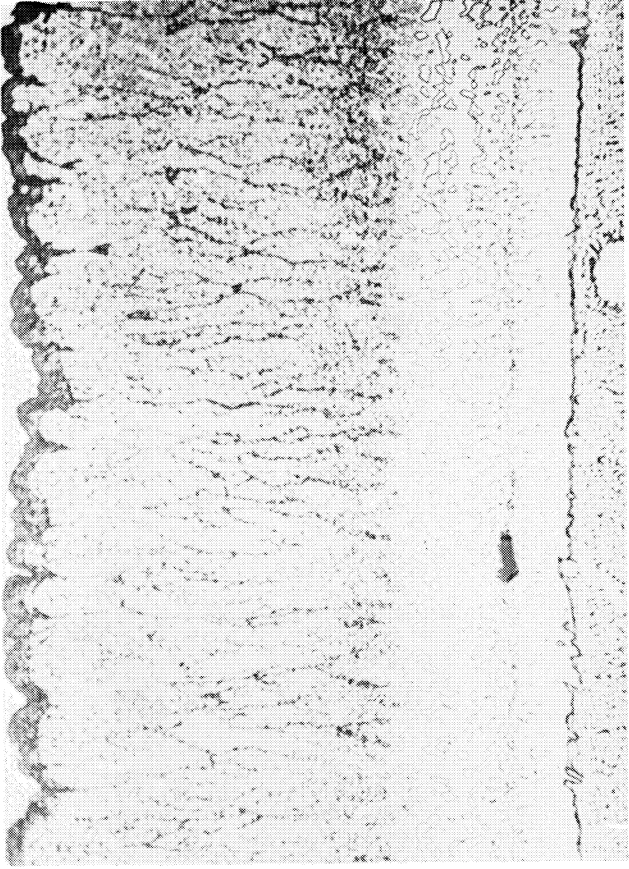
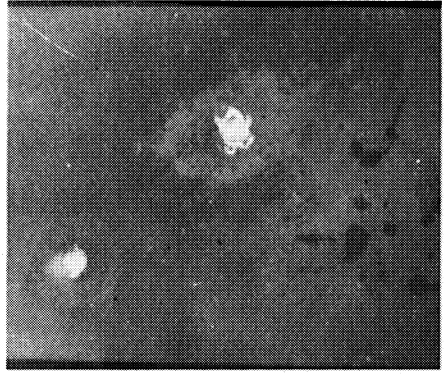


Figure 7 Representative Microstructure of Composition 5 Coating (500X Magnification)

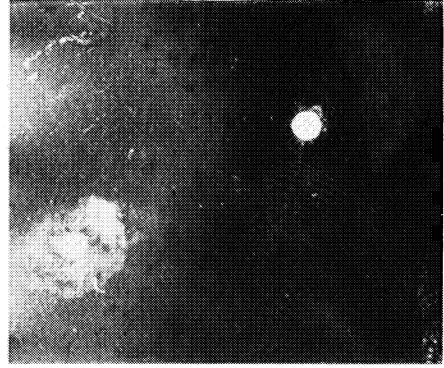
COMPOSITION 5 (Co-40Cr-20Al-0.5Y), SPECIMEN 300

TABLE II  
RESULTS OF BALLISTIC IMPACT TEST

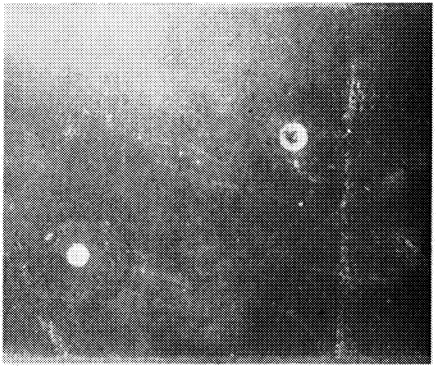
Composition No.	Specimen No.	Condition After Test
1	268	Very slight radial cracking 400 fps (122 m/sec), slight radial cracking 600 fps (183 m/sec)
1	269	No cracking evident
2	277	Radial cracking 400 and 600 fps (122 and 183 m/sec), very slight cracking backside of 600 fps (183 m/sec)
2	278	No cracking evident
3	285	Very slight circumferential cracking 400 and 600 fps (122 and 183 m/sec), cracking bottom of dent from 600 fps (183 m/sec), slight cracking backside of 600 fps (183 m/sec)
3	288	Slight circumferential cracking 400 and 600 fps (122 and 183 m/sec)
4	295	Extensive radial cracking 400 fps (122 m/sec) and 600 fps (183 m/sec), entire specimen face crazed with radial and circumferential pattern
4	296	Extensive radial cracking 400 and 600 fps (122 and 183 m/sec), entire specimen face crazed with radial and circumferential pattern
5	305	Radial and circumferential cracking 400 and 600 fps (122 and 183 m/sec), extensive crazing
5	306	Radial and circumferential cracking 400 and 600 fps (122 and 183 m/sec), extensive crazing



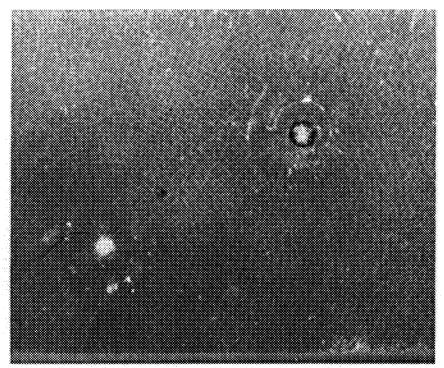
COMPOSITION 1 (Co-20Cr-12Al-0.5Y)  
SPECIMEN 269



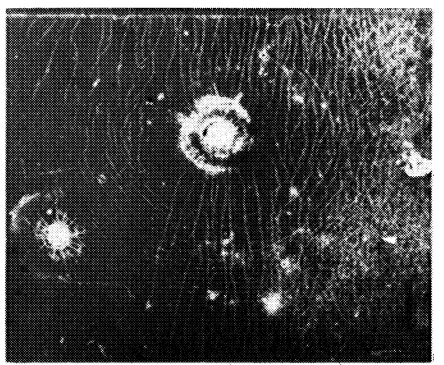
COMPOSITION 2 (Co-20Cr-20Al-0.5Y)  
SPECIMEN 277



COMPOSITION 3 (Co-30Cr-16Al-0.5Y)  
SPECIMEN 285



COMPOSITION 4 (Co-40Cr-12Al-0.5Y)  
SPECIMEN 295



COMPOSITION 5 (Co-40Cr-20Al-0.5Y)  
SPECIMEN 306

Figure 8 Front Views of Test Specimens Showing Result of 400 fps (122 m/sec) Ballistic Impact at Upper Left and 600 fps (183 m/sec) Impact at Lower Right of Each Specimen (1.9X Magnification)

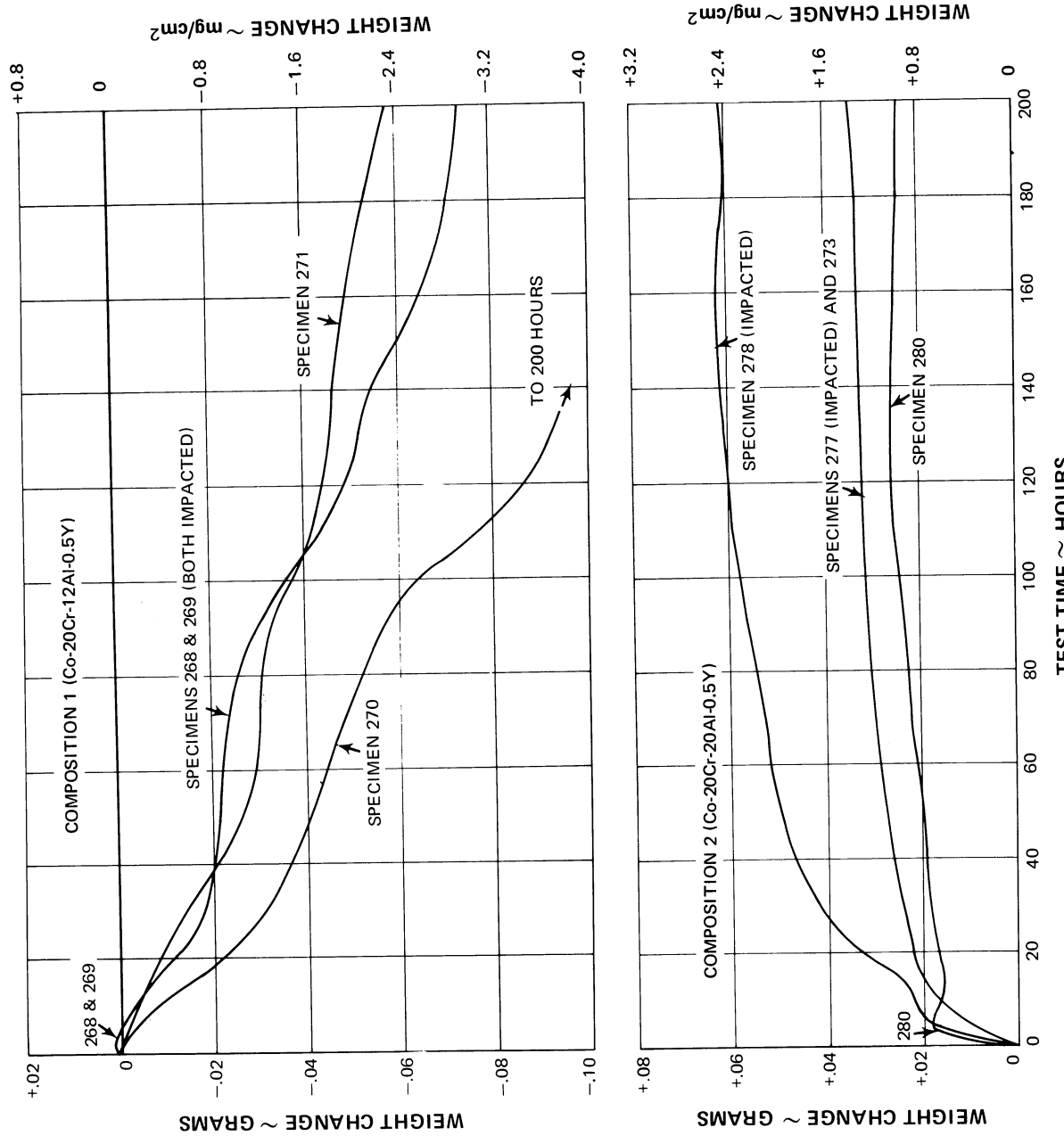


Figure 9 Furnace Oxidation Weight-Change Behavior of Both Impacted and Nonimpacted Specimens Coated With Compositions 1 and 2

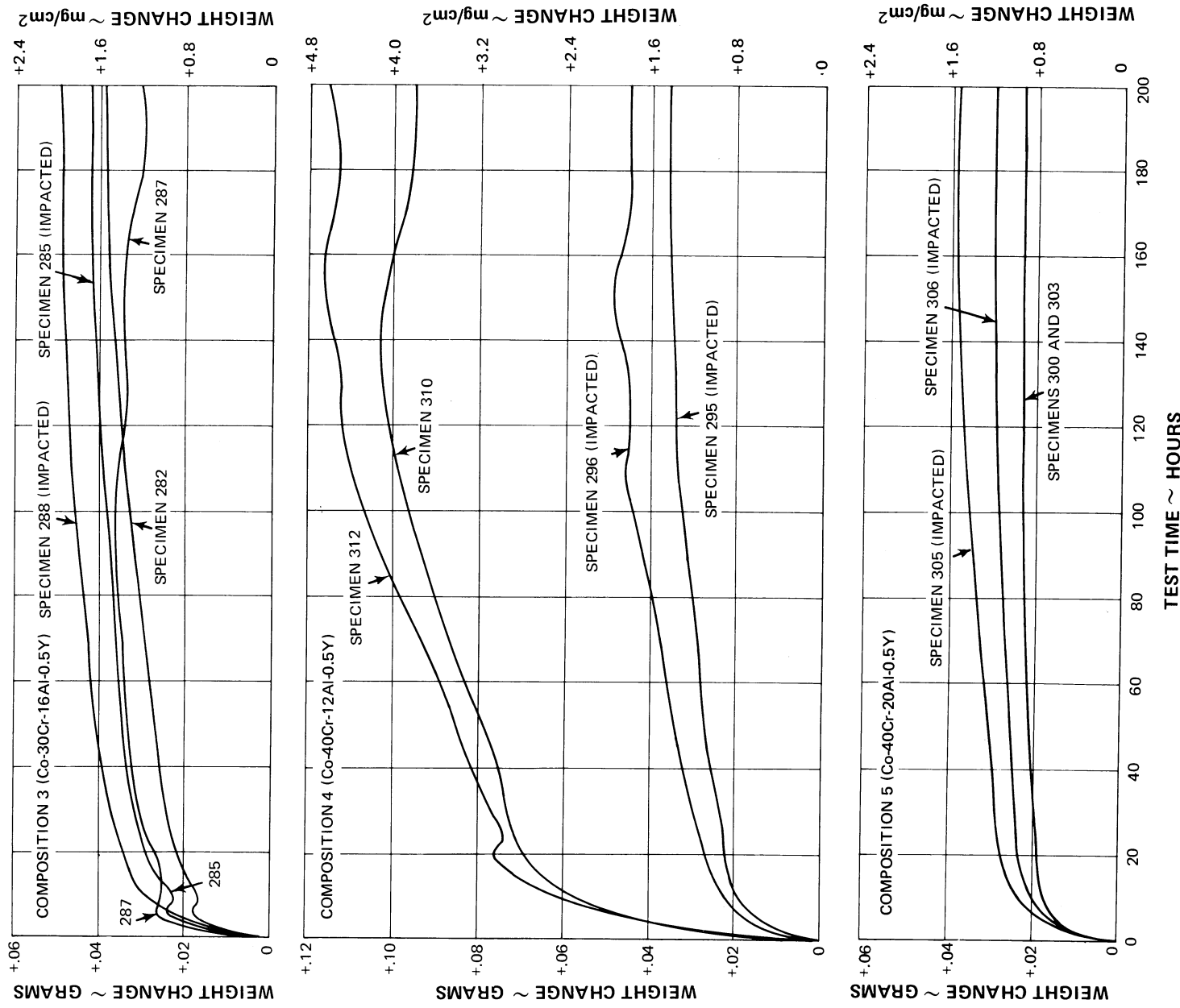
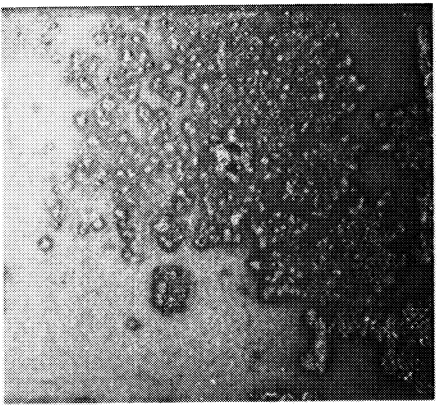
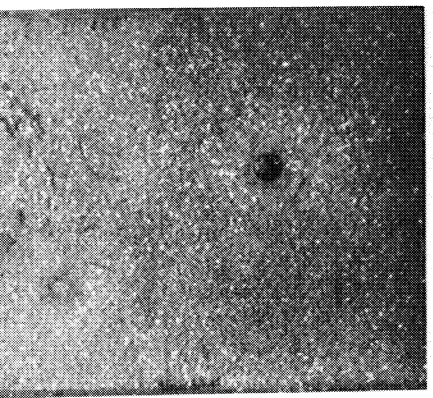


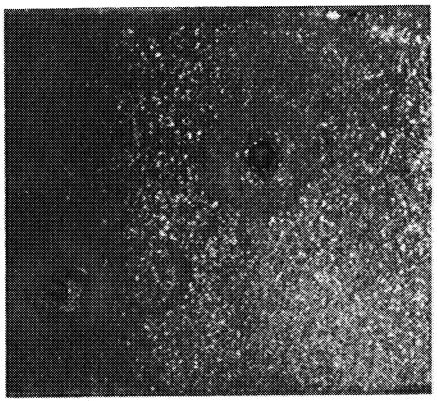
Figure 10 Furnace Oxidation Weight-Change Behavior of Both Impacted and Nonimpacted Specimens Coated With Compositions 3, 4, and 5



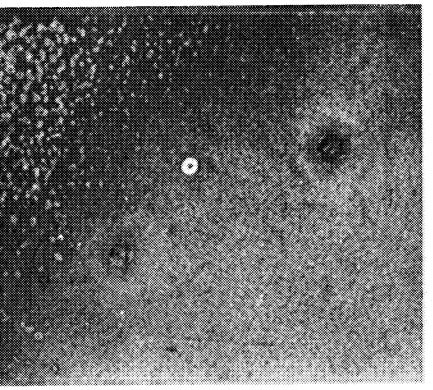
COMPOSITION 1 (Co-20Cr-12Al-0.5Y)  
SPECIMEN 268



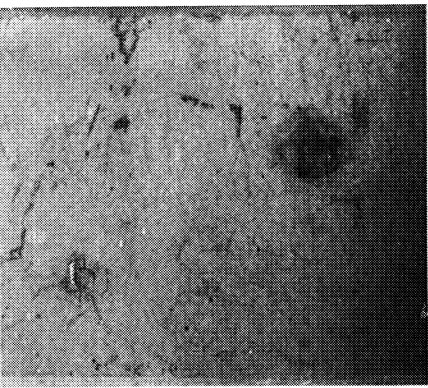
COMPOSITION 3 (Co-30Cr-16Al-0.5Y)  
SPECIMEN 288



COMPOSITION 2 (Co-20Cr-20Al-0.5Y)  
SPECIMEN 278



COMPOSITION 4 (Co-40Cr-12Al-0.5Y)  
SPECIMEN 296



COMPOSITION 5 (Co-40Cr-20Al-0.5Y)  
SPECIMEN 305

Figure 11      Front Views of Test Specimens After Ballistic Impact—400 fps (122 m/sec) Upper Left  
and 600 fps (183 m/sec) Lower Right of Each Specimen—and 200 Hours Exposure at  
2000°F (1366°K) in Static Furnace Oxidation Test (1.9X Magnification)

Composition 1 suffered a general pitting attack on all specimens tested. Composition 2 showed no visual ill effects from exposure; very light oxide spallation was noted as a general symptom of exposure. Composition 3 showed generally light oxide spallation as a consequence of exposure. Composition 4 exhibited a very light pitting attack similar to that of composition 1 but of significantly lower magnitude. Composition 5 remained virtually unchanged in appearance throughout testing.

Post-test metallographic examination showed that no test specimen had failed after 200 hours of furnace exposure. Composition 1 was considered to be in the worst condition; pitted areas had not penetrated to base metal although substantial oxide scale was associated with the pitting (Figure 12, upper photograph). Those areas not pitted showed little distress (Figure 12, lower photograph). Also, no distress was associated with impact (Figure 13).

Compositions 2 through 5 exhibited attack by oxidation at the columnar grain boundaries (Figures 14 and 15) which were evident in the microstructure prior to test. Ballistic impact had not initiated additional oxidative distress under these test conditions.

### C. DISCUSSION OF TEST RESULTS AND SELECTION OF ALLOY MODIFICATIONS FOR BURNER RIG TEST

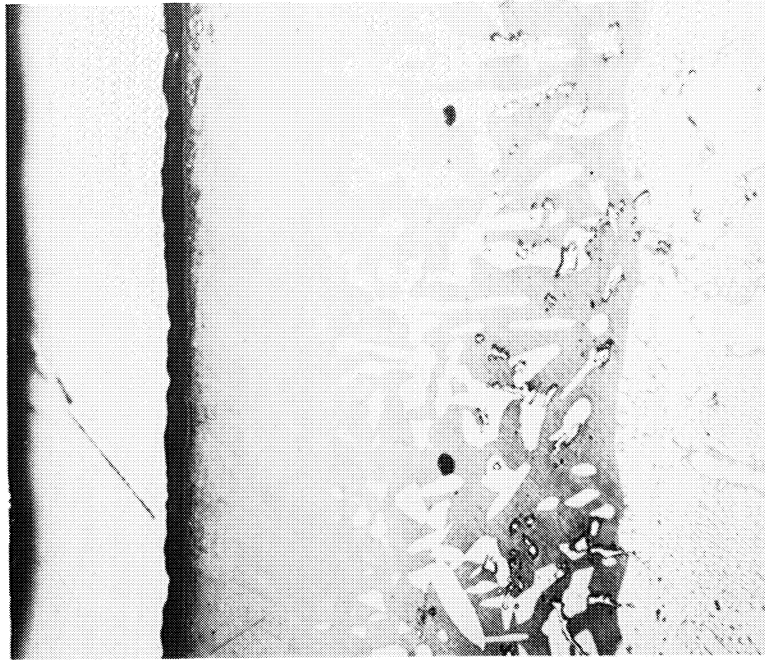
Oxidation resistance and resistance to foreign object damage are important criteria in establishing the usefulness of a coating system. Equally important is the adaptability of a coating to production manufacture. It was previously shown that ingots of compositions 2 and 5 were extremely difficult to machine. This drawback could limit the future usefulness of these two compositions when the electron beam vapor deposition process is employed. Compositions 2 through 5 could not be mechanically processed after coating successfully to produce a homogeneous noncolumnar structure. However, none of the specimens failed in oxidation testing, whether impacted or not.

The results of this portion of the program may best be expressed in tabular fashion. The tabulation below compares each coating system by use of a subjective ranking system, ranking 1 to 5, best to poorest.

<u>Ranking</u>	<u>Composition Number</u>		
	<u>Ingot Machining</u>	<u>Mechanical Processing</u>	<u>Ballistic Impact</u>
			<u>Oxidation Resistance</u>
1	1	1	5
2	3	4.5	2
3	4	2,3	4
4	2	4	3,4
5	5	5	1



PITTED AREA, SHOWING HEAVY SCALE (BRACKET)



AREA NOT PITTED

Figure 12 Microstructure of Composition 1, Co-20Cr-12Al-0.5Y, Coating (Specimen 270) in Pitted Area and in Area Not Pitted Following 2000°F (1366°K) Furnace Oxidation Exposure for 200 Hours (300X Magnification)



Figure 13 Microstructure of Composition 1, Co-20Cr-12Al-0.5Y, Coating (Specimen 268) in Area of 600 fps (183 m/sec) Ballistic Impact Indentation Following 2000°F (1366°K) Furnace Oxidation Exposure for 200 Hours (75X Magnification). The photomicrograph shows the severe plastic deformation of the coating at the periphery of the indentation.

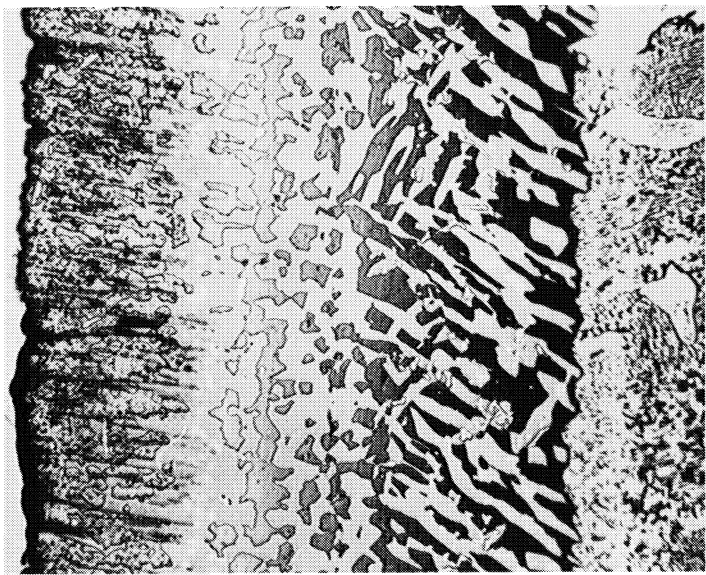
The results show that the coating alloys tested could be characterized in two groups:

- Group A alloys possess relatively good ductility but oxidation resistance less than that of Group B. Compositions 1, 3, and 4 belong in this category.
- Group B alloys possess the highest oxidation resistance but have relatively poor ductility. Compositions 2 and 5 are in this category.

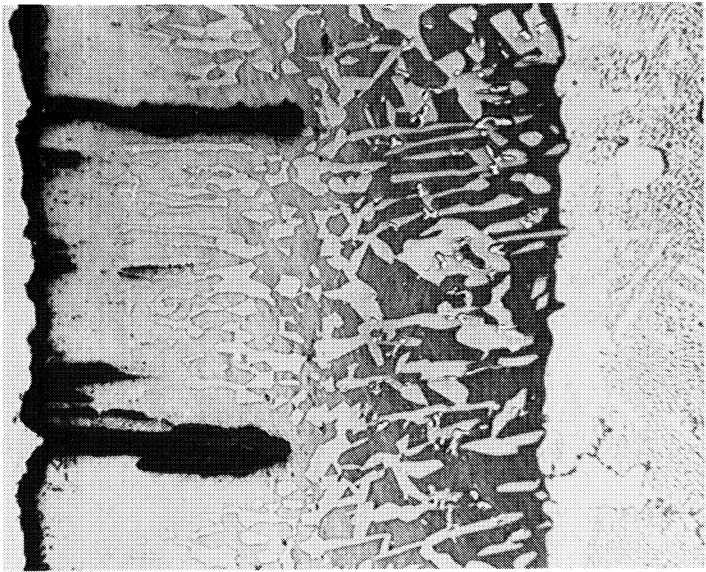
The objective for coating alloy modification for burner rig testing was twofold:

- Improve oxidation resistance of Group A alloys with minimal compromise in ductility.
- Improve ductility of Group B alloys with minimal compromise in oxidation resistance.

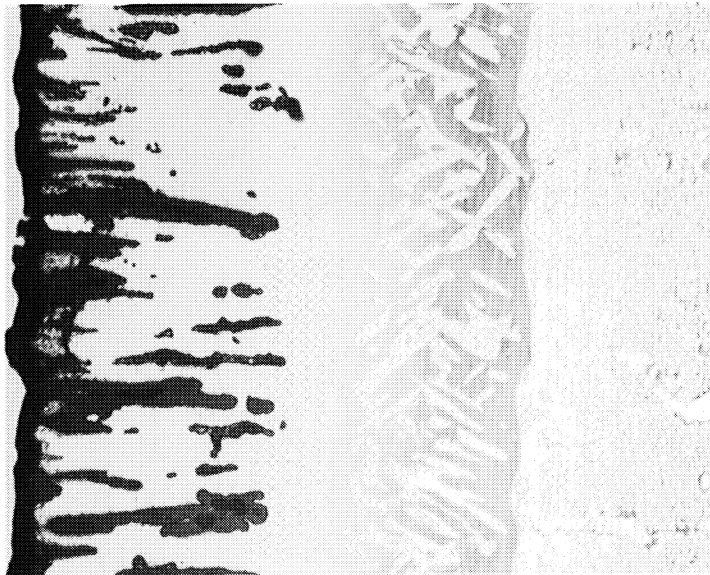
The data indicate that the best oxidation resistance is associated with higher aluminum content and modest chromium content, while the poorest resistance to ballistic impact appears to be associated with higher chromium content. The best balance of properties, therefore, should fall within the framework of the original factorial design.



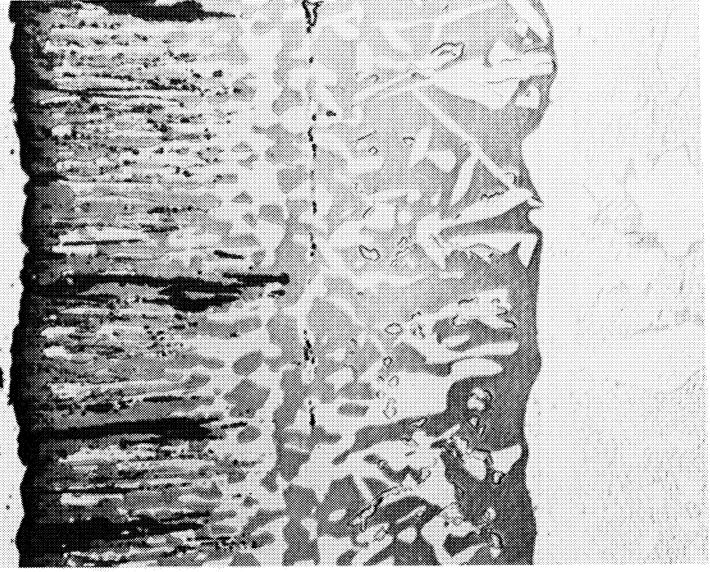
COMPOSITION 2 (Co-20Cr-20Al-0.5Y), SPECIMEN 310



COMPOSITION 3 (Co-30Cr-16Al-0.5Y), SPECIMEN 287

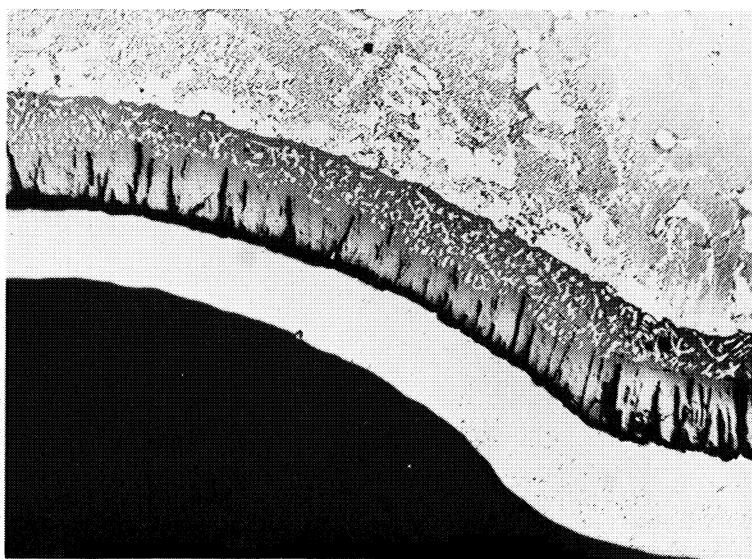


COMPOSITION 4 (Co-40Cr-12Al-0.5Y), SPECIMEN 310

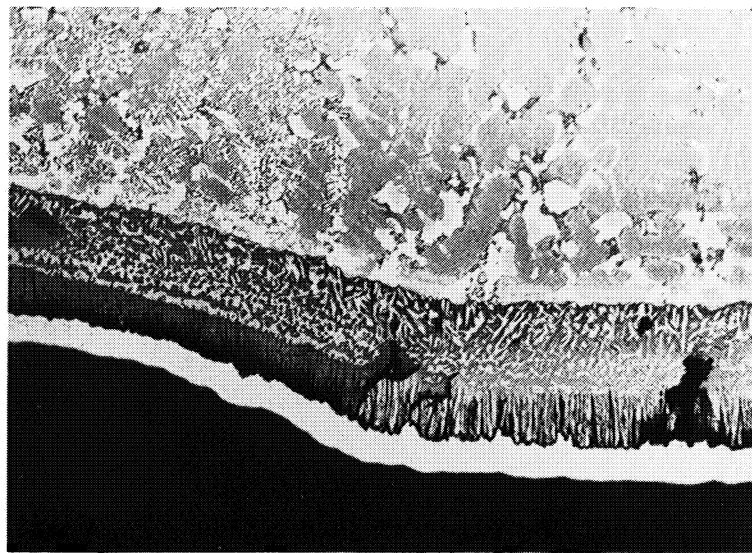


COMPOSITION 5 (Co-40Cr-20Al-0.5Y), SPECIMEN 300

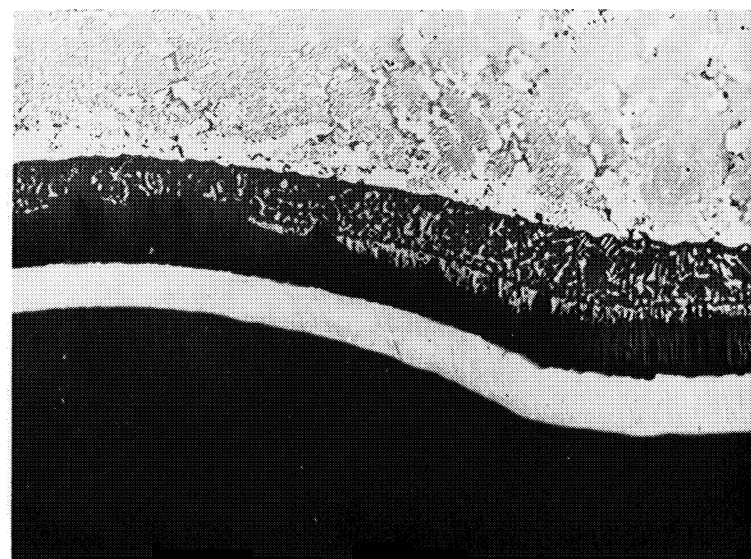
Figure 14 Microstructures of Compositions 2, 3, 4, and 5 Coatings Following 2000°F (1366°K)  
Furnace Oxidation Exposure for 200 Hours (300X Magnification)



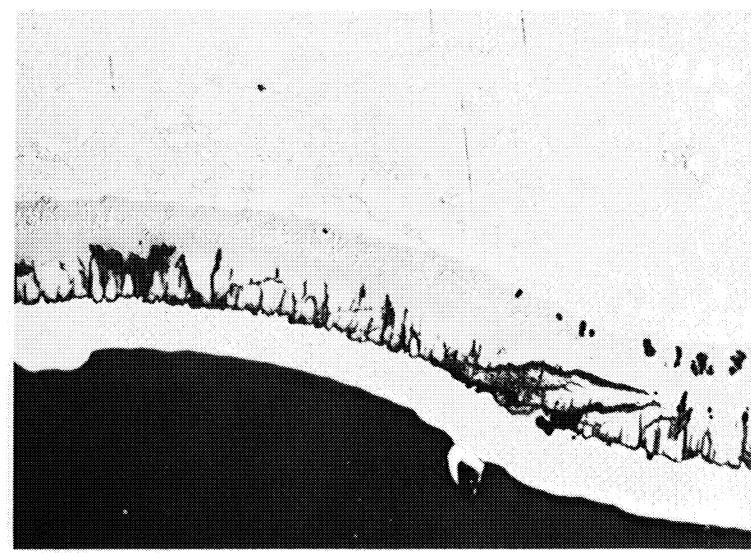
COMPOSITION 3 (Co-30Cr-16Al-0.5Y), SPECIMEN 288



COMPOSITION 4 (Co-40Cr-12Al-0.5Y), SPECIMEN 296



COMPOSITION 2 (Co-20Cr-20Al-0.5Y), SPECIMEN 278



COMPOSITION 5 (Co-40Cr-20Al-0.5Y), SPECIMEN 305

Following 2000°F (1366°K) Furnace Oxidation Exposure for 200 Hours (75X Magnification)  
Figure 15 Microstructures of Compositions 2, 3, 4, and 5 Coatings in Areas of 600 fps (183 m/sec) Ballistic Impact Indentations

In Group A, four compositional modifications were selected with a modest increase in chromium over composition 1 (Co-20Cr-12Al-0.5Y) and three different levels of aluminum above that of composition 1. These four modifications were designated compositions 6 through 9; target compositions are tabulated below, and the relationship of the new compositions to the original factorial design is illustrated graphically in Figure 16.

<u>Composition No.</u>	<u>Target Coating Composition</u>
6	Co - 25Cr - 16Al - 0.2Y
7	Co - 25Cr - 14Al - 0.2Y
8	Co - 25 Cr - 14Al - 0.7Y
9	Co - 25Cr - 15Al - 0.2Y

Yttrium content was varied in composition 8 in order to explore its effect as a variable.

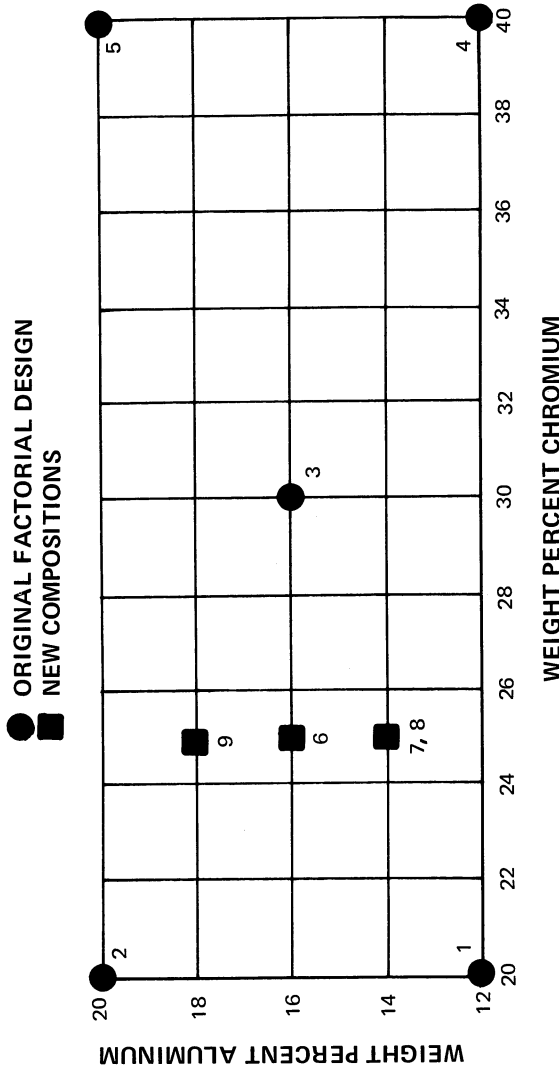


Figure 16 Chromium-Aluminum Content of the Five Initial Coating Compositions and of Compositional Variations 6 through 9 (Group A Modifications)

Composition 5 (Co-40Cr-20Al-0.5Y) was selected as the basis for Group B alloy modifications. Substitution of iron and nickel for cobalt in the best composition based on oxidation resistance was implemented in an effort to improve ductility without impairing oxidation resistance significantly. Composition of two modifications is tabulated below.

<u>Composition No.</u>	<u>Target Coating Composition</u>
10	Co - 40Cr - 20Fe - 20Al - 0.2Y
11	Co - 40Cr - 20Ni - 20Al - 0.2Y

## IV. 1100-HOUR BURNER RIG TEST

### A. COATING OF TEST SPECIMENS

Cast ingots of each of the five original compositions and each of the six compositional variations were prepared for evaporation by centerless grinding. Analyses of these compositions are summarized in Table III. Compositions 2, 5, and 10 were marginally acceptable for evaporation; compositions 6, 9, and 11 experienced slight to moderate chipping; and compositions 1, 3, 4, 7, and 8 were readily machinable (Figure 17).

Following ingot preparation, the coating of burner-rig paddle specimens was accomplished by the electron beam vapor deposition process. Chemical analyses of deposited coatings are summarized in Table IV. Specimens coated simultaneously are represented by one analysis.

One coated paddle specimen each of compositions 6 through 11 were run through a glass bead peening process. Compositions 6, 9, 10, and 11 could not be successfully processed. No attempt was made to process compositions 2 through 5, which failed earlier when it was attempted on sample coupons prior to ballistic impact and furnace oxidation testing. Both specimens of composition 1 were successfully processed and the second specimen of the compositions 7 and 8 were processed. One specimen of each of compositions 6, 9, 10, and 11 was recoated to replace those damaged by trial processing. All samples were given a 1975°F (1135°K) heat treatment in hydrogen for 4 hours. Representative microstructures for compositions 6 through 11 are shown in Figures 18 through 20. Microstructures for compositions 1 through 5 are shown in Figures 5 through 7.

TABLE III  
INGOT COMPOSITIONS FOR BURNER RIG TESTS

Composition No.	Target Composition for Casting	Chemical Analysis
1	Co - 20Cr - 12Al - 0.5Y	Co - 19.65Cr - 11.99Al - 0.42Y
2	Co - 20Cr - 20Al - 0.5Y	Co - 19.94Cr - 20.05Al - 0.38Y
3	Co - 30Cr - 16Al - 0.5Y	Co - 29.63Cr - 15.93Al - 0.68Y
4	Co - 40Cr - 12Al - 0.5Y	Co - 38.72Cr - 11.80Al - 0.70Y
5	Co - 40Cr - 20Al - 0.5Y	Co - 40.64Cr - 18.80Al - 0.33Y
6	Co - 25Cr - 16Al - 0.5Y	Co - 23.44Cr - 16.50Al - 0.61Y
7	Co - 25Cr - 14Al - 0.5Y	Co - 24.75Cr - 14.10Al - 0.44Y
8	Co - 25Cr - 14Al - 0.9Y	Co - 25.29Cr - 14.30Al - 0.80Y
9	Co - 25Cr - 18Al - 0.5Y	Co - 24.56Cr - 18.13Al - 0.49Y
10	Co - 40Cr - 20Fe - 20Al - 0.5Y	Co - 39.07Cr - 19.00Fe - 20.15Al - 0.33Y
11	Co - 40Cr - 20Ni - 20Al - 0.5Y	Co - 37.87Cr - 19.87Ni - 19.65Al - 0.80Y

Figure 17 Appearance of Cast Ingot of Each Composition After Grindding. Each ingot is 2 inches (50.8 mm) in diameter. The composition number is given under each ingot along with target composition.

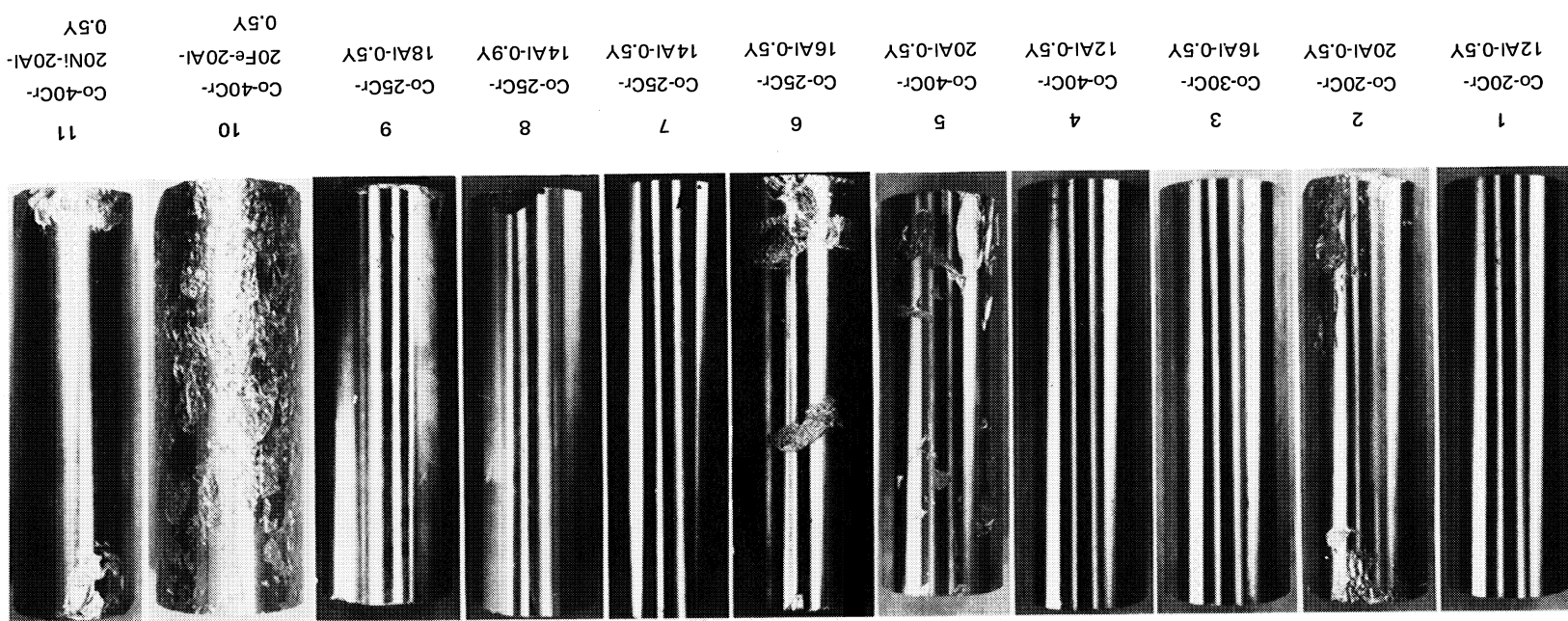
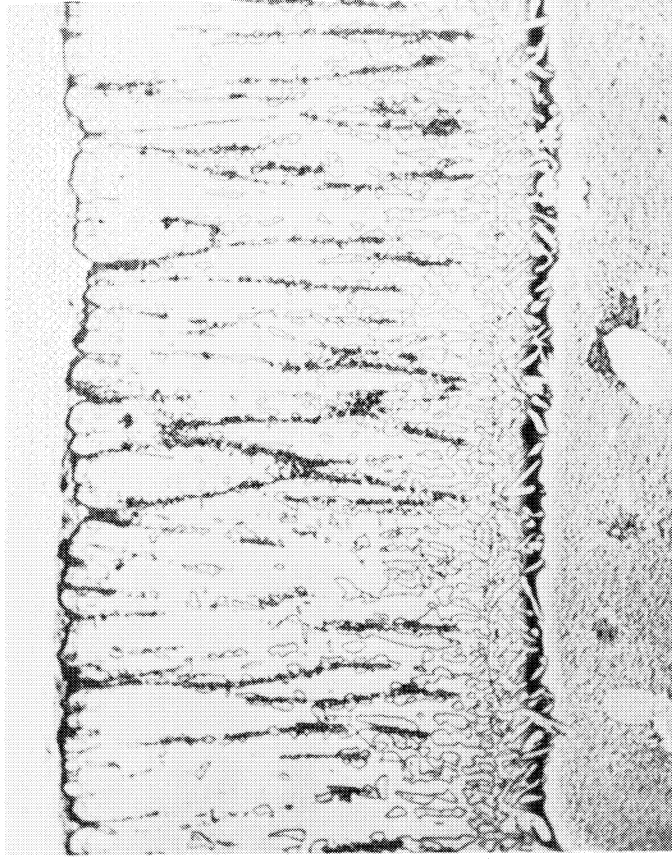


TABLE IV

CHEMICAL ANALYSIS OF VAPOR DEPOSITED COATINGS  
FOR BURNER RIG TEST AND EVALUATION

Composition No.	Specimen No.	Composition (Weight %)				Calculated Thickness (mils)	Calculated Thickness (μm)
		Co	Cr	Al	Y		
1	G4088B, G4088C	70.44	18.98	10.65	0.10	..	5.2, 5.3 132, 135
2	G4088F, G4088G	63.79	19.87	18.89	0.16	..	4.9, 4.9 124, 124
3	G4088H, G4088K	56.61	28.30	15.27	0.17	..	5.0, 4.8 127, 122
4	G4088L, G4088M	49.22	37.70	12.24	0.11	..	4.8, 4.8 122, 122
5	G4088N, G4088O	45.98	36.24	20.87	0.18	..	5.7, 5.7 145, 145
6	G4088S, G4088R	62.96	23.23	16.95	0.15	..	6.0, 6.1 152, 155
	G4092T	63.96	22.05	13.88	0.12	..	4.7 109
7	G4092H, G4092K	65.48	22.33	13.91	0.10	..	5.2, 5.2 132, 132
8	G4162P, G4092Q	58.75	26.37	13.55	0.61	..	4.5, 4.4 114, 112
9	G4094M, G4094C	63.96	21.13	17.46	0.19	..	5.8, 5.8 147, 147
	G4092M	60.49	24.39	16.26	0.25	..	5.1 130
	G4162I, G4162M	19.50	37.00	20.00	0.15	..	5.4, 5.3 137, 135
*10	G4161E, G4092I	25.54	33.02	18.50	0.20	..	4.9, 5.1 124, 130
*11	G4162N, G4162O	23.00	35.70	20.40	0.07	22.1	5.4, 5.3 137, 135
	G4092B, G4092S	19.85	38.64	20.00	0.10	21.24	5.2, 5.0 132, 127

\* Analyzed by x-ray solution except for aluminum which was done by atomic absorption spectrophotometry

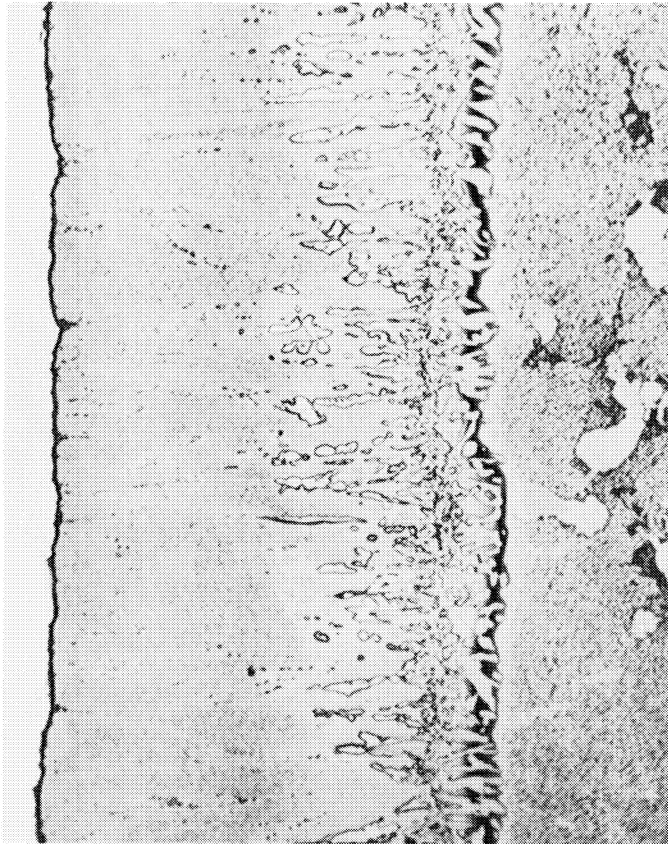


COMPOSITION 6 (Co-25Cr-16Al-0.5Y), SPECIMEN G4092T

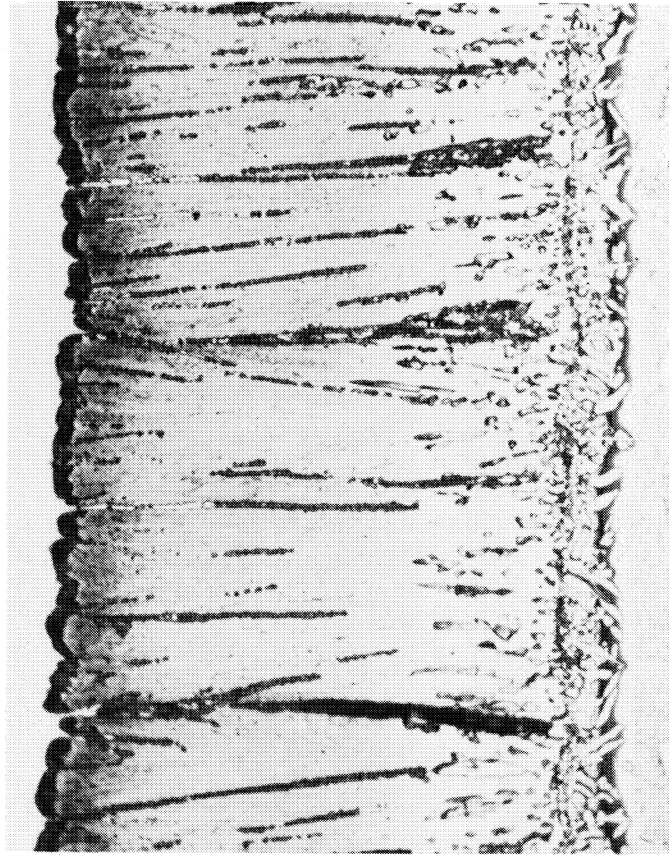


COMPOSITION 7 (Co-25Cr-14Al-0.5Y), SPECIMEN G4092K

Figure 18 Representative Microstructures of Compositions 6 and 7 Coatings (500X Magnification)

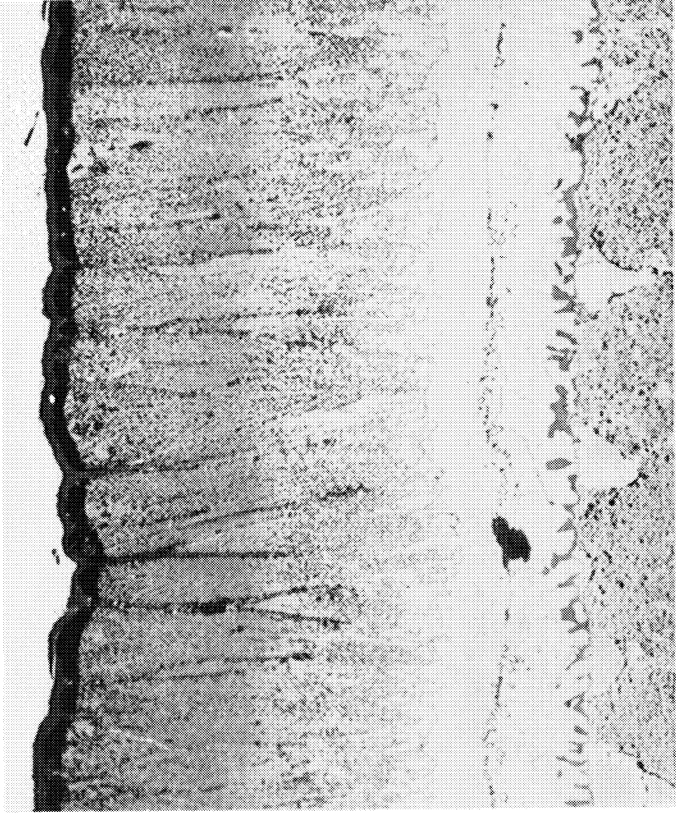


COMPOSITION 8 (Co-25Cr-14Al-0.9Y)  
SPECIMEN G4092Q



COMPOSITION 9 (Co-25Cr-18Al-0.5Y)  
SPECIMEN G4092M

Figure 19 Representative Microstructures of Compositions 8 and 9 Coatings (500X Magnification)



COMPOSITION 10 (Co-40Cr-20Fe-20Al-0.5Y)  
SPECIMEN G4161E



COMPOSITION 11 (Co-40Cr-20Ni-20Al-0.5Y)  
SPECIMEN G4092S

Figure 20 Representative Microstructures of Compositions 10 and 11 Coatings (500X Magnification)

Figure 20

## B. BURNER RIG TEST

Specimens coated with the 11 coating compositions were placed in the burner rig along with a control specimen of B-1900 with a commercially applied aluminide coating (designated here as NASA Standard 43 and later replaced by NASA Standard 45).

Each thermal cycle consisted of 1 hour exposure at test temperature of 2000°F (1366°K) followed by a 3-minute forced air cool. Specimens were weighed after each 20 hours of exposure at temperature for the first 100 hours and thereafter at intervals no greater than 100 hours. Test duration was 1100 hours or until specimen failure as evidenced visually or by weight loss exceeding 20 milligrams, whichever occurred first. Specimens which failed before 1100 hours were replaced by nickel-base specimens coated with a standard aluminide coating (designated as P&WA Standards 17 and 19).

The results of burner rig testing are summarized in Table V, and weight-change curves are plotted in Figures 21 and 22.

Compositions 1, 5, 7, and 8 were run through the entire 1100 hours without failure, while the remaining seven compositions failed after test periods ranging from 137 to 605 hours. Determination of failure was in some cases by visual examination (subsequently confirmed by metallographic examination) and in some cases by measured weight loss.

Photographs showing the appearance of the specimens following burner rig testing are provided in Figures 23 through 27, while coating microstructures of the same test specimens are shown in Figures 28 through 30. A standard aluminide coated specimen is shown in Figure 23, specimens which failed are compared in Figures 24 and 25, and the appearance of compositions 1, 5, 7, and 8 after 1100 hours of test exposure is shown in Figures 26 and 27. The microstructures shown in Figures 28 through 30 are in the failed areas of the seven coatings which failed, and in areas exhibiting visual distress in the case of the four compositions which completed 1100 hours of testing without failure.

Compositions 2, 3, 4, 6, and 9 failed by massive oxidative attack along original columnar grain boundaries. Oxide retention was good. Compositions 10 and 11 exhibited a more general attack with occasional oxide penetration along original deposition grain boundaries. Composition 5 showed oxidative attack along columnar grain boundaries which had not penetrated to the substrate. Compositions 1 and 8 were similar, showing occasional breaches in the coating which may be associated with the original deposition structure. Composition 7 exhibited light surface oxidation and appeared capable of running considerably longer in test.

TABLE V

## SUMMARY OF RESULTS OF 2000°F (1366°K) BURNER RIG TEST

Composition No.	Specimen No.	Test Time (hours)	Failure Time (hours)	Final Weight Change (grams)	Failure Criterion
Aluminide	NASA Standard 43	284	275*	-0.0234	Weight Loss
Aluminide	NASA Standard 45	404	381*	-0.0377	Weight Loss
Aluminide	P&WA Standard 19	238	235*	-0.0207	Weight Loss
Aluminide	P&WA Standard 17	121	No Failure	+0.0060	---
1	G4088B	1100	No Failure	-0.0113	---
2	G4088F	200	200	+0.1000	Visual
3	G4088H	251	251	+0.0206	Visual
4	G4088L	251	251	-0.0168	Visual
5	G4088N	1100	No Failure	+0.1110	---
6	G4088S	285	276*	-0.0313	Visual, Weight
7	G4092H	1100	No Failure	+0.0131	---
8	G4162P	1100	No Failure	+0.0549	---
9	G4094M	285	285	+0.1068	Visual
10	G4092I	200	137*	-0.0827	Weight Loss
11	G4092B	609	605*	-0.0203	Weight Loss

\* Determined from weight change curve.

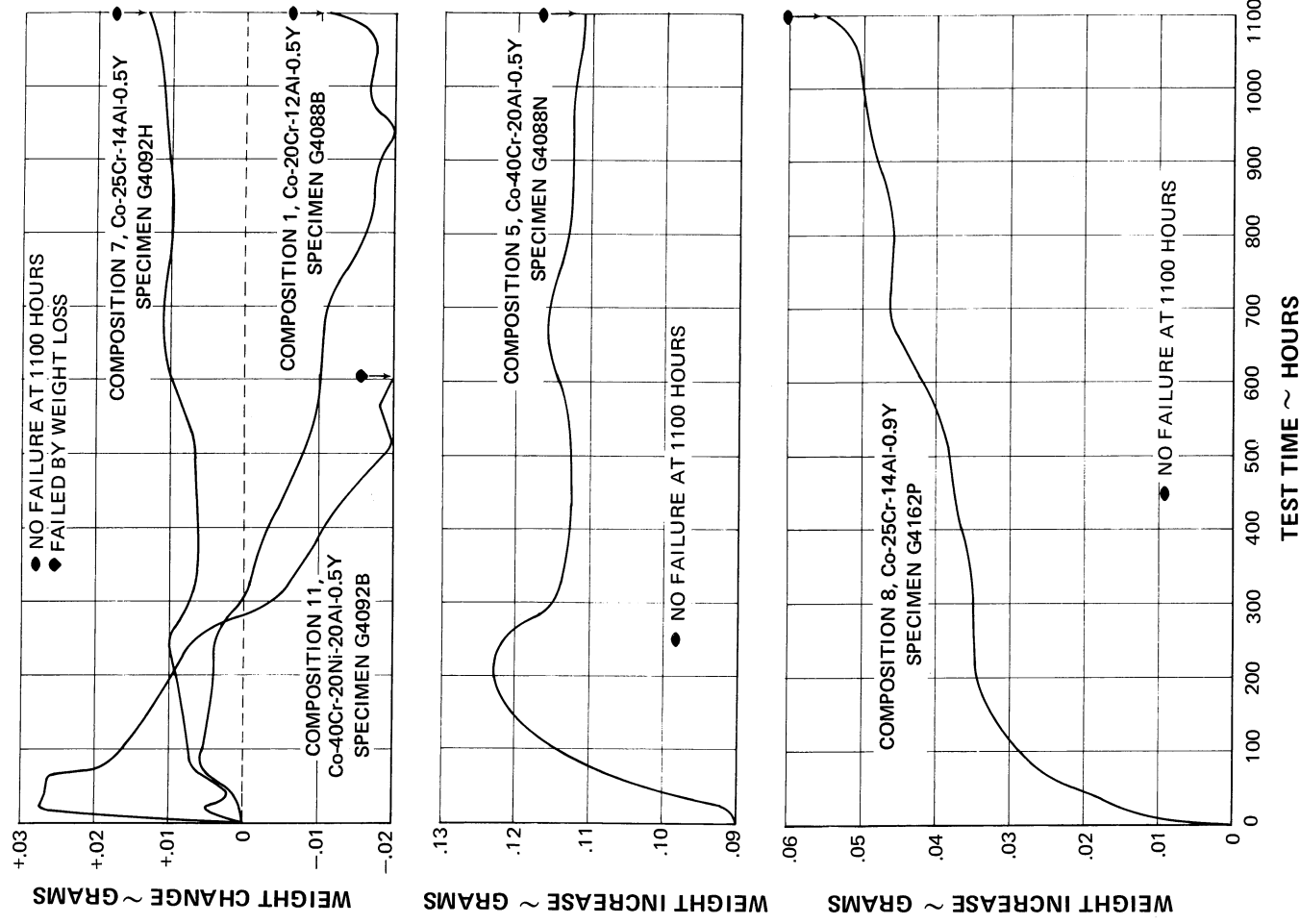


Figure 21 Burner Rig Weight-Change Behavior of Specimens Coated With Compositions 1, 5, 7, 8, and 11

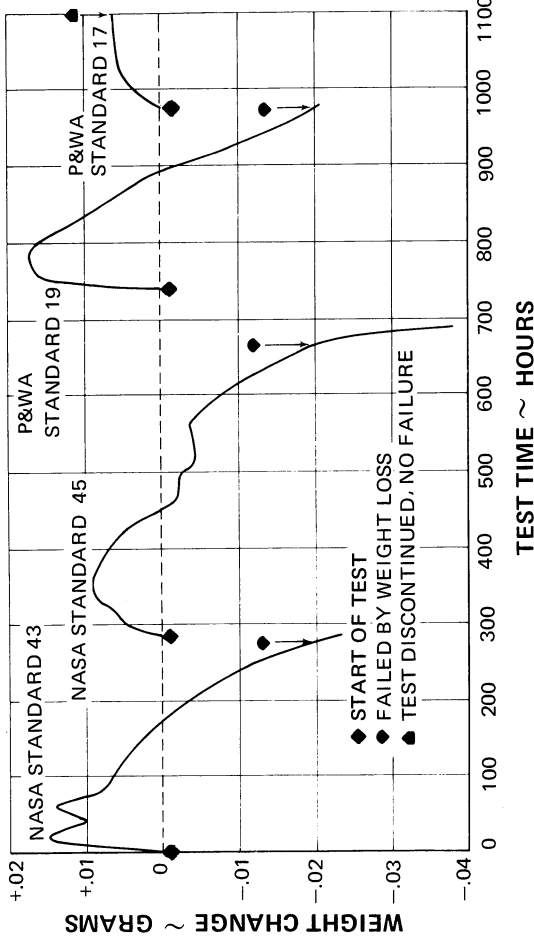
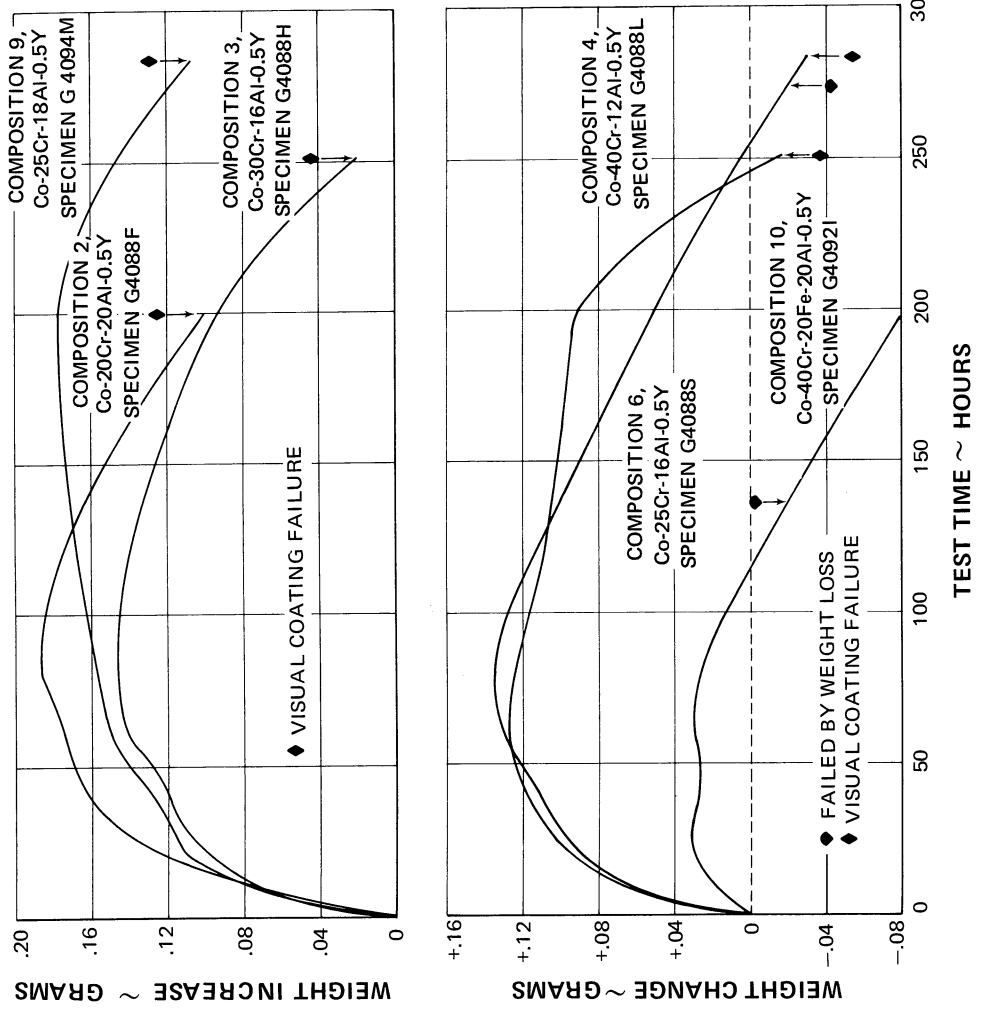
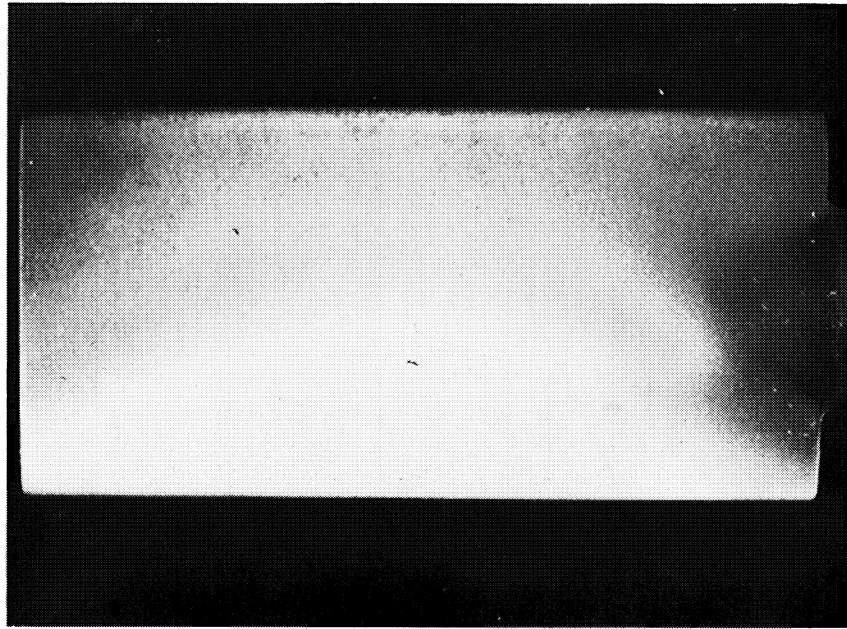


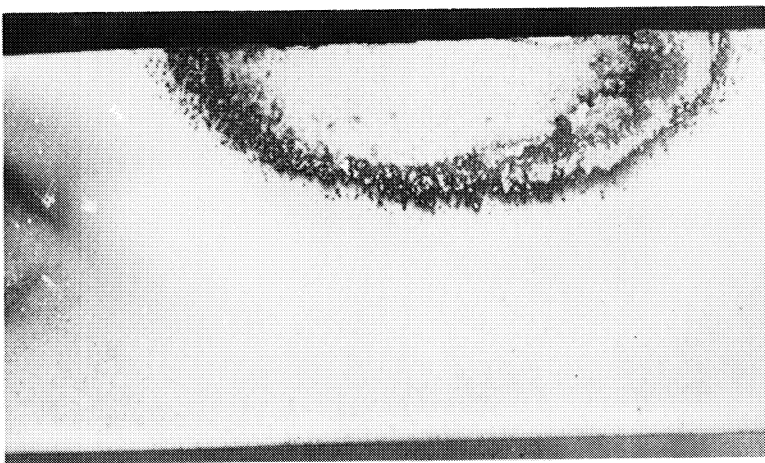
Figure 22 Burner Rig Weight-Change Behavior of Specimens Coated With Compositions 2, 3, 4, 6, 9, and 10 and of the Four Aluminide Standard Coated Specimens



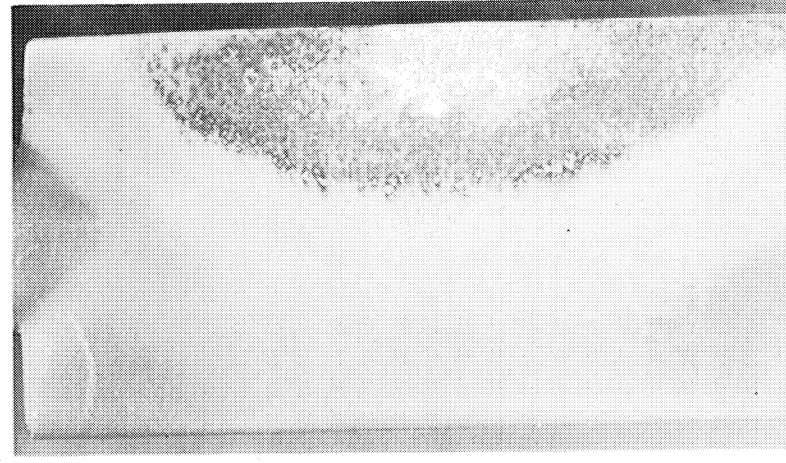
NASA STANDARD 43

Figure 23 Convex Side of Aluminide Standard Coated Test Specimen After 284 Hours of Burner Rig Testing (2X Magnification)

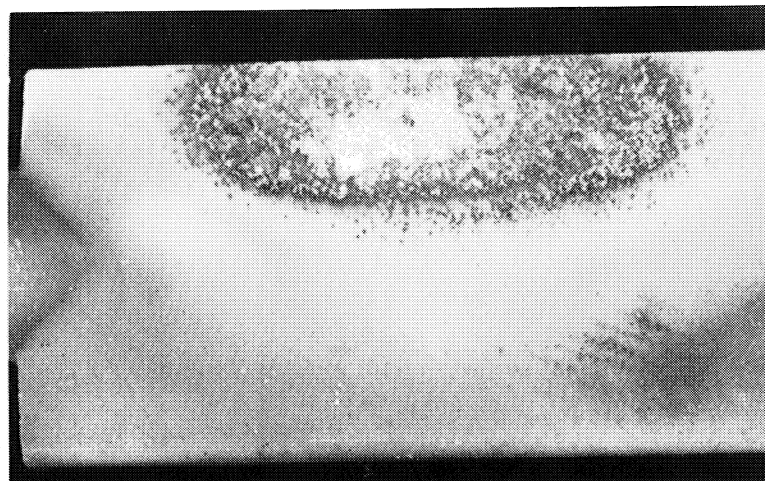
Figure 24 Convex Side of Compositions 2, 3, 4, and 6 Coated Test Specimens After Burner Rig Testing for the Times Given (2X Magnification)



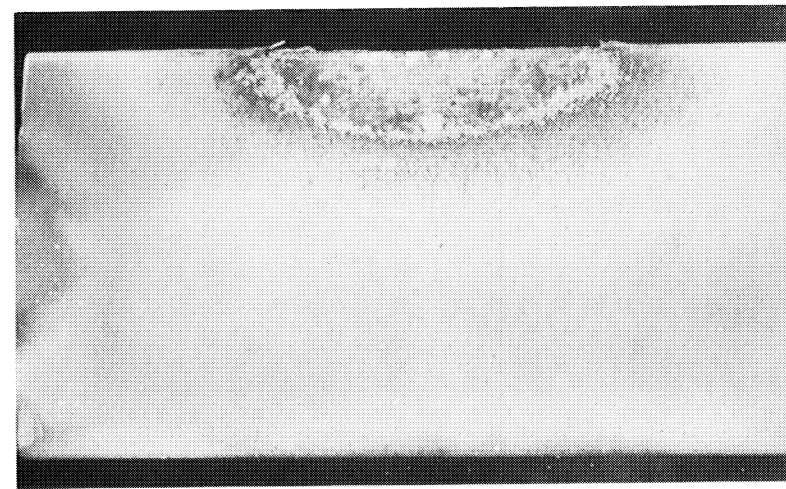
COMPOSITION 3 (Co-30Cr-16Al-0.5Y), SPECIMEN G4088H  
251 HOURS



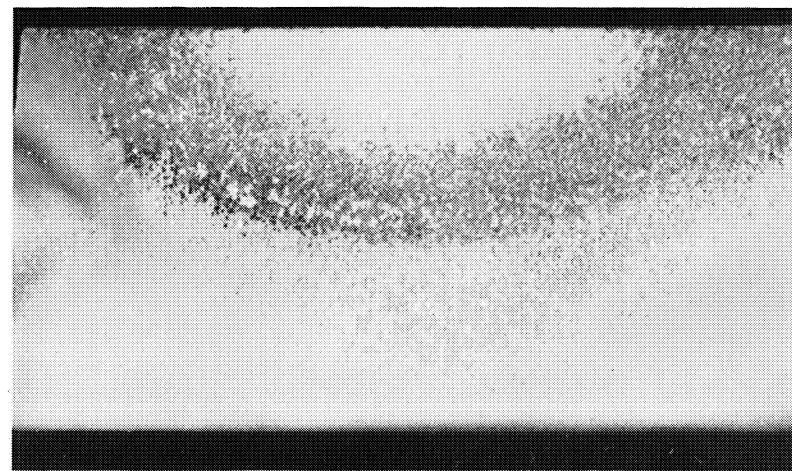
COMPOSITION 4 (Co-40Cr-12Al-0.5Y), SPECIMEN G4088L  
251 HOURS



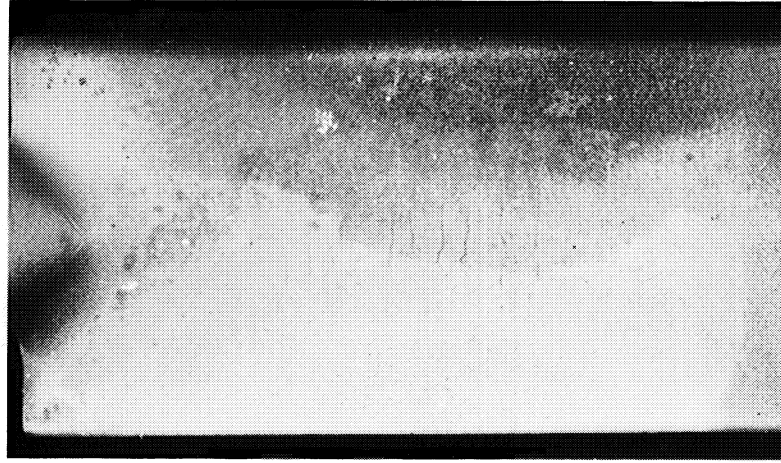
COMPOSITION 2 (Co-20Cr-20Al-0.5Y), SPECIMEN G4088F  
200 HOURS



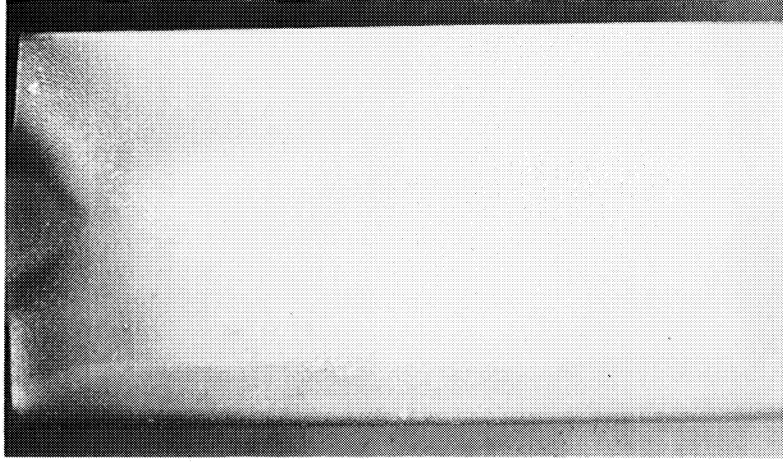
COMPOSITION 6 (Co-25Cr-16Al-0.5Y), SPECIMEN G4088S  
285 HOURS



COMPOSITION 9 (Co-25Cr-18Al-0.5Y), SPECIMEN G4094M, CONVEX SIDE  
285 HOURS

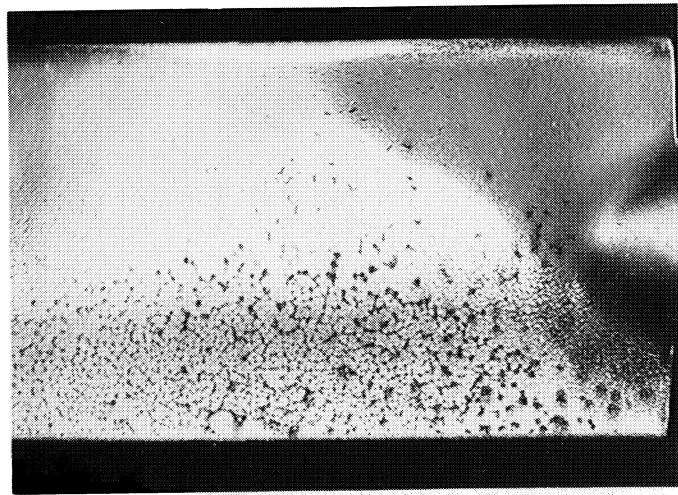


COMPOSITION 10 (Co-40Cr-20Fe-20Al-0.5Y), SPECIMEN G4092I, CONVEX SIDE  
200 HOURS

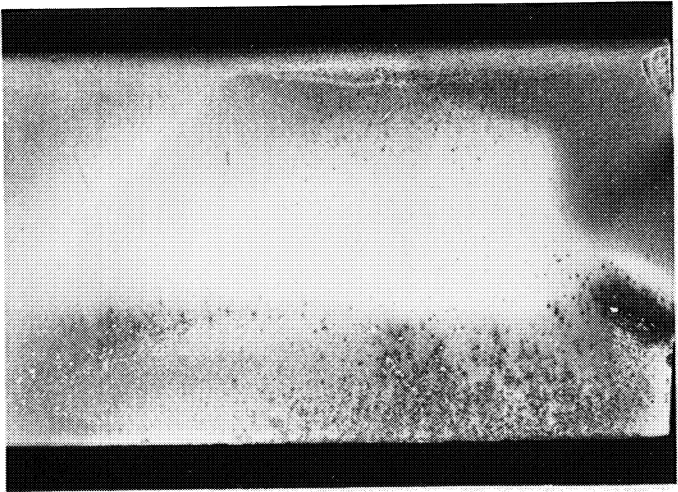


COMPOSITION 11 (Co-40Cr-20Ni-20Al-0.5Y), SPECIMEN G4092B, CONVEX SIDE  
609 HOURS

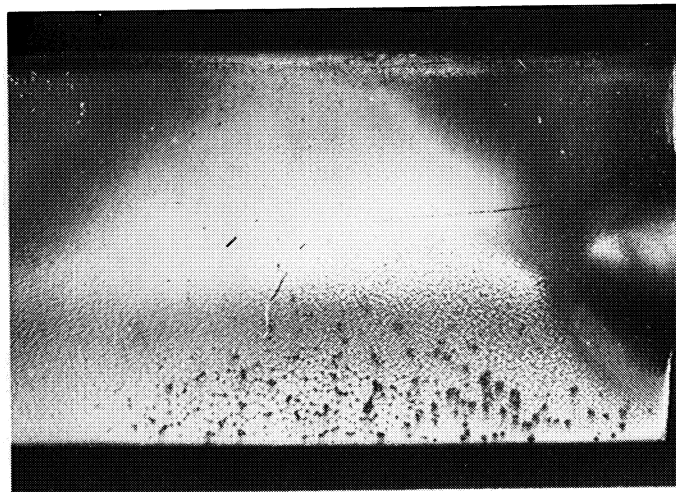
Figure 25 Compositions 9, 10, and 11 Coated Test Specimens After Burner Rig Testing for the Times Given (2X Magnification)



COMPOSITION 1 (Co-20Cr-12Al-0.5Y)  
SPECIMEN G4088B

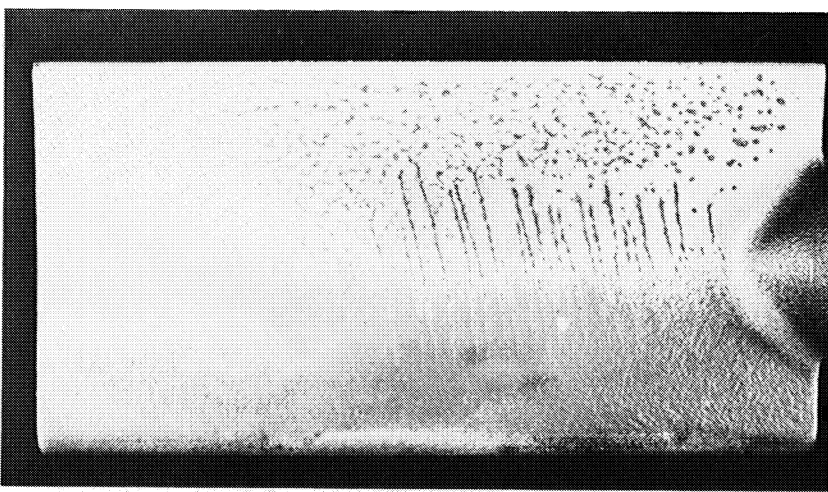


COMPOSITION 5 (Co-40Cr-20Al-0.5Y)  
SPECIMEN G4088N



COMPOSITION 7 (Co-25Cr-14Al-0.5Y)  
SPECIMEN G4092H

Figure 26 Convex Side of Compositions 1, 5, and 7 Coated Test Specimens After Burner Rig Testing  
for 1100 Hours (2X Magnification)



CONVEX SIDE,

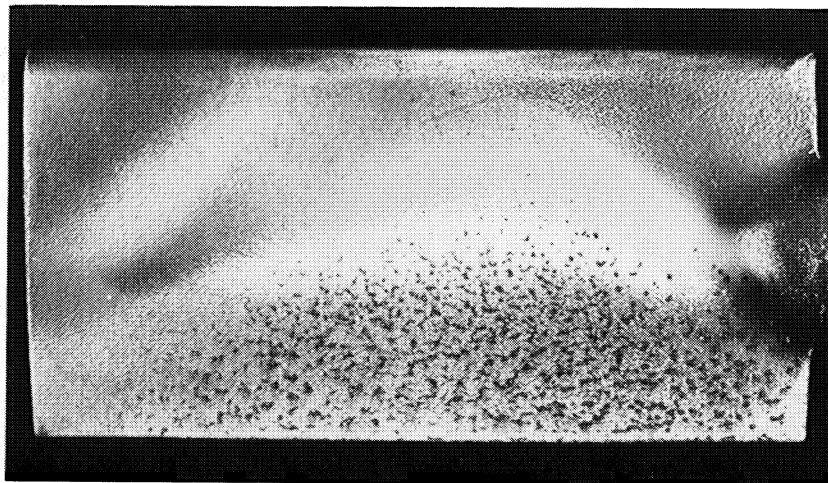
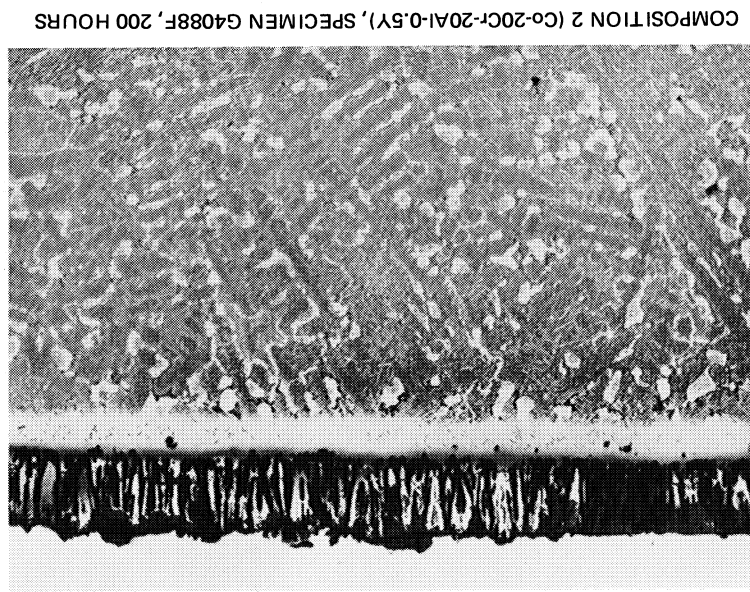
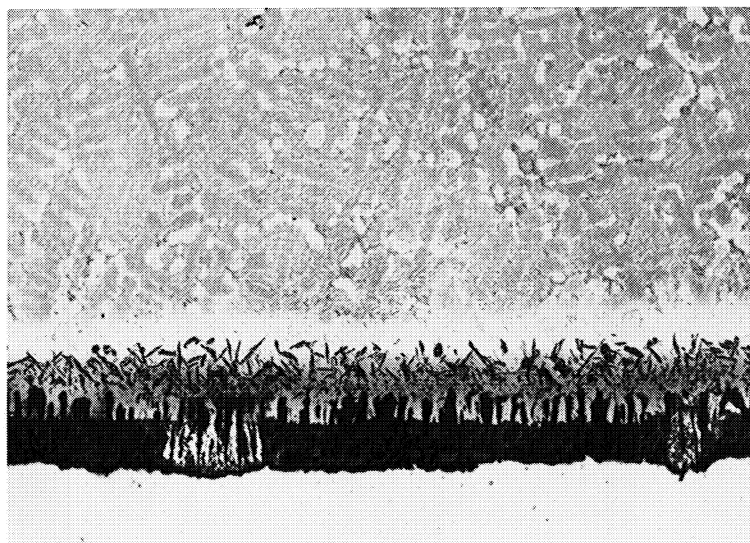


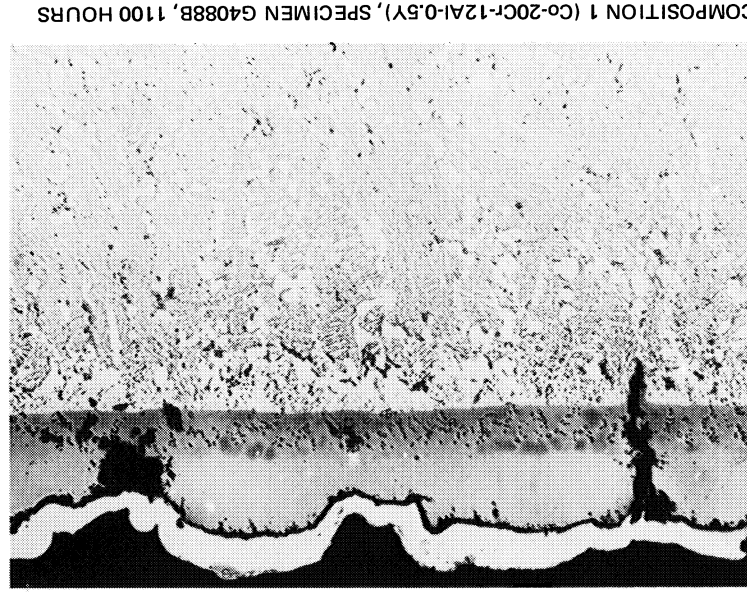
Figure 27      Composition 8 (Co-25Cr-14Al-0.9Y) Coated Test Specimen G4162P After Burner Rig  
Testing for 1100 Hours (2X Magnification)



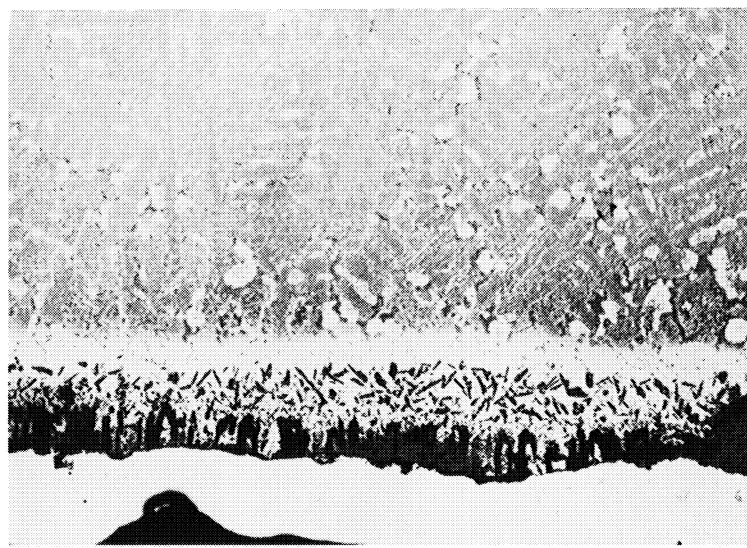
COMPOSITION 2 (Co-20Cr-20Al-0.5Y), SPECIMEN G4088F, 200 HOURS



COMPOSITION 3 (Co-30Cr-16Al-0.5Y), SPECIMEN G4088H, 251 HOURS

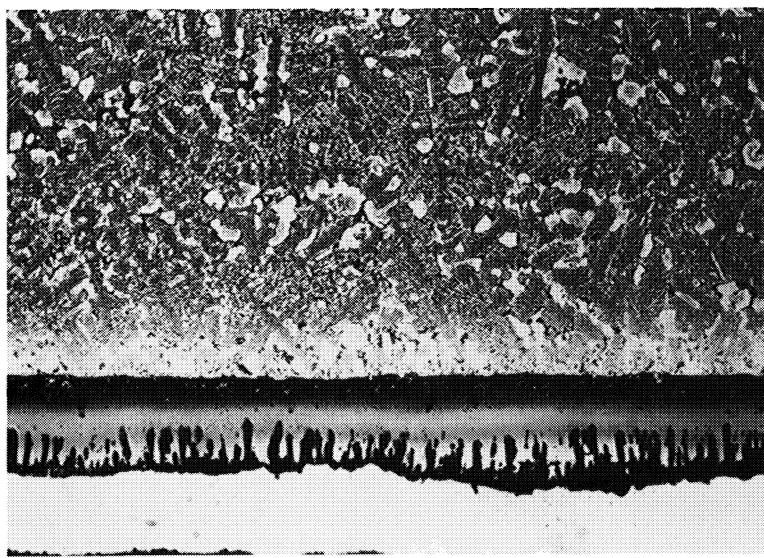


COMPOSITION 4 (Co-40Cr-12Al-0.5Y), SPECIMEN G4088L, 251 HOURS

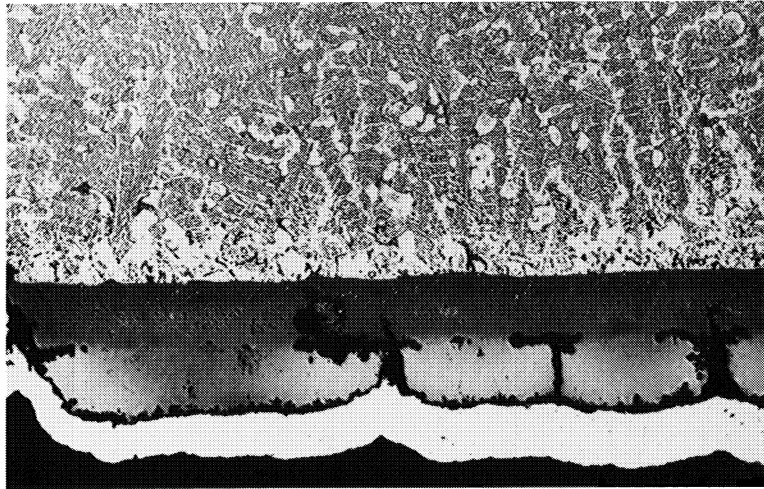


COMPOSITION 1 (Co-20Cr-12Al-0.5Y), SPECIMEN G4088B, 110 HOURS

Figure 28 Microstructures of Compositions 1, 2, 3, and 4 Coatings After Burmet Rig Testing for the Times Given (75X Magnification)

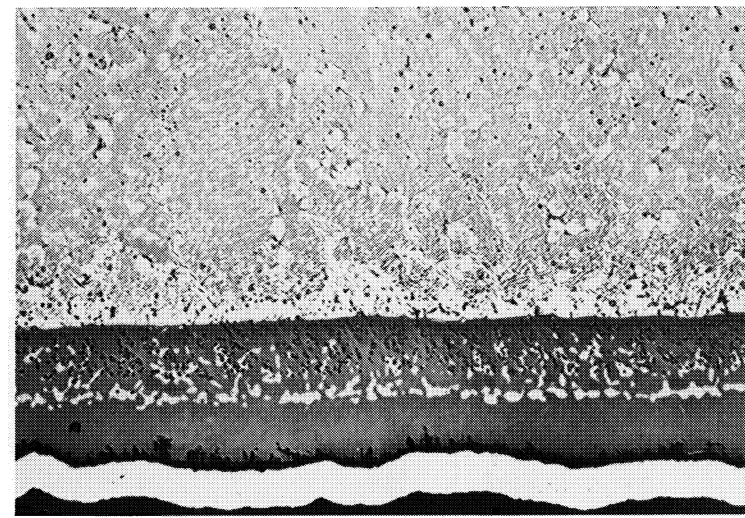


COMPOSITION 6 (Co-25Cr-16Al-0.5Y), SPECIMEN G4088S, 285 HOURS



COMPOSITION 7 (Co-25Cr-14Al-0.5Y), SPECIMEN G4092H, 1100 HOURS

COMPOSITION 8 (Co-25Cr-14Al-0.9Y), SPECIMEN G4162P, 1100 HOURS



COMPOSITION 5 (Co-40Cr-20Al-0.5Y), SPECIMEN G4088N, 1100 HOURS

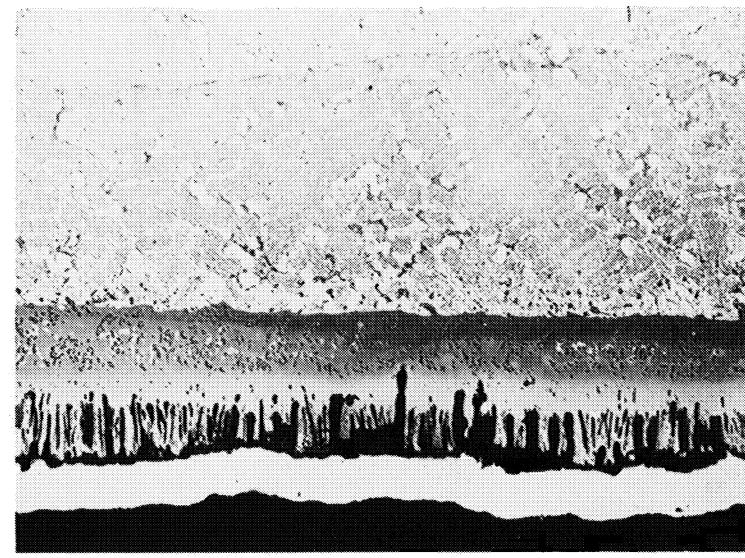


Figure 29 Microstructures of Compositions 5, 6, 7, and 8 Coatings After Burner Rig Testing for the Times Given (75X Magnification)

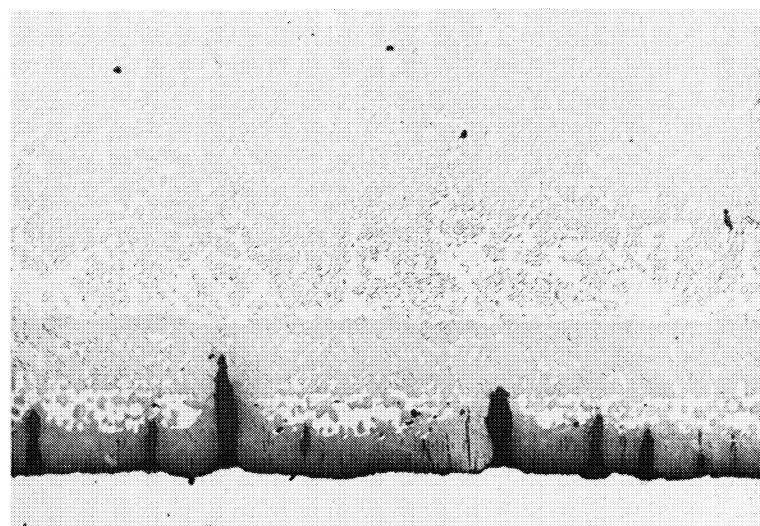
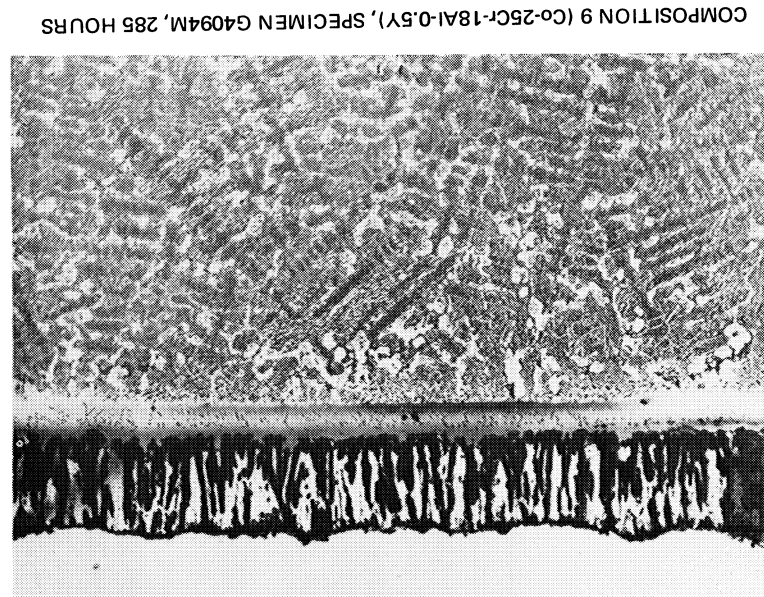
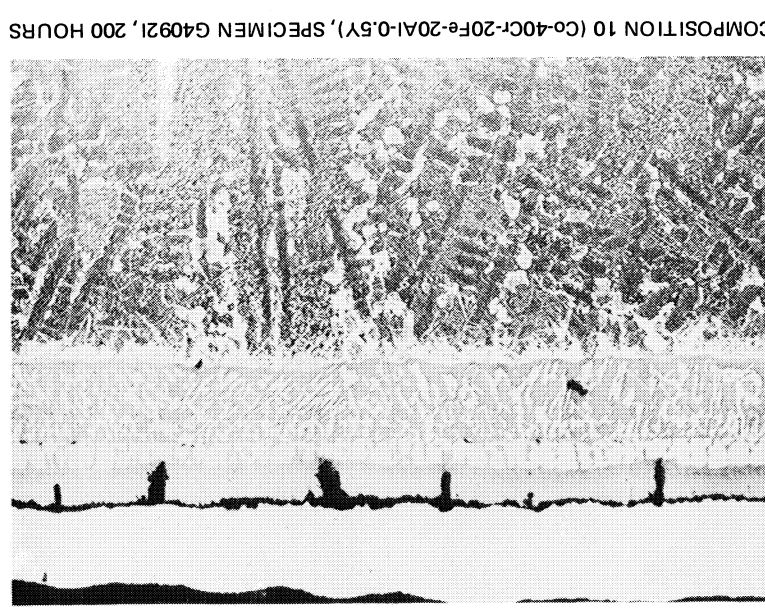


Figure 30 Microstructures of Compositions 9, 10, and 11 Coatings After Burner Rig Testing for the Times Given (75X Magnification)

C. DISCUSSION OF TEST RESULTS AND SELECTION OF COMPOSITIONS FOR  
CHARACTERIZATION BY TENSILE AND STRESS-TO-RUPTURE TESTS

A qualitative comparison, including ingot machining and coating processing, of the eleven coatings in burner rig testing is tabulated below by means of subjective ranking of the coatings by composition number.

<u>Ranking</u>	<u>Composition Number</u>	<u>Ingot Machining</u>	<u>Processing</u>	<u>Oxidation Resistance</u>
1	1,3,4,7		1,7	7
2	8		8	5
3	9		11,10	1,8
4	11		6,4*	11
5	6		9,3*,2*,5*	6
6	5			9
7	2			3,4
8	10			10,2

\* Compositions 2, 3, 4 and 5 not processed because of previous lack of success. They are ranked under processing here for comparative purposes.

As stated in Section III. C, the objective established in the coating modification program following ballistic impact and furnace oxidation testing was twofold: to improve oxidation resistance of Group A alloys with minimal compromise in ductility and to improve ductility of Group B alloys without impairing oxidation resistance. The first of these two goals was accomplished successfully with compositions 7 and 8. Compositions 10 and 11, which were modifications of composition 5 in Group B, were only partially successful. The substitution of nickel for cobalt (composition 11) improved ingot machinability and processability but impaired oxidation resistance significantly. The substitution of iron for cobalt (composition 10) effected slight improvement in processability but drastically reduced oxidation resistance.

Composition 7 was selected for further characterization by tensile and stress-to-rupture testing as being the best in all categories. Composition 1, despite its relatively poor behavior in furnace oxidation tests, was selected in favor of composition 8 because compositions 7 and 8 were too similar. There is no apparent explanation for the improved performance of composition 1 in burner rig tests over furnace oxidation tests. Compositions 1 and 7 (Co-20Cr-12Al-0.5Y and Co-25Cr-14Al-0.5Y respectively) provide a successful composition range which can be used to advantage if either composition were to prove deleterious from a mechanical properties standpoint.

## V. TENSILE AND STRESS-TO-RUPTURE TESTS

### A. PROGRAM

Two of the eleven coating compositions which had been burner rig tested were then evaluated for their effect upon the elevated-temperature tensile and stress-to-rupture properties of NASA-TRW VI-A nickel-base alloy. Uncotted specimens were tested for comparison purposes. Tensile tests were conducted at 1400° and 1800°F (1033° and 1255°K) and stress-to-rupture tests at 1800°F (1255°K). Duplicate specimens were tested in all cases; the specimens were 0.250 inch (6.35 mm) diameter round cast to size.

### B. SPECIMEN COATING AND HEAT TREATMENT

Twelve specimens were coated with compositions 1 and 7 (six specimens of each composition) using ingot material left from the coating of 1100-hour burner rig specimens. Sample plate analysis and calculated coating thickness for these specimens are shown in Table VI. Following coating processing, all coated and uncoated specimens were heat treated at  $1975^{\circ}\pm25^{\circ}$ F ( $1353^{\circ}\pm14^{\circ}$ K) for 4 hours in hydrogen, followed by cooling in hydrogen at a rate equal to or faster than air cool. All specimens were subsequently aged at 1600°F (1144°K) for 35 hours in argon.

TABLE VI  
CHEMICAL ANALYSIS OF TENSILE AND  
STRESS-TO-RUPTURE TEST SPECIMENS

Composition No.	Specimen No.	Composition (Weight %)			Calculated Thickness (mils)	Calculated Thickness (μm)
		Co	Cr	Al		
1	G4069A	Bal.	17.89	11.50	0.09	5.09
	G4069B		16.81	11.53	0.10	5.16
1	G4069C		16.82	11.45	0.12	4.71
	G4069D		17.94	11.40	0.12	4.90
1	G4070K		16.73	11.93	0.17	5.47
	G4070L		17.40	11.27	0.15	5.54
7	G4069E		21.53	12.98	0.21	4.92
	G4069G		22.22	12.73	0.22	5.52
7	G4069I		20.72	13.07	0.28	5.07
	G4069J		22.29	12.75	0.26	5.46
7	G4070M		21.81	12.76	0.19	5.20
	G4070N		21.51	12.69	0.17	5.05

### C. RESULTS AND CONCLUSIONS

Elevated-temperature tensile data are presented in Table VII. Visual inspection of tensile specimens after testing revealed that composition 7 underwent a ductile-to-brittle transition between 1400° and 1800°F (1033° and 1255°K). This was indicated by the presence of transverse coating cracks along the gauge section of the specimen tested at 1400°F (1033°K) and the absence of cracking at 1800°F (1255°K), as shown in Figure 31. Inspection after testing of specimens coated with composition 1 indicated that its ductile-to-brittle transition temperature lies below 1400°F (1033°K), as shown by the absence of coating cracks at 1400°F (1033°K) in Figure 32.

Results of stress-to-rupture testing are given in Table VIII. Visual inspection of tested specimens revealed no unusual conditions.

An analysis of all mechanical properties test results indicated that no significant difference existed between values obtained for uncoated compared to coated specimens. Compositions 1 and 7 were therefore judged to have not adversely affected the elevated-temperature tensile or stress-to-rupture properties of NASA-TRW VI-A alloy at the temperatures tested.

TABLE VII  
RESULTS OF ELEVATED TEMPERATURE TENSILE TESTING

Composition No.	Test Specimen No.	Test Temp. (°F)	Temp. (°K)	0.02% Yield Strength (ksi)	0.02% Yield Strength (MN/m <sup>2</sup> )	0.20% Yield Strength (ksi)	0.20% Yield Strength (MN/m <sup>2</sup> )	Ultimate Tensile Strength (ksi)	Ultimate Tensile Strength (MN/m <sup>2</sup> )	Room Temperature % Elongation	% Reduction in Area
*	G4069H	1400	1033	100.2	691	129.4	892	142.0	979	2.0	6.26
*	G4069K	1400	1033	104.2	718	130.6	900	155.7	1074	**	4.59
1	G4069A	1400	1033	104.2	718	132.0	910	157.9	1090	2.7	6.12
1	G4069D	1400	1033	113.2	780	135.7	936	162.0	1117	3.5	6.85
7	G4069E	1400	1033	118.9	820	141.8	978	161.5	1114	3.1	3.92
7	G4069J	1400	1033	116.0	800	136.8	943	146.3	1009	2.4	5.40
*	G4069L	1800	1255	54.5	376	72.5	500	92.5	638	2.1	4.59
*	G4070J	1800	1255	52.8	364	74.7	515	93.2	643	3.3	4.13
1	G4069B	1800	1255	47.3	326	67.3	484	84.1	580	2.5	3.69
1	G4069C	1800	1255	59.5	410	77.8	536	91.9	634	2.0	2.17
7	G4069G	1800	1255	50.3	347	70.3	485	81.7	563	1.2	2.14
7	G4069I	1800	1255	54.9	379	76.9	530	94.4	651	2.0	4.66

\* Uncoated.

\*\* No gauge marks.

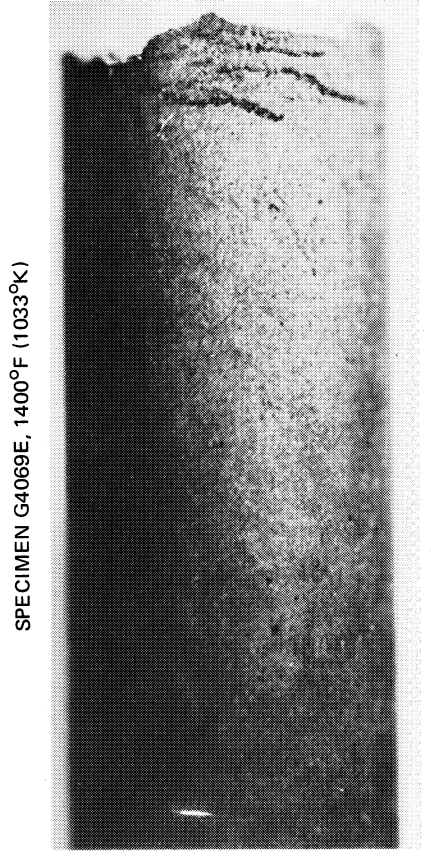
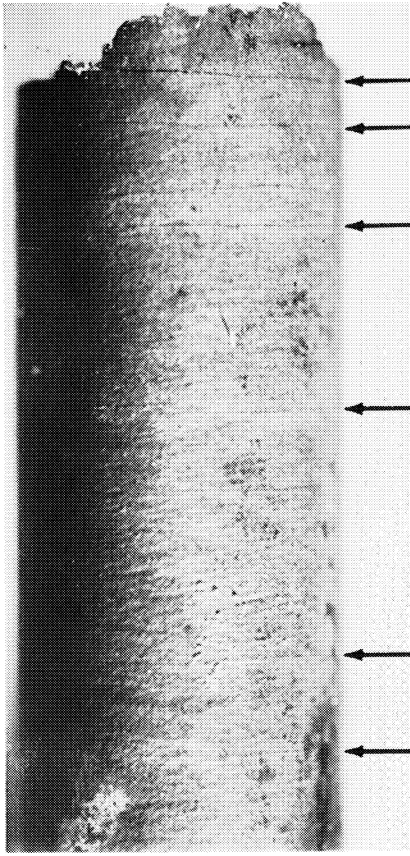


Figure 31

Composition 7 (Co-25Cr-14Al-0.5Y) Coated Test Specimens After Tensile Testing at the Temperatures Given (8X Magnification). Transverse coating cracks on the 1400°F (1033°K) specimen are identified by the arrows.

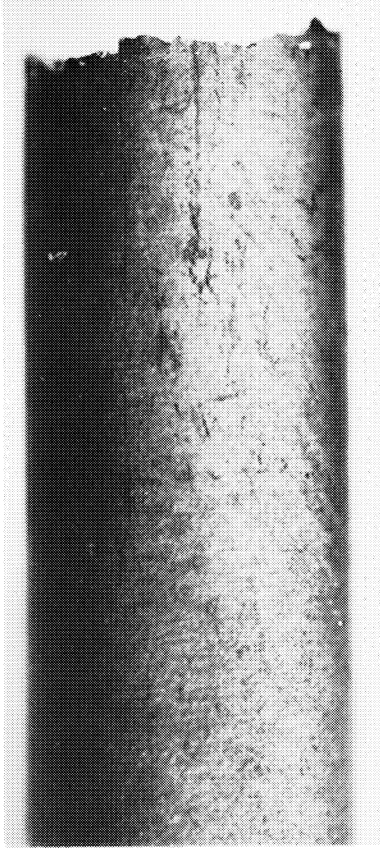


Figure 32

Composition 1 (Co-20Cr-12Al-0.5Y) Coated Test Specimen G4069D After 1400°F (1033°K) Tensile Testing (8X Magnification). No cracks are present in the coating.

TABLE VIII  
RESULTS OF STRESS-TO-RUPTURE TESTING AT  
1800°F (1255°K) WITH A STRESS OF 29,000 PSI (200 MN/m<sup>2</sup>)

Composition No.	Specimen No.	Time to Rupture (hours)			Room Temperature	Elongation %	Reduction of Area %
		58.4	51.9	46.1			
*	G4070O	58.4	51.9	46.1	2.93	4.11	4.11
*	G4070P				6.80	6.94	6.94
1	G4070K				4.71	6.11	6.11
1	G4070L				4.18	6.75	6.75
7	G4070M	76.7	49.3	49.3	3.38	5.17	5.17
7	G4070N				3.64	3.86	3.86

\*Uncoated.

## VI. ANALYTICAL CHARACTERIZATION OF COATINGS

### A. X-RAY DIFFRACTION ANALYSIS

Phases present at the surfaces of the Co-Cr-Al-Y coated specimens were identified by x-ray diffraction on representative test specimens of each composition prior to test and on burner rig test specimens after test. Analyses conducted following test were performed on surfaces immediately adjacent to the failure site, or on areas of high distress on unfailed specimens. The results are presented in Table IX for untested specimens and in Table X for tested specimens.

No meaningful correlations could be made concerning coating life as a function of metallic phases present prior to test. All specimens had major amounts of  $\beta$ CoAl present. After test, all specimens had major or minor amounts of  $\alpha$  Al<sub>2</sub>O<sub>3</sub>, Co<sub>3</sub>O<sub>4</sub>, and Co (solid solution) in common at the surface. None of the specimens had formed oxides involving chromium, indicating that chromium does not participate in the oxidation reactions at the surface. Aluminum is selectively oxidized, forming the protective oxide Al<sub>2</sub>O<sub>3</sub>. Specimens which had failed early generally had major amounts of Co<sub>3</sub>O<sub>4</sub> present in the scale. All specimens had major or minor amounts of Co (solid solution) present at the surface after test.

TABLE IX  
PHASES PRESENT ON COATING ALLOY SURFACES PRIOR TO TEST

Composition No.	Specimen No.	Phases Identified				$\frac{\beta\text{CoAl}(110)}{\text{Solid Sol'n}}/\text{Co}$	Intensity Ratio $\frac{\beta\text{CoAl}(110)}{\text{Solid Sol'n}}$
		$\beta$ CoAl	$\delta$ Co(Solid Sol'n)	$\alpha$ Al <sub>2</sub> O <sub>3</sub>	$\sigma$ CrCo		
1	--	Major	Major	--	--	--	--
2	--	Major	--	Minor	--	--	100/0
3	--	Major	--	Minor	Minor	--	100/0
4	--	Major	--	Trace	Minor	--	100/0
5	--	Major	--	Trace	--	--	100/0
6	G4092T	Major	Major	Minor	--	Trace Indication	--
7	G4092K*	Major	Major	--	Trace	--	100/150
7	G4092K*	Major	Major	--	--	Trace Indication	--
8	G4092Q	Major	Minor	--	Trace Indication	--	100/160
8	G4092Q*	Major	Major	Trace	Trace	--	100/99
9	G4092M	Major	Major	--	--	Trace Indication	--
9	G4092M*	Major	Minor	--	--	--	100/41
10	G4161E	Major	Major	Trace	--	Trace	100/6
10	G4161E*	Major	--	--	--	--	100/0
11	G4092S	Major	--	--	--	--	100/183
11	G4092S*	Major	--	--	--	--	100/42
						--	100/111
						--	100/0
						--	100/0
						--	100/0

\*Specimen lightly sanded.

TABLE X  
PHASES PRESENT ON COATING ALLOY SURFACES  
AFTER BURNER RIG TEST

Compo- sition No.	Specimen No. G4088B	Test Time (hours)	Phases Identified			Trace	Indication
			Major	Minor			
1	G4088B	1100	$\alpha\text{Al}_2\text{O}_3,\text{Co}(\text{Sol}.\text{Sol}'\text{n})$	$\text{Co}_3\text{O}_4$			$\text{YAlO}_3$
2	G4088F	200	$\alpha\text{Al}_2\text{O}_3,\text{Co}_3\text{O}_4$	$\text{Co}(\text{Sol}.\text{Sol}'\text{n})$		--	$\text{YAlO}_3$
3	G4088H	251	$\text{Co}_3\text{O}_4,\text{Co}(\text{Sol}.\text{Sol}'\text{n})$	$\alpha\text{Al}_2\text{O}_3$		--	$\text{YAlO}_3$
4	G4088L	251	$\text{Co}_3\text{O}_4,\text{Co}(\text{Sol}.\text{Sol}'\text{n})$	$\alpha\text{Al}_2\text{O}_3$		--	--
5	G4088N	1100	$\text{Co}_3\text{O}_4,\text{Co}(\text{Sol}.\text{Sol}'\text{n})$	$\alpha\text{Al}_2\text{O}_3$		--	$\text{YAlO}_3$
6	G4088S	285	$\text{Co}_2\text{O}_4$	$\alpha\text{Al}_2\text{O}_3,\text{Co}(\text{Sol}.\text{Sol}'\text{n})$		--	$\text{YAlO}_3$
7	G4092H	1100	$\alpha\text{Al}_2\text{O}_3,\text{Co}(\text{Sol}.\text{Sol}'\text{n})$	$\text{Co}_3\text{O}_4$		--	--
8	G4162P	1100	$\text{Co}(\text{Sol}.\text{Sol}'\text{n})$	$\alpha\text{Al}_2\text{O}_3,\text{Co}_3\text{O}_4$		$\text{Al}_2\text{Y}_4\text{O}_9$	--
9	G4092M	285	$\alpha\text{Al}_2\text{O}_3,\text{Co}_3\text{O}_4,\text{Co}(\text{Sol}.\text{Sol}'\text{n})$	--		--	--
10	G4092I	200	$\text{Co}(\text{Sol}.\text{Sol}'\text{n}),\text{CoFe}_2\text{O}_4$	$\alpha\text{Al}_2\text{O}_3,\text{Co}_3\text{O}_4$	$\sigma(\text{Fe},\text{Co})\text{Cr}$	$\text{YAlO}_3$	
11	G4092B	609	$\alpha\text{Al}_2\text{O}_3$	$\text{Co}_3\text{O}_4,\text{Co}(\text{Sol}.\text{Sol}'\text{n})$	$(\text{Ni},\text{Co})\text{O}^\bullet$	$\sigma\text{CoCr}$	$(\text{Ni},\text{Co})_3\text{O}_4$

### B. ELECTRON MICROPROBE ANALYSIS

Electron microprobe analysis was performed on sections through each coating on representative samples prior to test (Figures 33 through 41) and on samples which had been tested in the burner rig test (Figures 42 through 52). Concentration profiles were made across the coating and into the substrate by translating the specimen beneath the electron beam while simultaneously recording x-ray intensity. These profiles were transposed to one or two charts for each specimen and correlated with a photomicrograph showing the precise area examined. Chemical compositions are indicated at several key locations on each profile. Although a profile for yttrium was run on each specimen, it was not shown on the composite profile unless it showed significant changes occurring across the coating. A generalized summary of microprobe results is presented in Table XI, in which chemical compositions for the outer layers of the coating are listed. The numbers given are not accurate representations of coating composition but are representative of actual coating compositions.

No specific conclusions could be drawn relative to coating life and chemistry. The format of this program did not lend itself well to an analytical approach to determination of the role of each of the constituents in the coatings. For an example, the differing lengths of exposure time for each composition studied precluded the determination of such things as depletion rate of aluminum and microstructural change as a function of time. Substantial microstructural differences due to process variation rather than compositional variation obscured the role that composition played in coating life. Further, the scope of the program did not permit a more complete analysis.

The longer lived coatings generally had higher amounts of aluminum retained in the outer portion of the coating despite the much longer exposure times. Analysis results indicate that formation of NiAl in a diffusion zone at the coating-basis interface occurred during burner rig tests for all specimens. The chromium content of all specimens remained relatively unchanged during the course of testing, indicating low mobility of chromium in this coating system. Tungsten and tantalum were present in insignificant amounts in the outer layers of all the coatings. Compositions 1 and 7 had fine, evenly distributed two-phase microstructures prior to test, one phase being chromium rich and aluminum poor, while the other phase was aluminum rich and chromium poor. The coatings studied appeared to have degraded by loss of aluminum through consumption to form  $\text{Al}_2\text{O}_3$  at the surface and through diffusion into the substrate. Chromium apparently played a passive role in the oxidation process in the compositional range studied. The small amounts of yttrium present in the oxide scale after test indicate an active participation of yttrium in the formation of the protective scale.

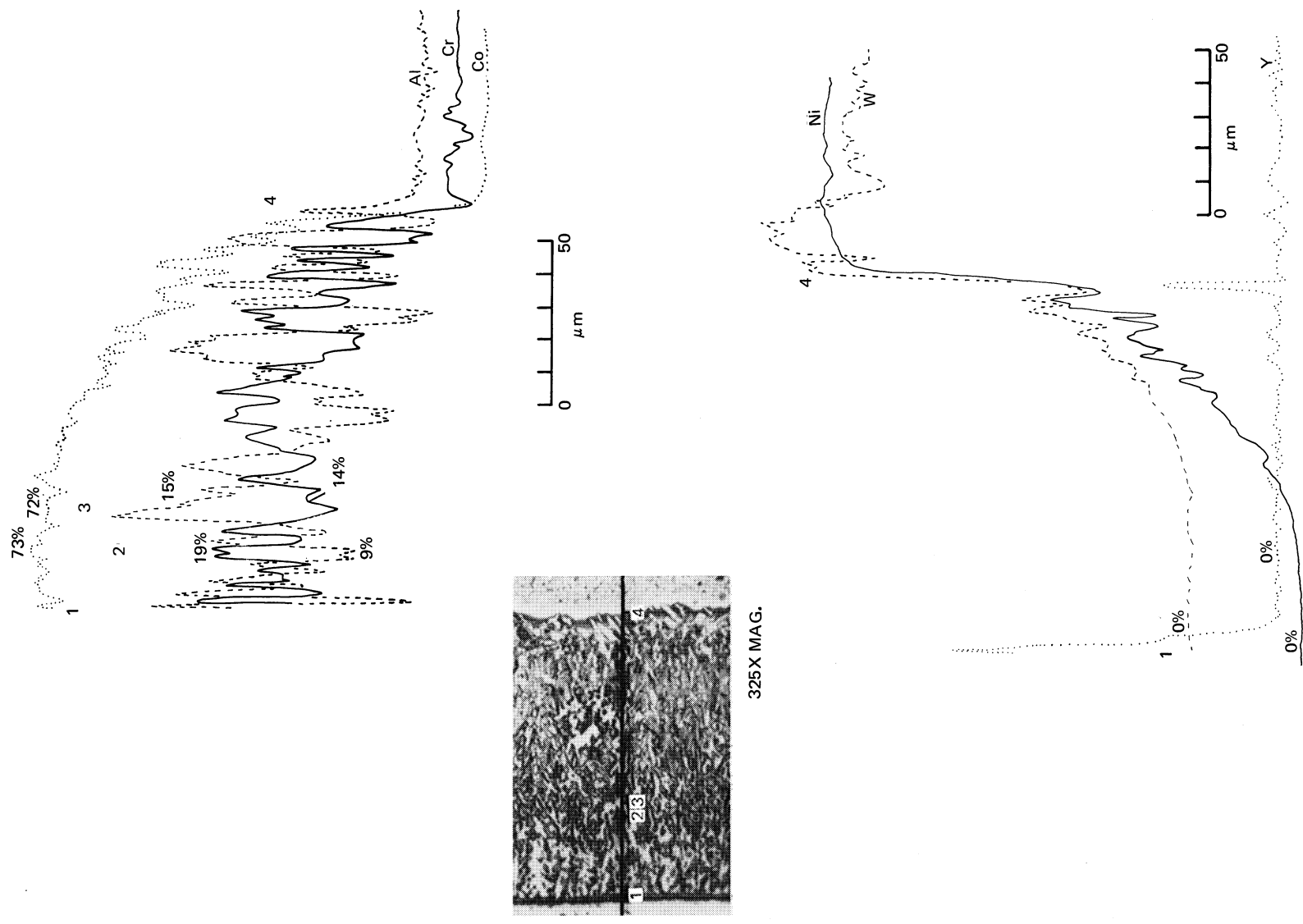


Figure 33 Electron Microprobe Analysis of Composition 1 (Co-20Cr-12Al-0.5Y) Coating  
(Specimen 271) Prior to Test

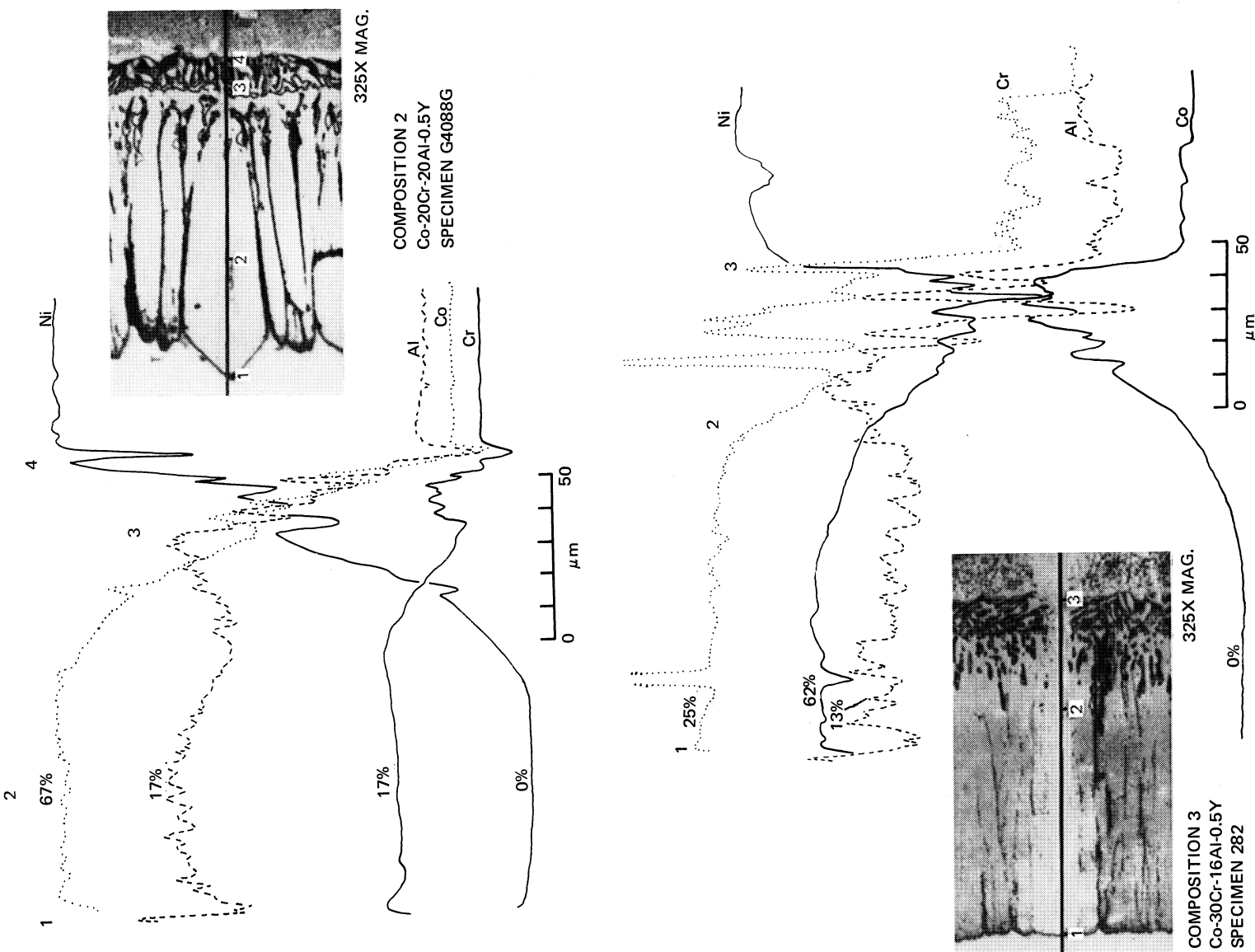


Figure 34 Electron Microprobe Analyses of Compositions 2 (Top) and 3 (Bottom) Coatings Prior to Test

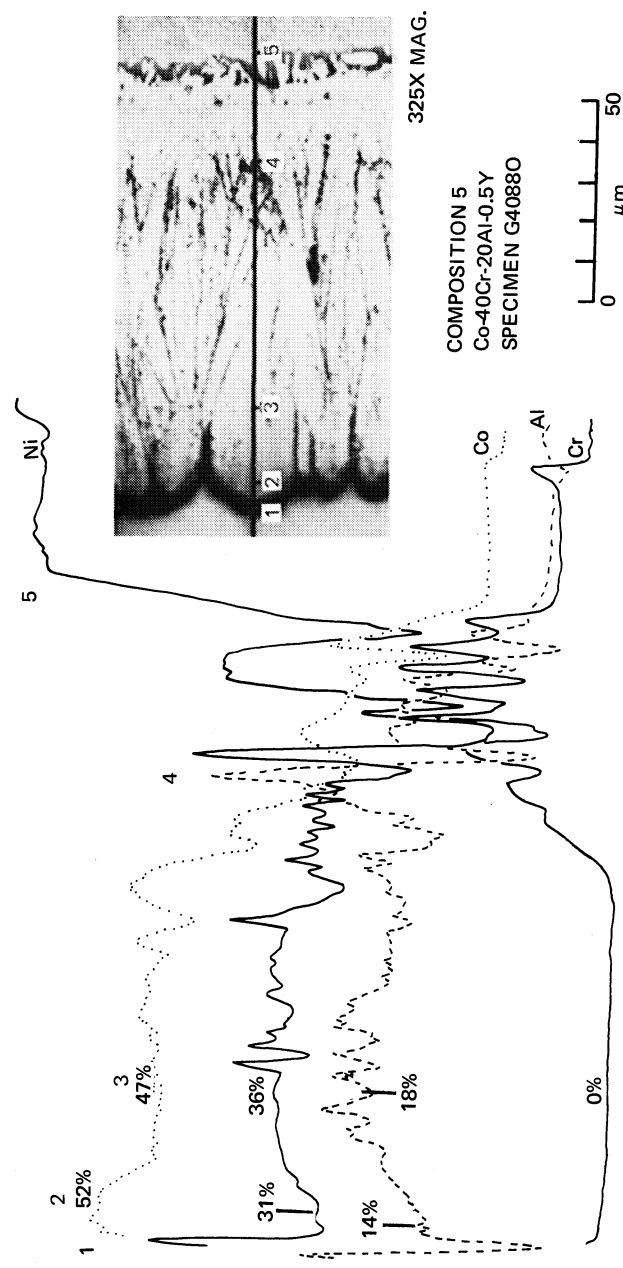
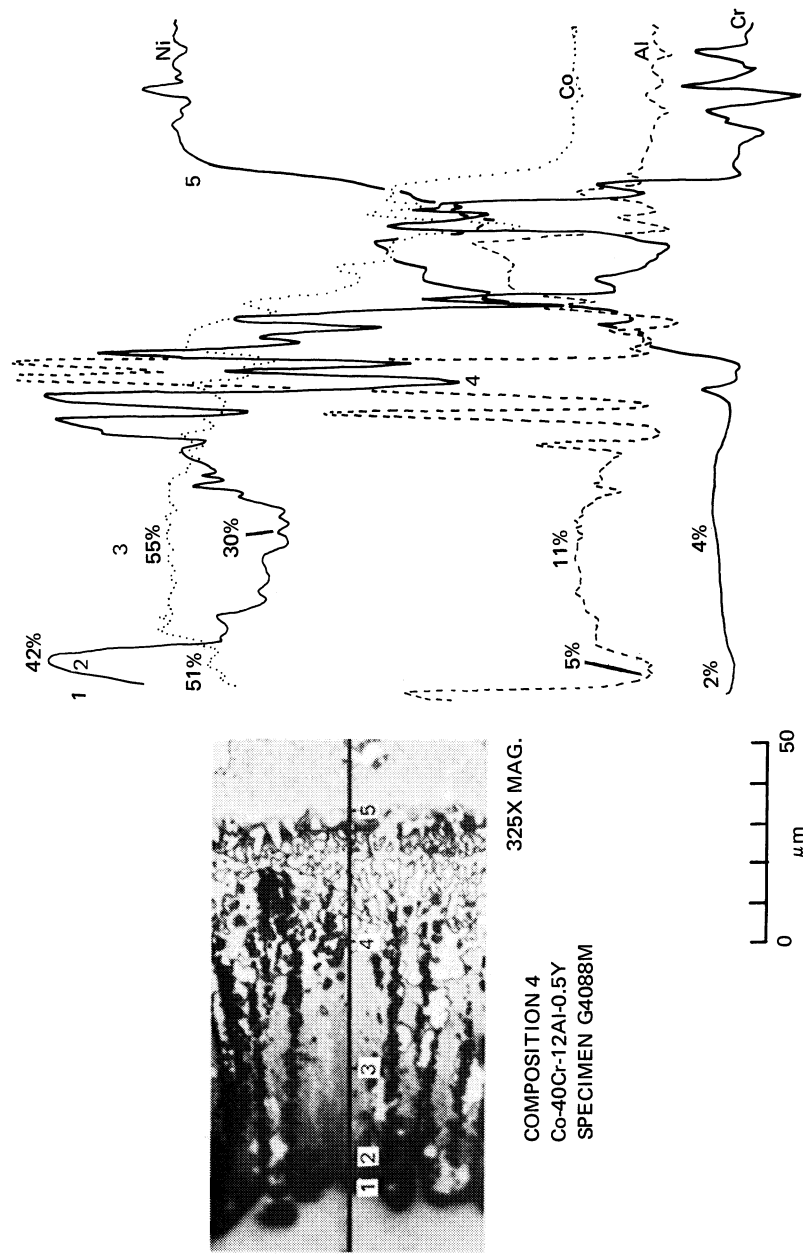


Figure 35 Electron Microprobe Analyses of Compositions 4 (Top) and 5 (Bottom) Coatings Prior to Test

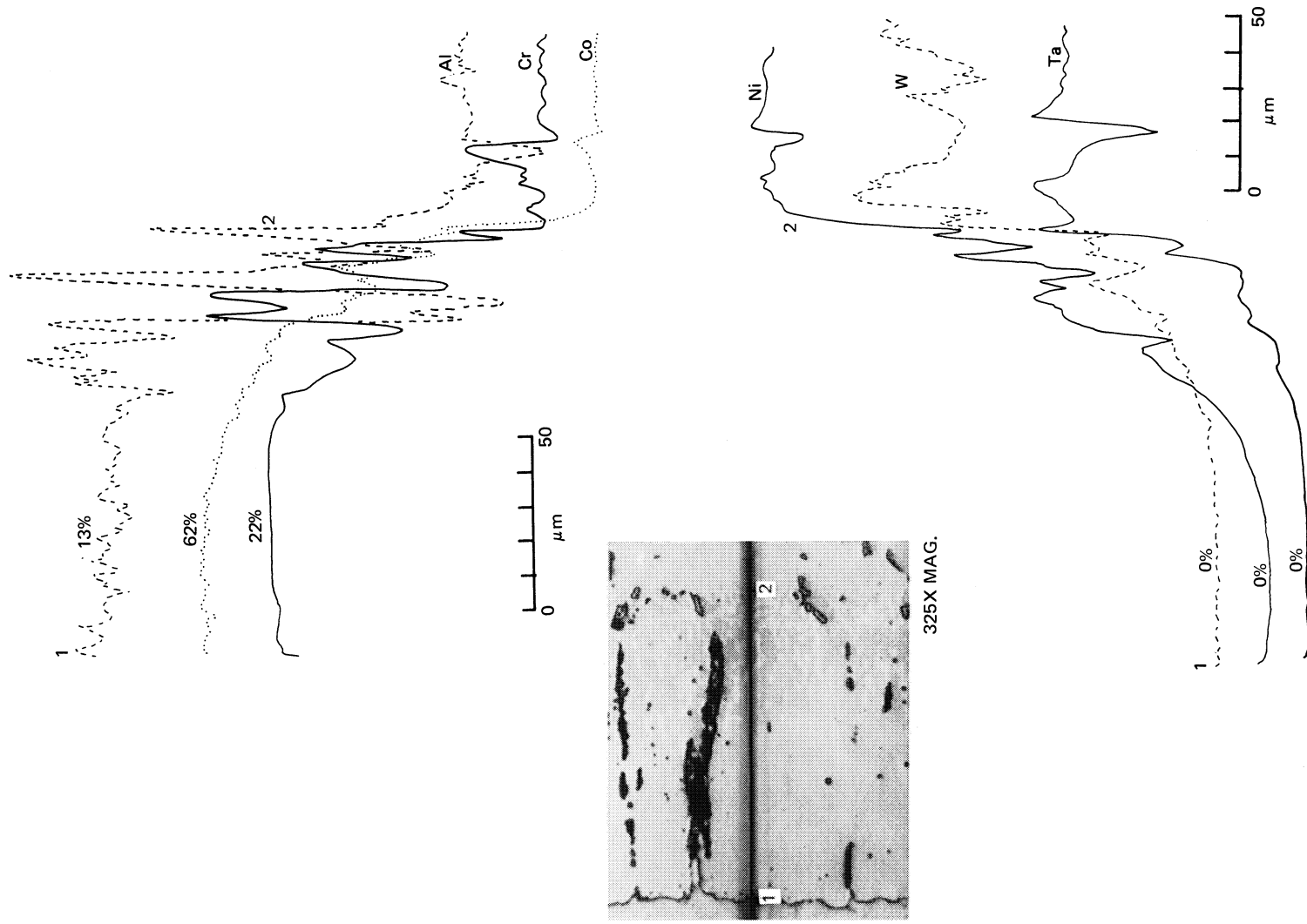


Figure 36 Electron Microprobe Analysis of Composition 6 (Co-25Cr-16Al-0.5Y) Coating  
(Specimen G4092T) Prior to Test

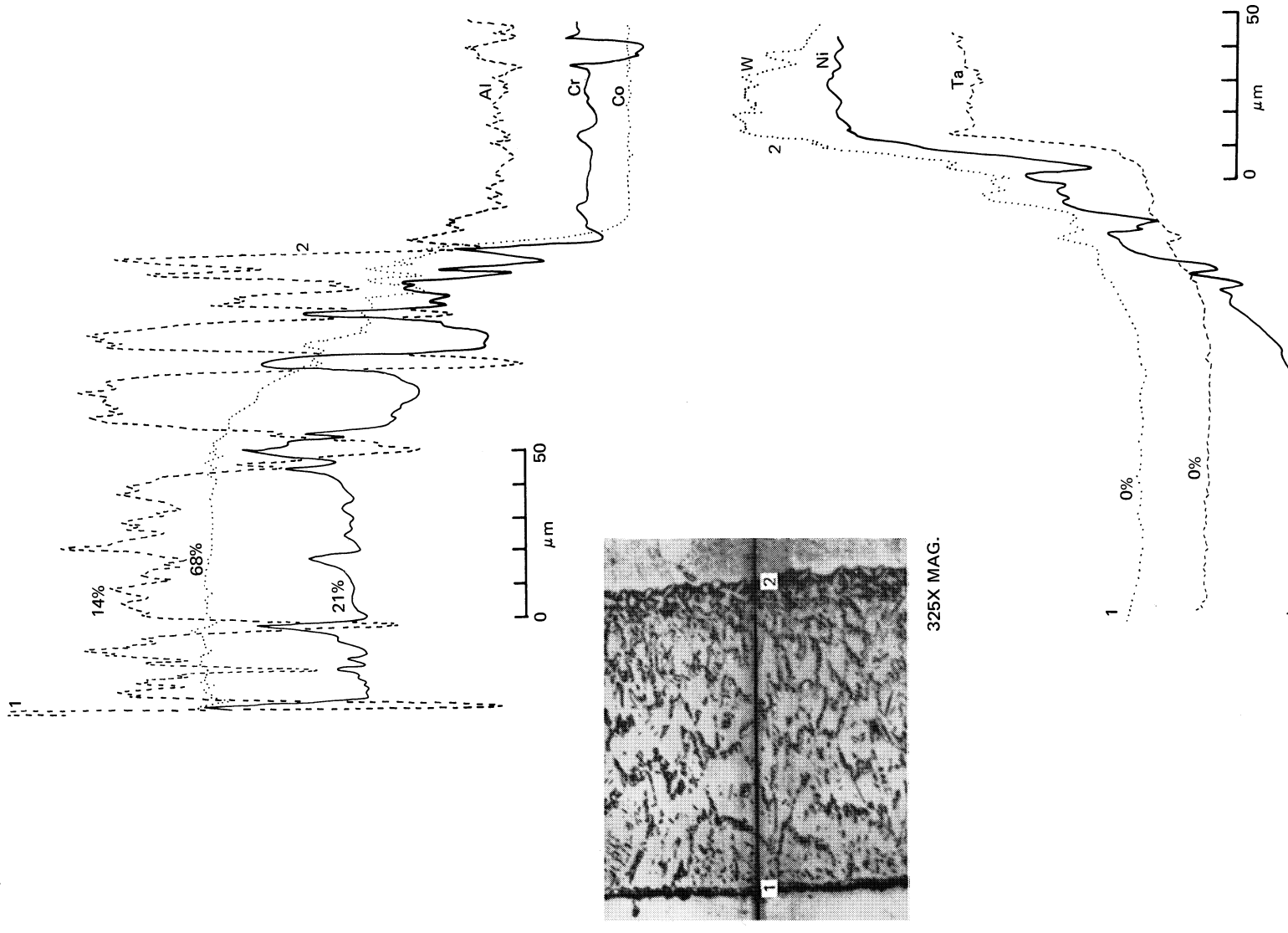


Figure 37 Electron Microprobe Analysis of Composition 7 (Co-25Cr-14Al-0.5Y) Coating  
(Specimen G4092K) Prior to Test

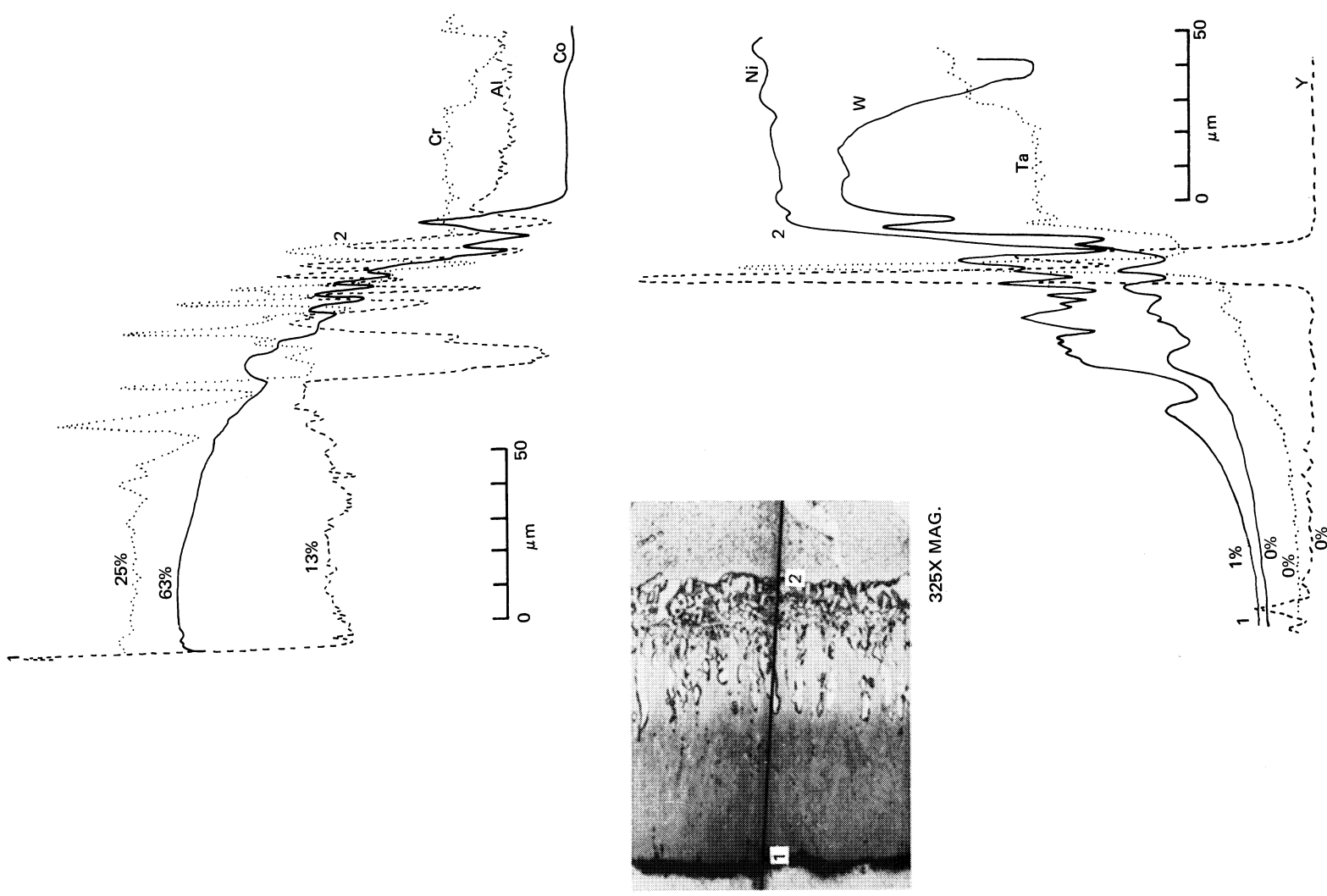


Figure 38 Electron Microprobe Analysis of Composition 8 (Co-25Cr-14Al-0.9Y) Coating (Specimen G4092Q) Prior to Test

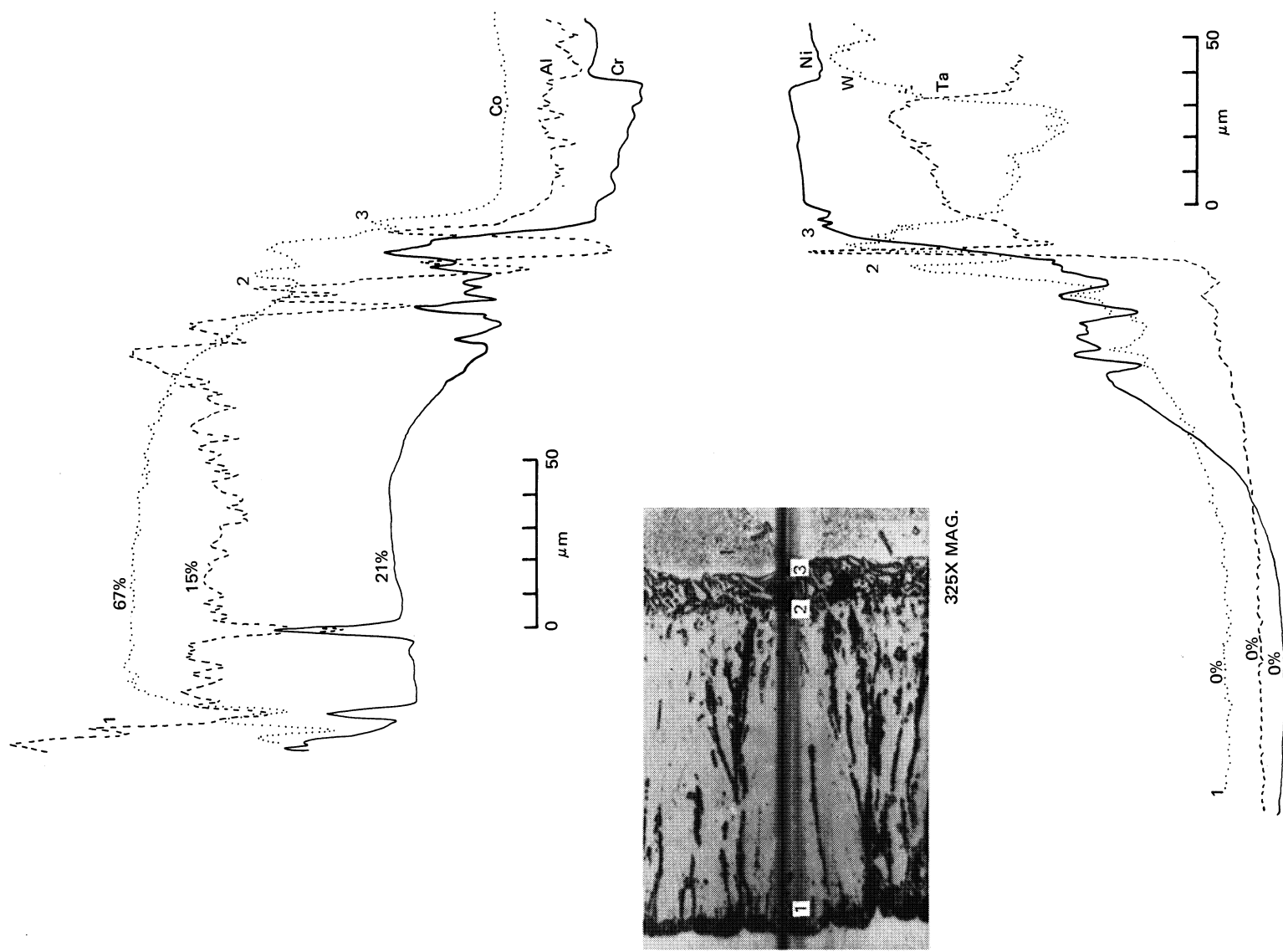


Figure 39  
Electron Microprobe Analysis of Composition 9 (Co-25Cr-18Al-0.5Y) Coating  
(Specimen G4092M) Prior to Test

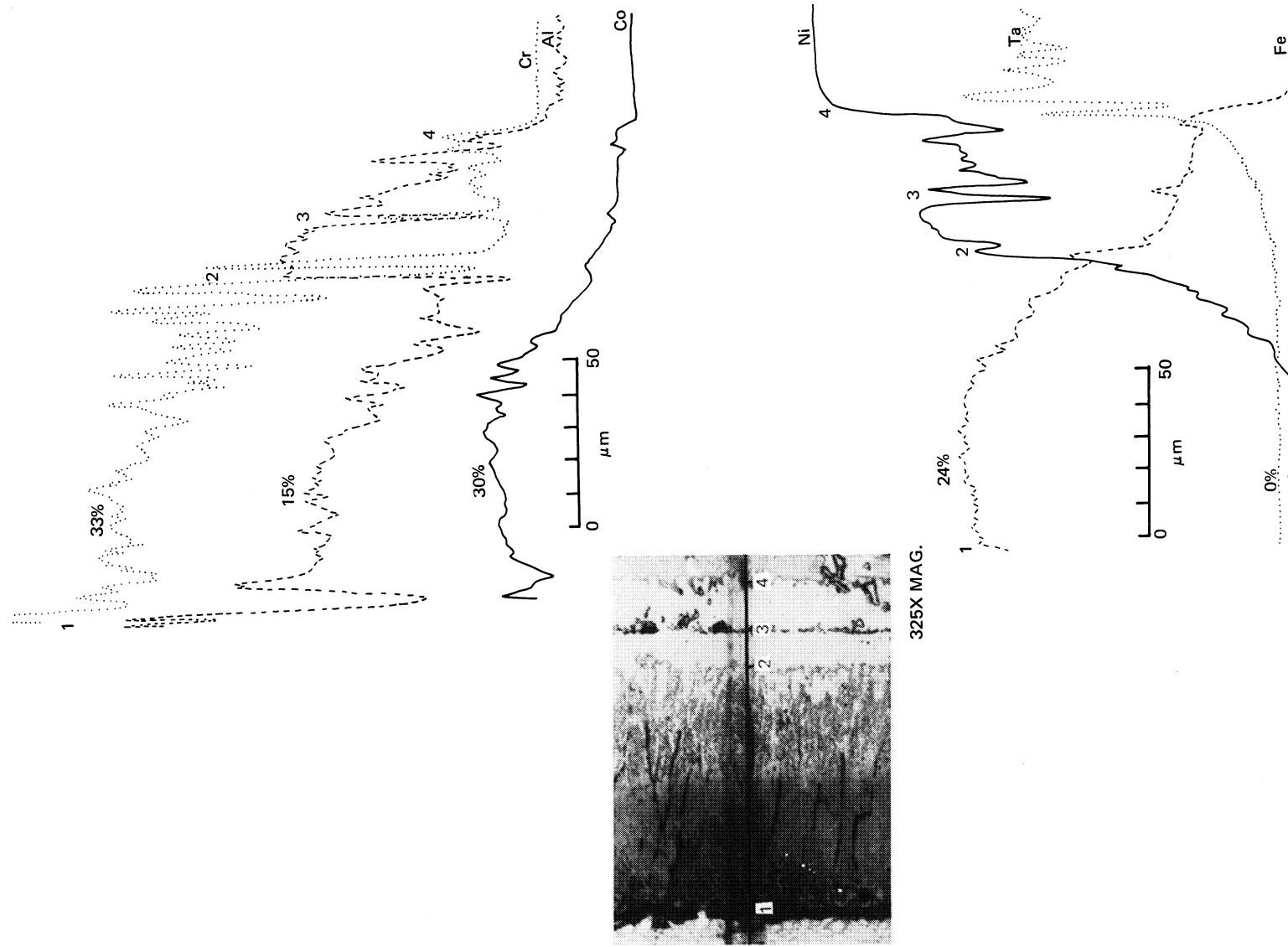


Figure 40

Electron Microprobe Analysis of Composition 10 (Co-40Cr-20Fe-20Al-0.5Y) Coating  
(Specimen G4161E) Prior to Test

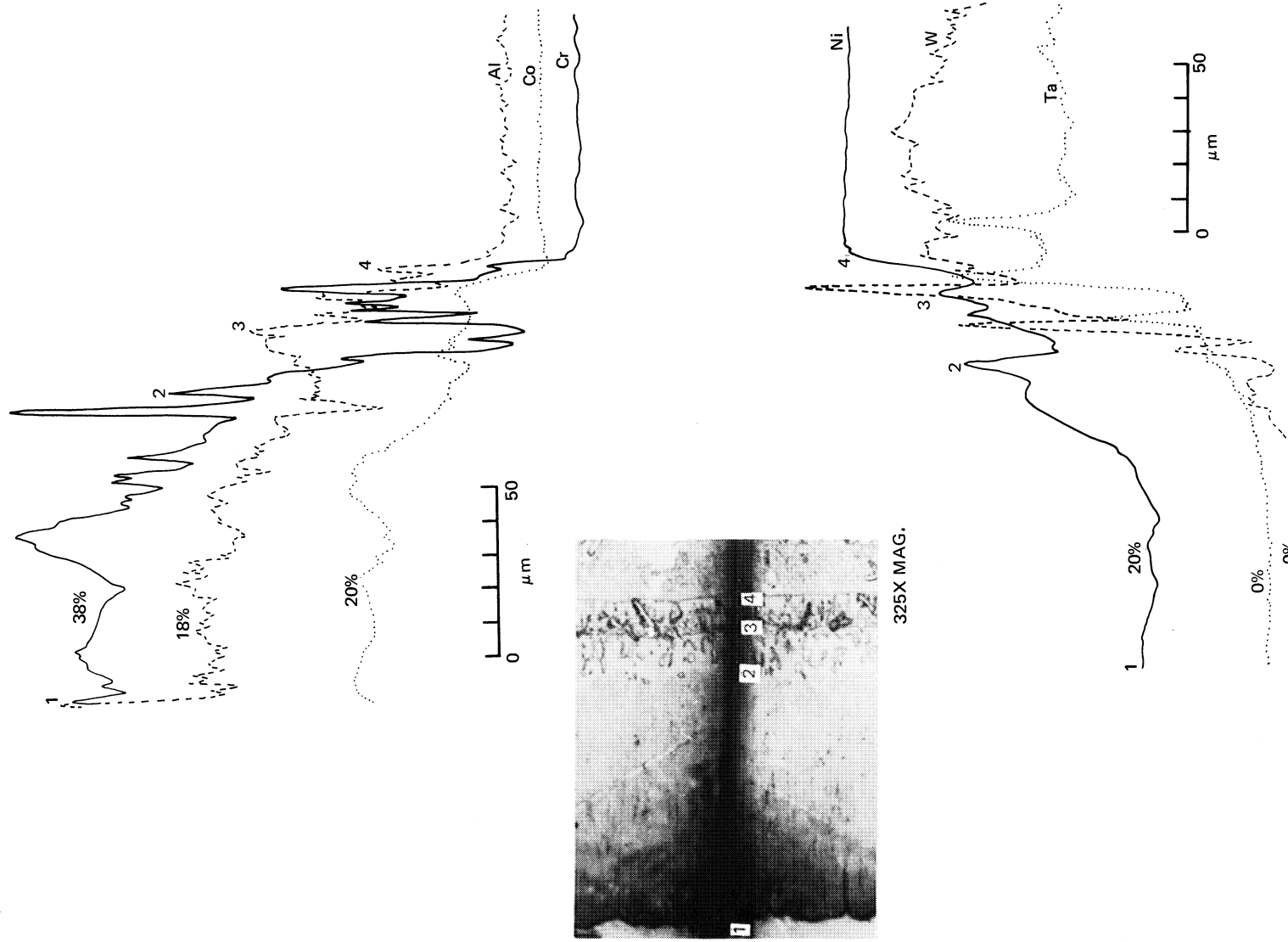


Figure 41 Electron Microprobe Analysis of Composition 11 (Co-40Cr20Ni20Al10.5Y) Coating  
(Specimen G4092S) Prior to Test

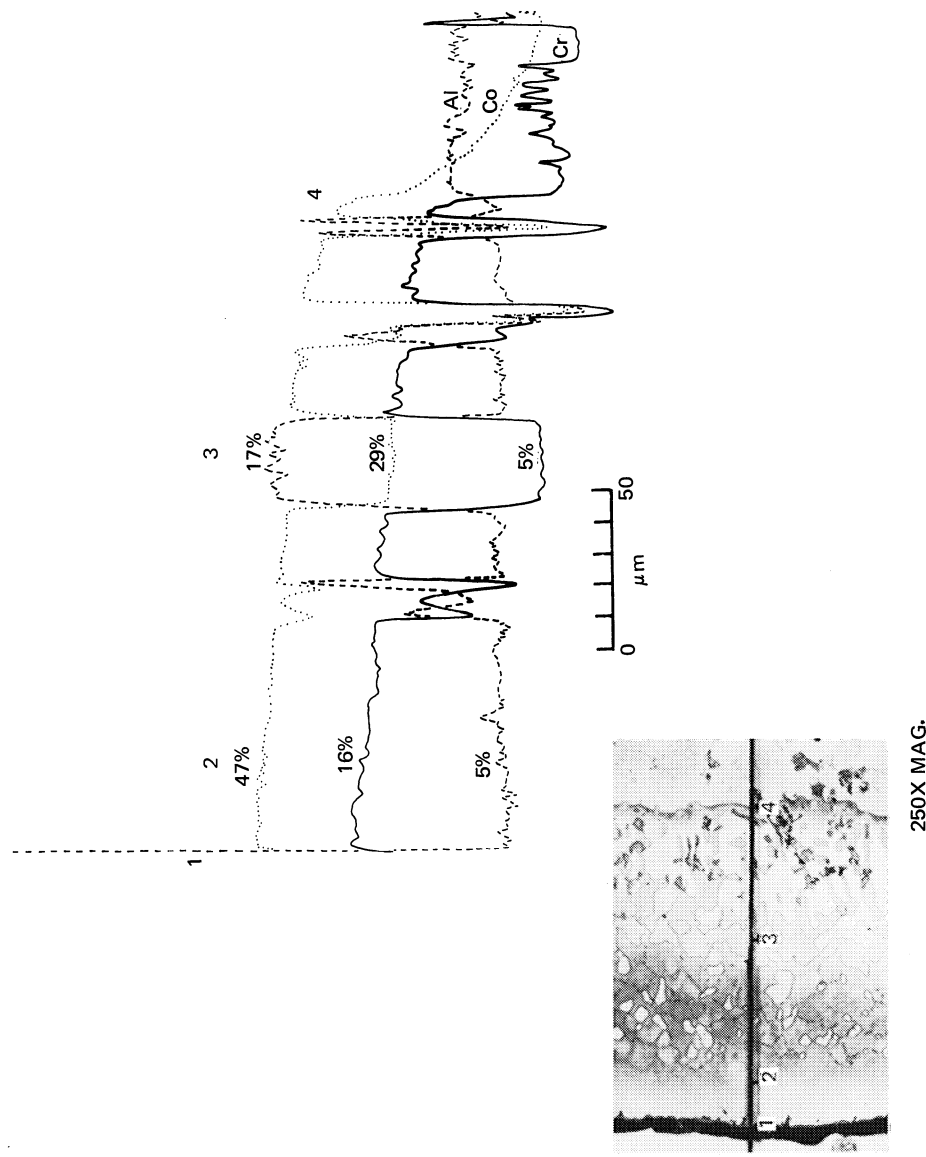


Figure 42 Electron Microprobe Analysis of Composition 1 (Co-20Cr-12Al-0.5Y) Coating (Specimen G4088B) After 1100 Hours of Burner Rig Testing

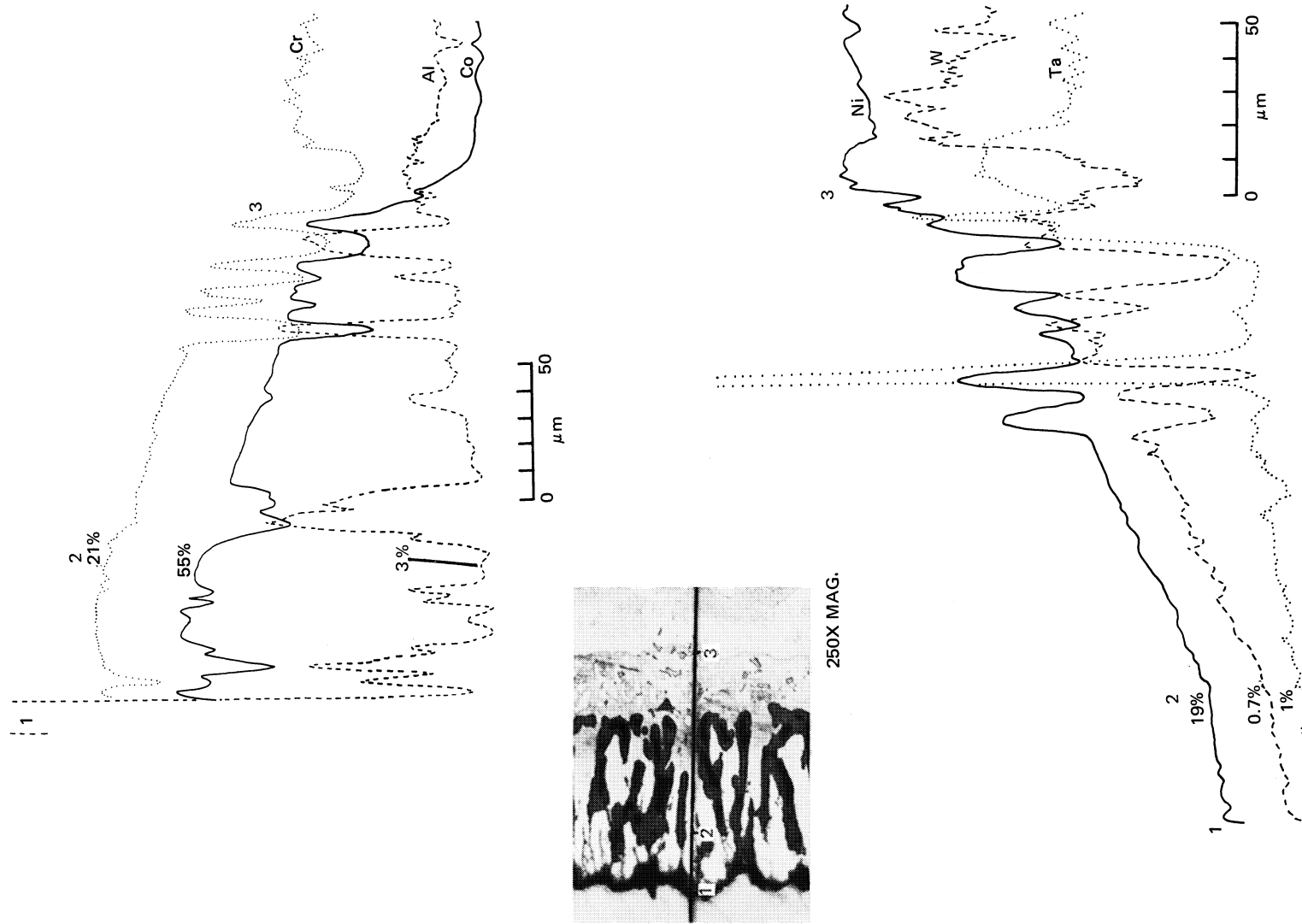


Figure 43  
Electron Microprobe Analysis of Composition 2 (Co-20Cr-20Al-0.5Y) Coating  
(Specimen G4088F) After 200 Hours of Burner Rig Testing

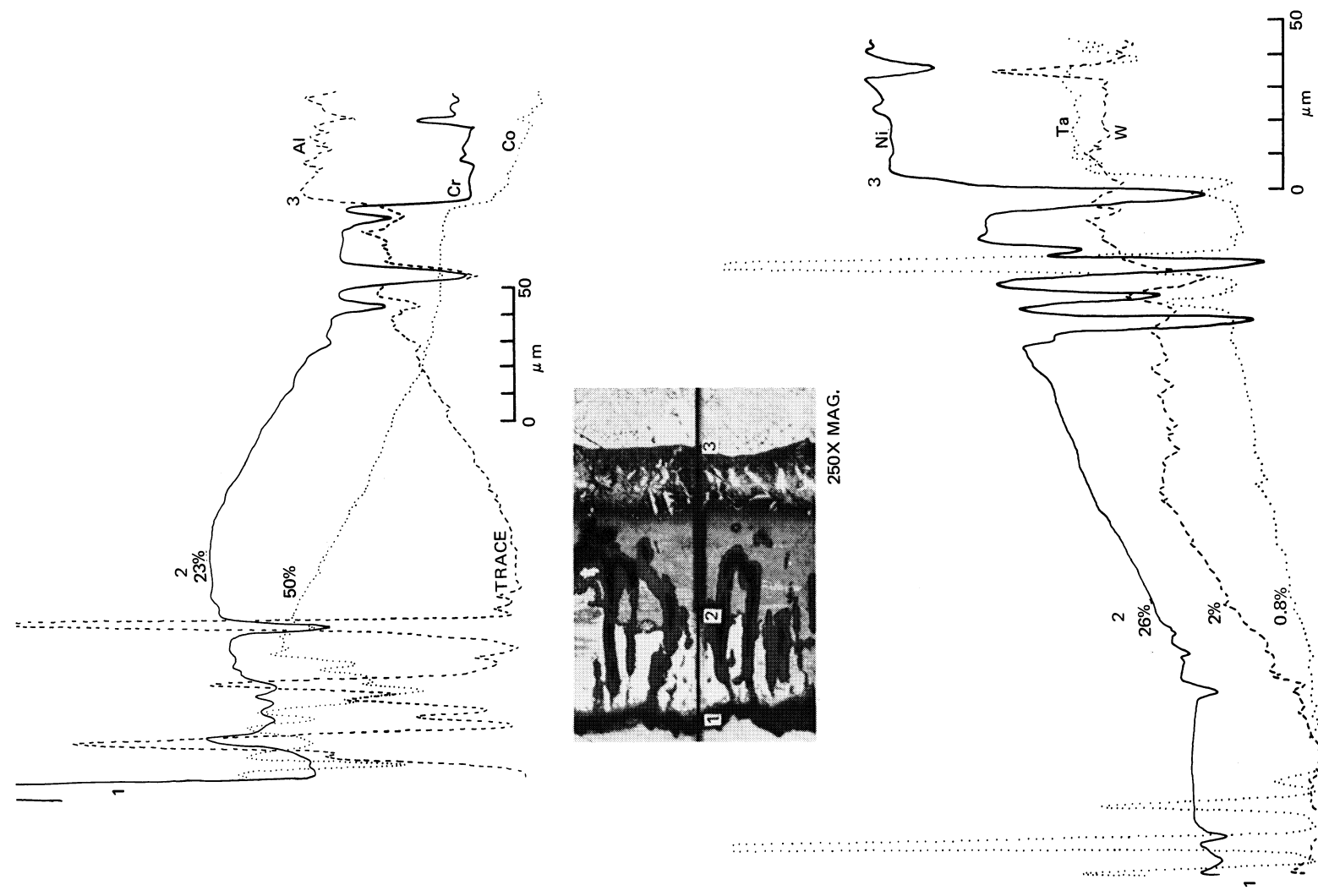


Figure 44  
Electron Microprobe Analysis of Composition 3 (Co-30Cr-16Al-0.5Y) Coating  
(Specimen G4088H) After 251 Hours of Burner Rig Testing

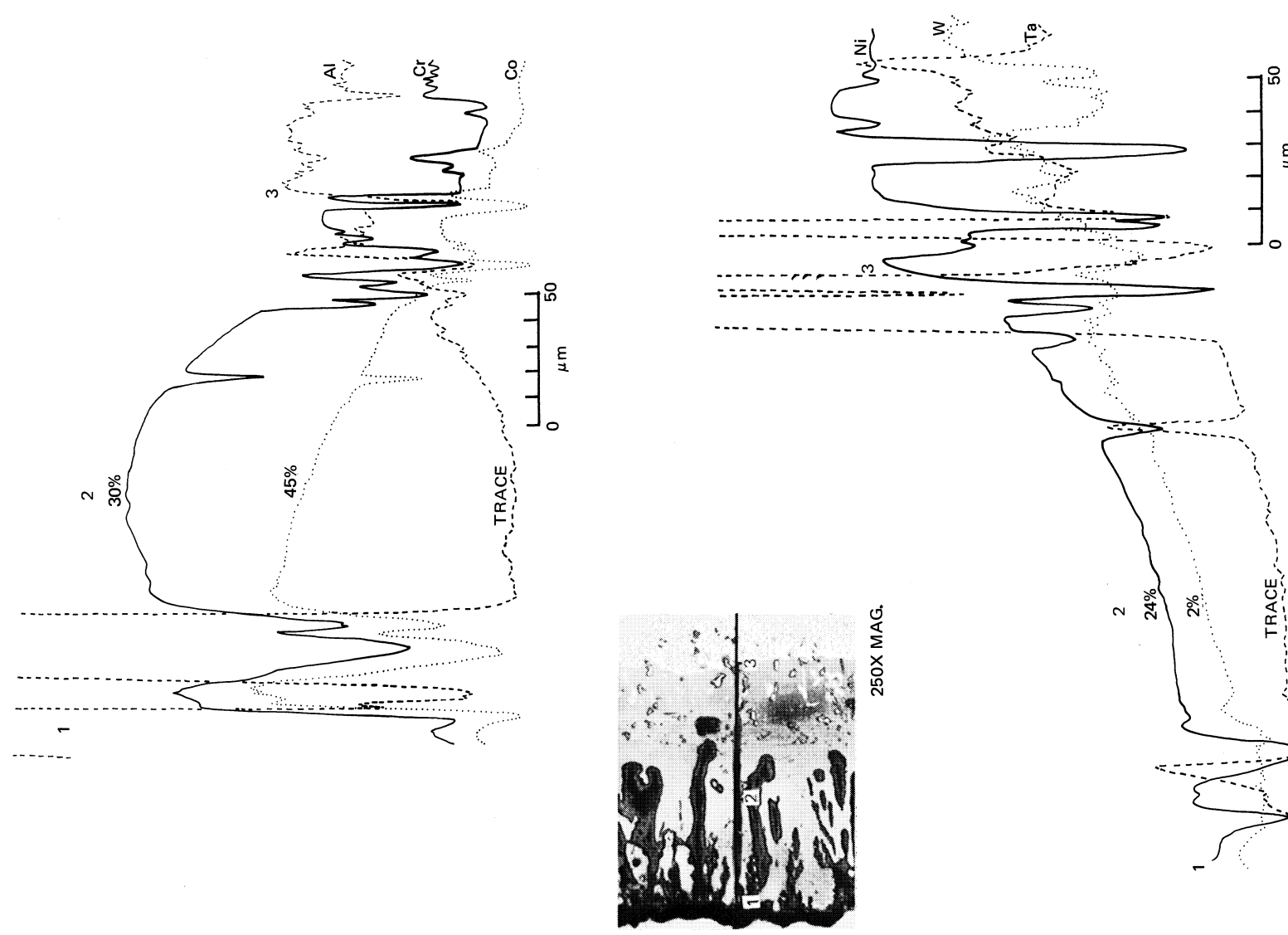


Figure 45 Electron Microprobe Analysis of Composition 4 (Co-40Cr-12Al-0.5Y) Coating (Specimen G4088L) After 251 Hours of Burner Rig Testing

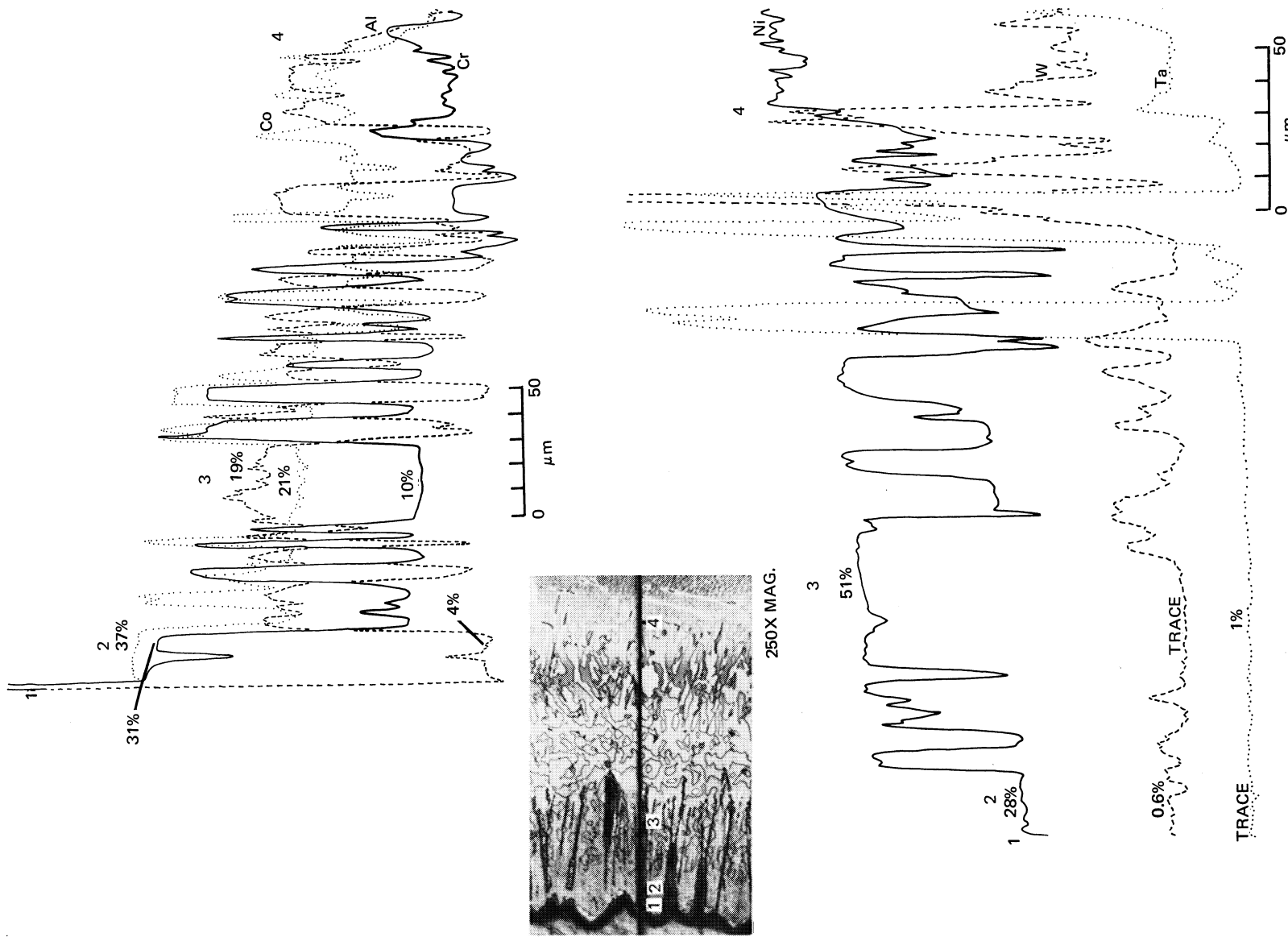


Figure 46 Electron Microprobe Analysis of Composition 5 (Co-40Cr-20Al-0.5Y) Coating  
(Specimen G4088N) After 1100 Hours of Burner Rig Testing

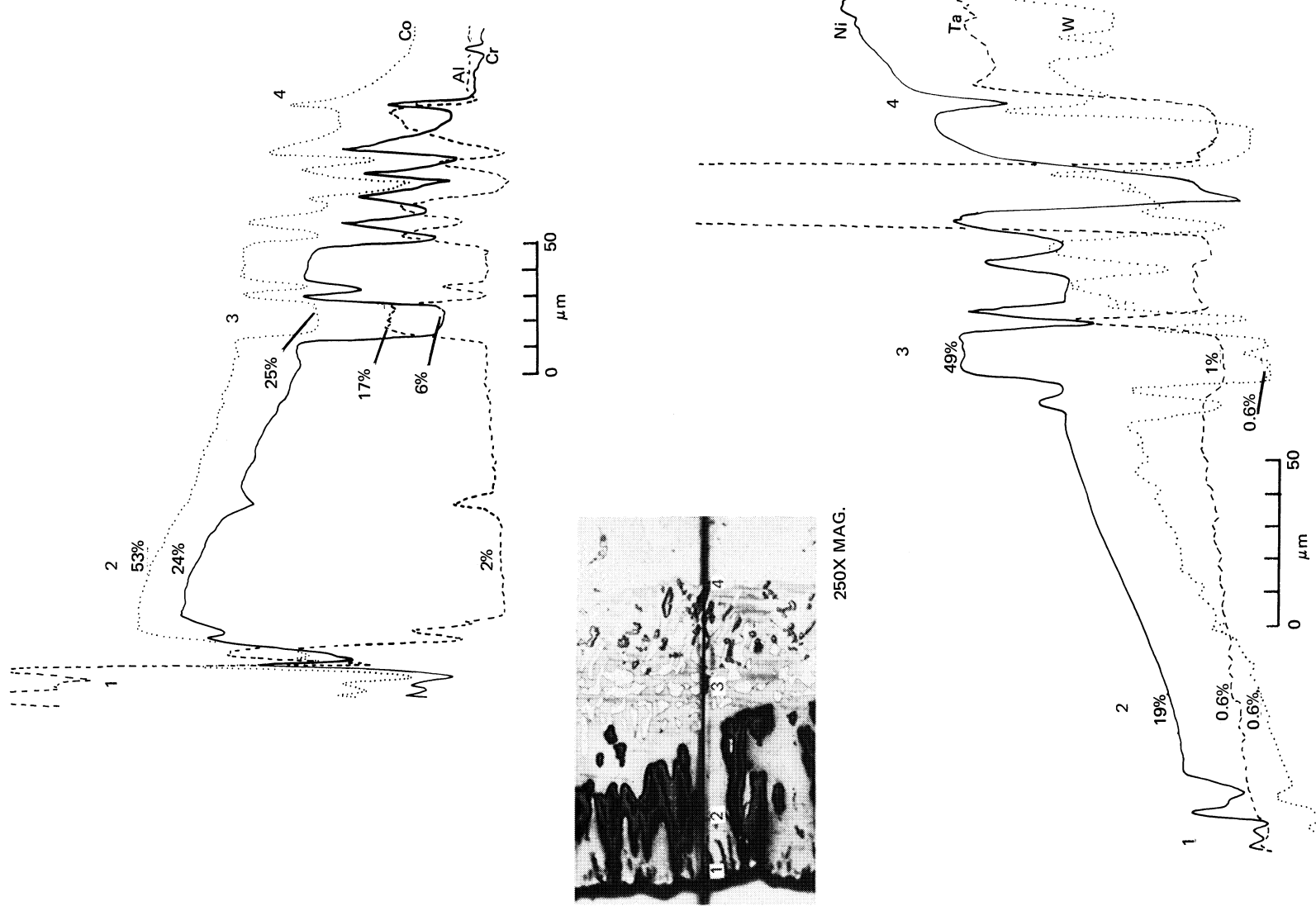


Figure 47  
Electron Microprobe Analysis of Composition 6 (Co-25Cr-16Al-0.5Y) Coating  
(Specimen G4088S) After 285 Hours of Burner Rig Testing

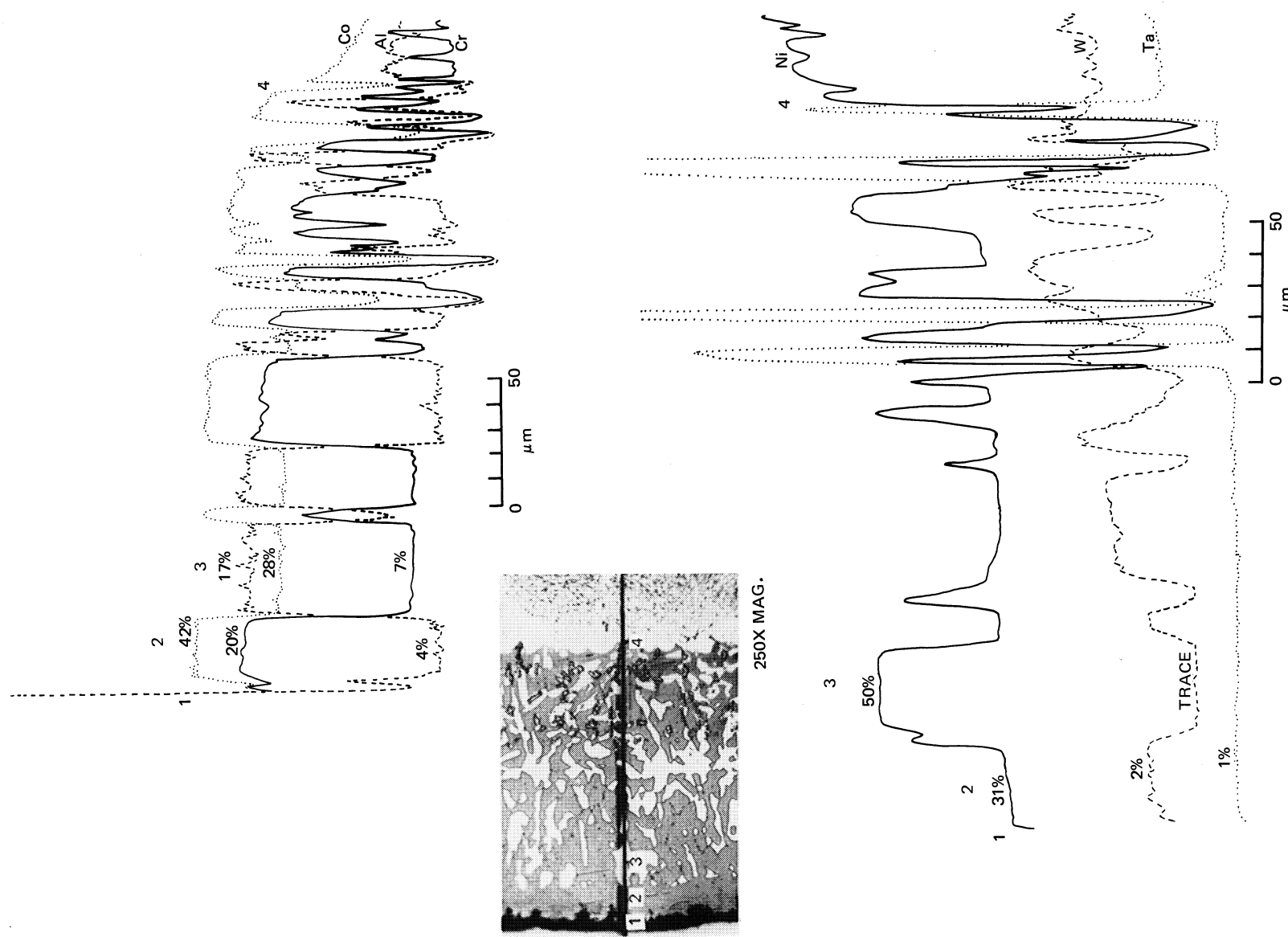


Figure 48 Electron Microprobe Analysis of Composition 7 (Co-25Cr-14Al-0.5Y) Coating (Specimen G4092H) After 1100 Hours of Burner Rig Testing

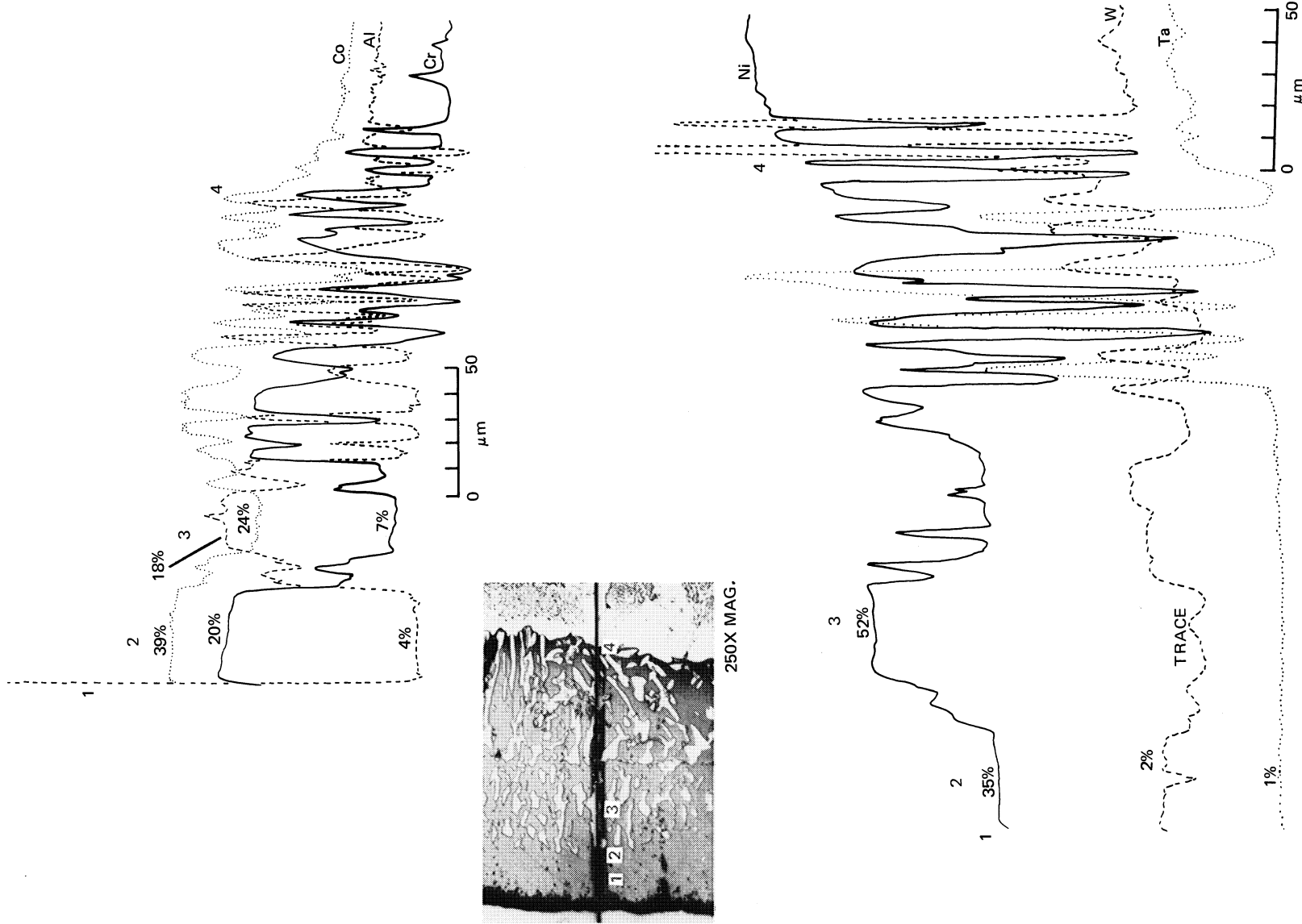


Figure 49 Electron Microprobe Analysis of Composition 8 (Co-25Cr-14Al-0.9Y) Coating  
(Specimen G4162P) After 1100 Hours of Burner Rig Testing

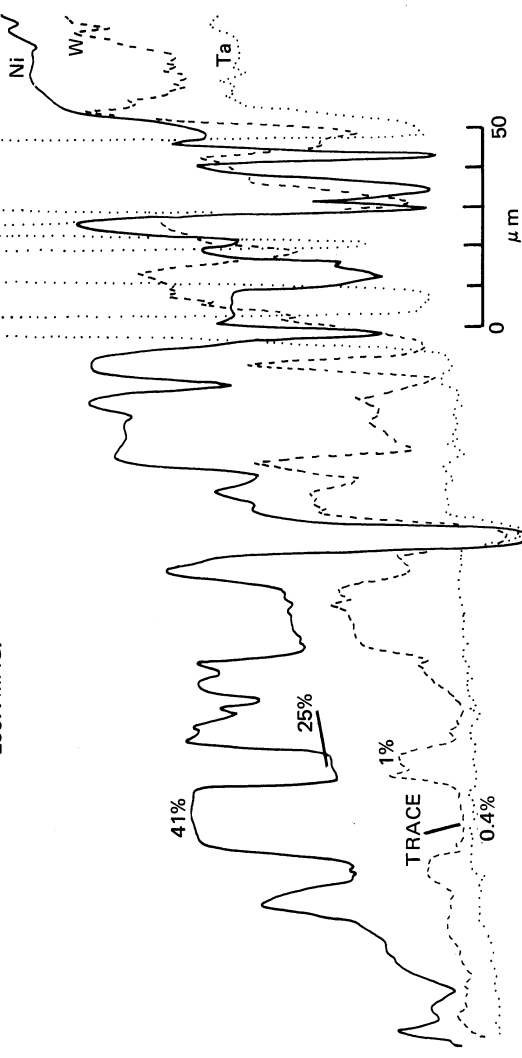
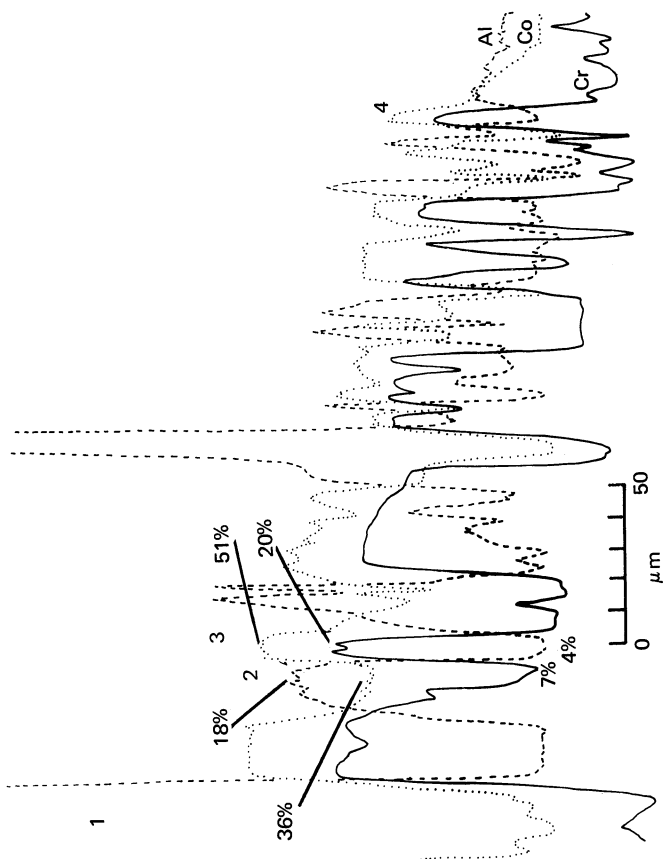


Figure 50 Electron Microprobe Analysis of Composition 9 (Co-25Cr-18Al-0.5Y) Coating  
(Specimen G4094M) After 285 Hours of Burner Rig Testing

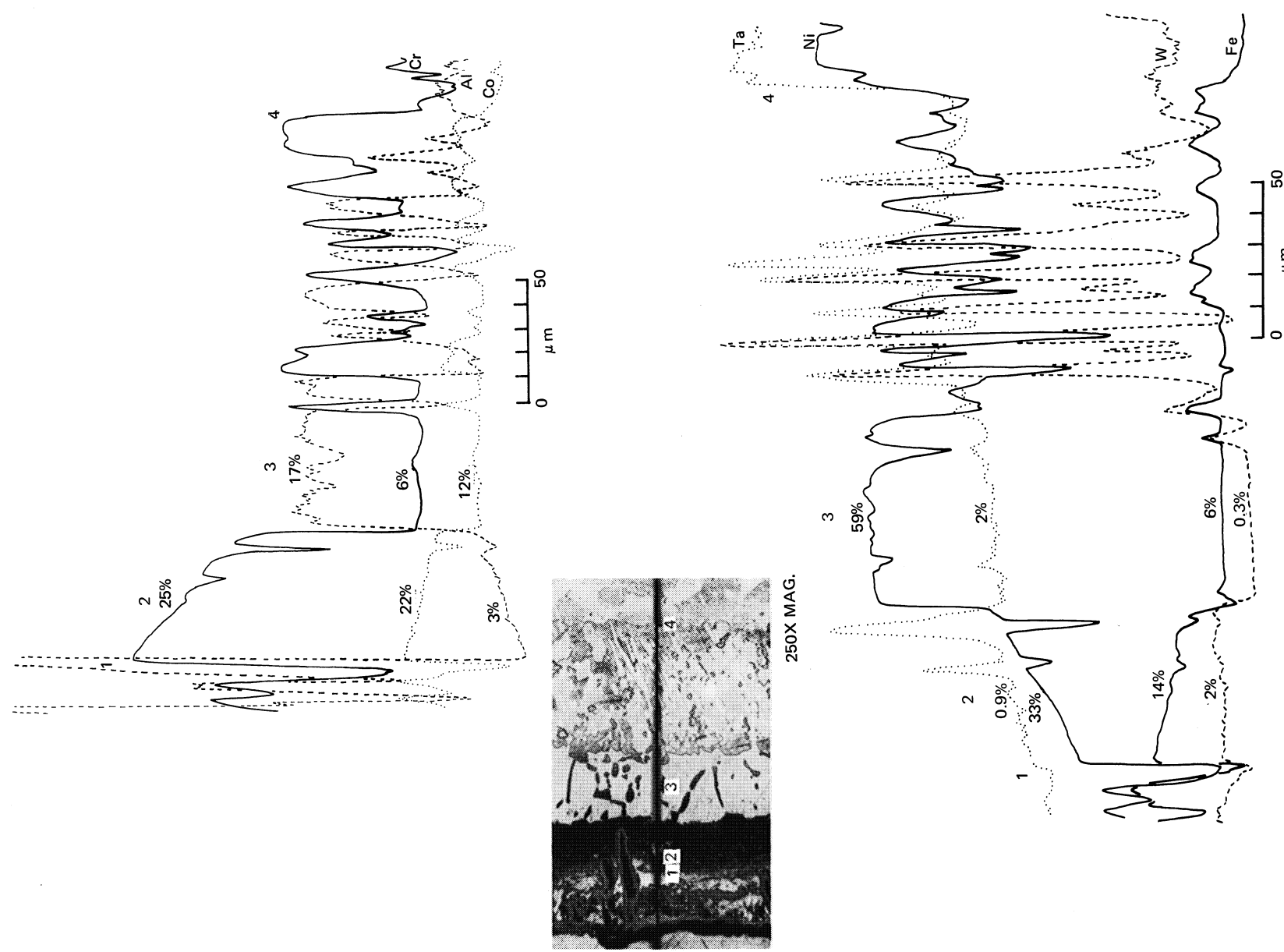


Figure 51 Electron Microprobe Analysis of Composition 10 (Co-40Cr-20Fe-20Al-0.5Y) Coating  
(Specimen G4092I) After 200 Hours of Burner Rig Testing

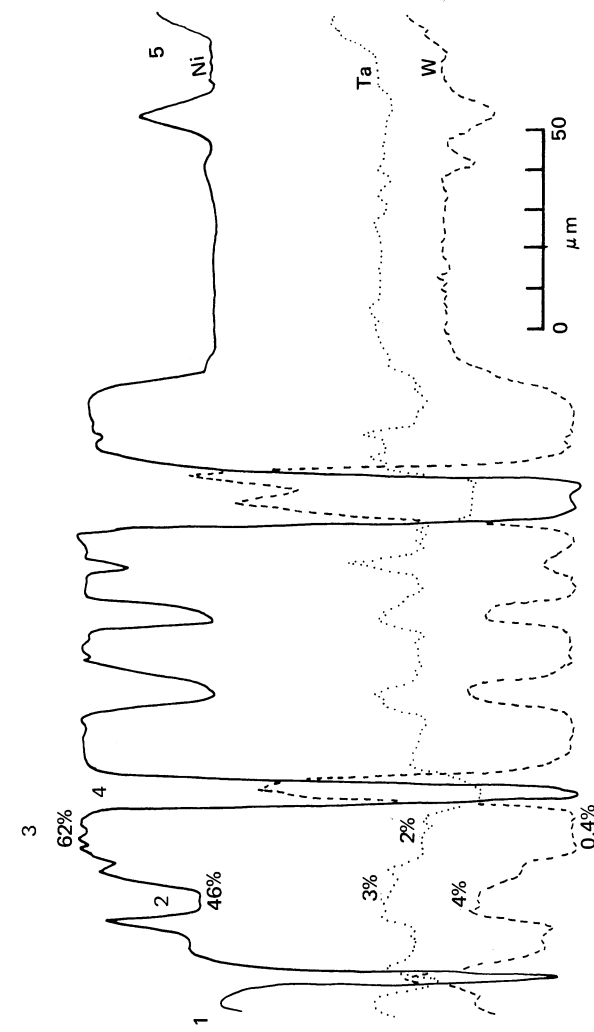
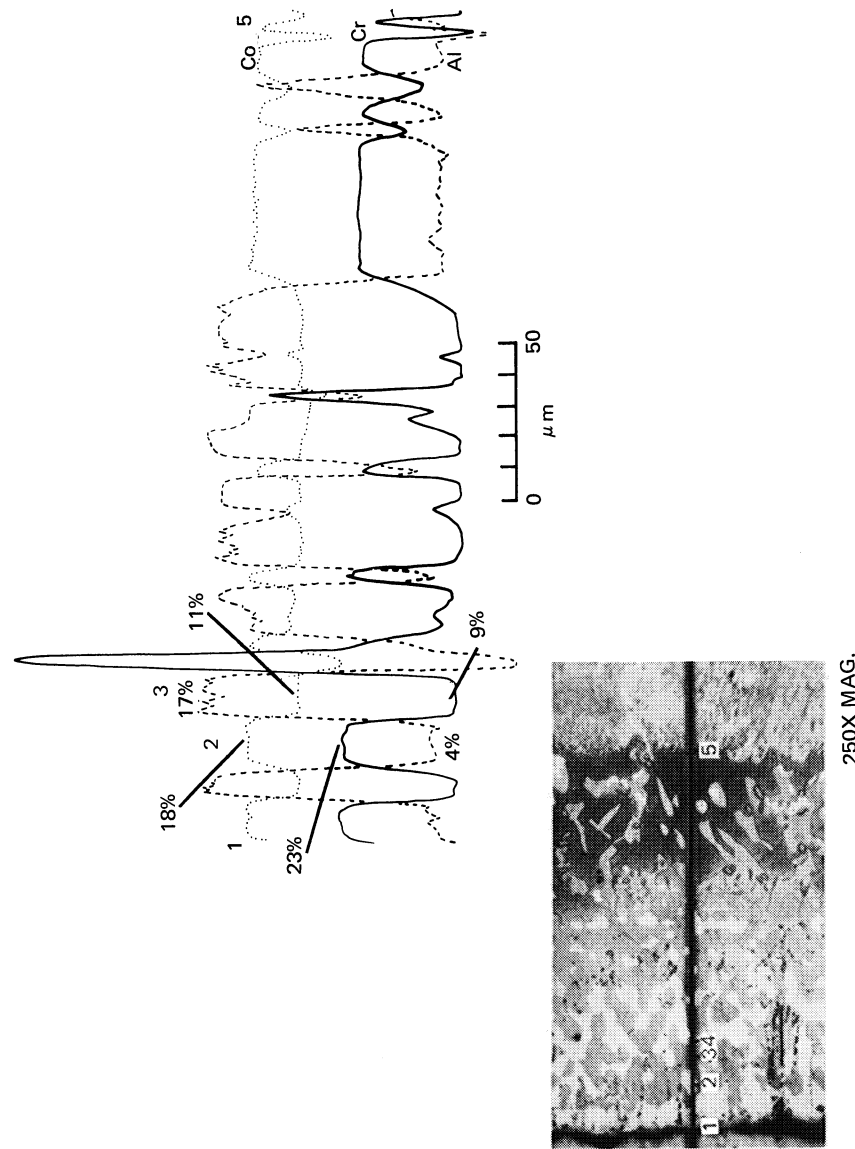


Figure 52 Electron Microprobe Analysis of Composition 11 (Co-40Cr-20Ni-20Al-0.5Y) Coating (Specimen G-4092B) After 609 Hours of Burner Rig Testing

**TABLE XI**  
**GENERALIZED SUMMARY OF MICROPROBE RESULTS**

Compo- sition No.	Specimen No.	Composition (Weight %)				Test Time (hours)		
		Co	Cr	Al	Ni	Fe	W	Ta
<u>PRE-TEST</u>								
1	271	72	14-19.2	9-15	0	N.A.	0	N.A.
2	G4088G	66.6	17.0	17.4	0	N.A.	N.A.	N.A.
3	282	61.7	25	13.4	0	N.A.	N.A.	N.A.
4	G4088M	55.2	30.2	11.2	2.1-4.3	N.A.	N.A.	N.A.
5	G4088O	47.0	36.0	18.0	0	N.A.	N.A.	N.A.
6	G4092T	62.1	21.9	13.4	0	N.A.	0	0
7	G4092K	68.2	21.4	14.3	0	N.A.	0	0
8	G4092Q	63.2	25.1	13.2	1.0	N.A.	0	0
9	G4092M	66.9	21.1	14.7	0	N.A.	0	0
10	G4161E	29.6	32.8	15.4	0	23.7	N.A.	0
11	G4092S	20.4	37.8	18.3	19.7	N.A.	0	0
<u>POST-TEST</u>								
1	G4088B	47.3	16.4	4.7	29.1	N.A.	2.1	1.4
2	G4088F	54.8	20.7	3.0	19.3	N.A.	0.7	1.1
3	G4088H	49.5	23.4	Trace	26.2	N.A.	1.8	0.8
4	G4088L	45.2	29.9	Trace	23.9	N.A.	1.5	Trace
5	G4088N	36.6	31.3	3.9-19.0	27.8	N.A.	0.6	1.2
6	G4088S	52.7	23.6	2.3	18.6	N.A.	0.6	0.6
7	G4092H	27.9-42.1	7.2-19.5	4.3-17.0	30.9	N.A.	2.1	1.4
8	G4162P	39.0	19.6	4.4	35.3	N.A.	2.1	1.0
9	G4094M	35.6-50.8	7.3-20.2	4.2-18.3	24.6-40.9	N.A.	Trace	0.4
10	G4092I	22.4	25.0	2.5	32.7	14.0	1.7	0.9
11	G4092B	10.8-17.5	8.8-22.5	4.4-17.0	46.4-61.9	N.A.	3.8	2.6

N. A. = Not Analyzed

## VII. SUMMARY OF RESULTS

The objective of this program was to evaluate electron beam vapor deposited coatings based on the Co-Cr-Al-Y system and designed to protect the nickel-base alloys, such as NASA-TRW VI-A, from excessive oxidation at temperatures up to 2000°F (1366°K) for extended times in jet engine combustion products. Four of the eleven compositions studied protected the NASA-TRW VI-A alloy for at least 1100 hours in burner rig tests at 2000°F (1366°K) metal temperature in the combustion products of JP-5 fuel and air. Three standard aluminiide coatings were failed during the 1100-hour burner rig test, showing that the advanced coatings exhibited more than a three-to-one life advantage. Ballistic impact tests and subsequent furnace oxidation tests showed that the advanced coatings have good resistance to impact and that impact initiated no significant increases in oxidative attack in that test.

Representative coated specimens in the as-coated and in the environmentally exposed conditions were studied by electron microprobe, x-ray diffraction, x-ray emission, and optical metallurgical techniques. The results of these evaluations showed that, in the Co-Cr-Al-Y system, aluminum is responsible for the formation of a protective oxide scale ( $\text{Al}_2\text{O}_3$ ) and that yttrium also participates in the oxidation processes leading to the formation of a protective scale. The role of chromium in the coating system remained largely undefined.

The coatings evidently degraded by consumption of aluminum through protective scale formation and by aluminum depletion in the coating through interdiffusion with the substrate. Microstructure had a significant influence on coating performance. The coatings which could not be peened to produce a homogeneous structure suffered oxidative degradation along columnar grain boundaries.

The most successful coating, Co-25Cr-14Al-0.5Y, was characterized by a fine, evenly distributed two-phase microstructure consisting of a chromium-rich and aluminum-poor phase, while the other phase was aluminum rich and chromium poor.

The effects of the coatings (Co-20Cr-12Al-0.5Y and Co-25Cr-14Al-0.5Y) on base-metal properties was negligible, as judged from tensile and stress-to-rupture test results on coated and uncoated specimens.



*Report Distribution:*

- Mr. J. Gangler/RRM  
NASA Headquarters  
600 Independence Avenue  
Washington, D. C. 20546
- Mr. G. M. Ault, MS 3-13  
NASA Lewis Research Ctr.  
21000 Brookpark Road  
Cleveland, Ohio 44135
- Mr. J. C. Freche, MS 49-1  
NASA Lewis Research Ctr.  
21000 Brookpark Road  
Cleveland, Ohio 44135
- Mr. S. J. Grisaffe, MS 49-1 (15 cys.)  
NASA Lewis Research Ctr.  
21000 Brookpark Road  
Cleveland, Ohio 44135
- Mr. F. H. Harf, MS 49-1 (3 cys.)  
NASA Lewis Research Ctr.  
21000 Brookpark Road  
Cleveland, Ohio 44135
- Mr. S. S. Manson  
NASA Lewis Research Ctr.  
21000 Brookpark Road  
Cleveland, Ohio 44135
- Mr. N. T. Saunders, MS 105-1  
NASA Lewis Research Ctr.  
21000 Brookpark Road  
Cleveland, Ohio 44135
- Library, MS 60-3 (2 cys.)  
NASA Lewis Research Ctr.  
21000 Brookpark Road  
Cleveland, Ohio 44135
- Aeronautics Proc. Sec. MS 77-3  
NASA Lewis Research Ctr.  
21000 Brookpark Road  
Cleveland, Ohio 44135
- Patent Counsel, MS 500-311  
NASA Lewis Research Ctr.  
21000 Brookpark Road  
Cleveland, Ohio 44135
- Report Control Off., MS 5-5  
NASA Lewis Research Ctr.  
21000 Brookpark Road  
Cleveland, Ohio 44135
- Technology Util. Off. MS 3-19  
NASA Lewis Research Ctr.  
21000 Brookpark Road  
Cleveland, Ohio 44135
- Mr. G. C. Deutscher/RRM  
NASA Headquarters  
600 Independence Avenue  
Washington, D. C. 20546
- Mr. R. H. Raring/RRM  
NASA Headquarters  
600 Independence Avenue  
Washington, D. C. 20546
- Mr. H. Rosenthal, MRL  
Metallurgy Research Lab.  
Frankfort Arsenal  
Philadelphia, Pa. 19137
- Mr. P. Goodwin, AIR-5203  
Naval Air Systems Command  
Navy Department  
Washington, D. C. 20360
- Mr. I. Petker  
Composite Structures Dept.  
Aerojet-General Corp.  
Azusa, Calif. 91702
- Reports Acquisition  
Aerospace Corporation  
P. O. Box 95085  
Los Angeles, Calif. 90045
- Supervisor, Materials Engineering  
Airesearch Company  
402 East 36th Street  
Phoenix, Arizona 85034
- Mr. R. Pride, 188A  
NASA  
Langley Research Center  
Langley Field, Virginia 23365
- Library  
NASA  
Ames Research Center  
Moffett Field, Calif. 94035
- Library  
NASA  
Goddard Space Flight Ctr.  
Greenbelt, Md. 20771
- Library  
NASA Flight Research Ctr.  
P. O. Box 273  
Edwards, Calif. 93523
- Library  
Jet Propulsion Laboratory  
4800 Oak Grove Drive  
Pasadena, Calif. 91102
- Library  
NASA  
Langley Research Center  
Langley Field, Virginia 23365
- Library  
NASA  
Manned Space Flight Ctr.  
Houston, Texas 77058
- Library  
NASA  
Marshall Space Flight Center  
Huntsville, Alabama 35812
- General J. C. Maxwell  
FAA Headquarters  
890 Independence Avenue  
Washington, D. C. 20553
- Mr. F. B. Howard, SS-210  
FAA Headquarters  
890 Independence Avenue  
Washington, D. C. 20553
- Mr. A. K. Forney  
FAA Headquarters  
890 Independence Avenue  
Washington, D. C. 20553
- Mr. W. Rentz  
Ford Motor Company  
2000 Rotunda Drive  
P. O. Box 2053  
Dearborn, Mich. 48123
- Mr. W. E. Binz  
Boeing Company  
P. O. Box 3733  
Seattle, Washington 98124
- Mr. M. Negrin  
Chromalloy Corp.  
169 Western Highway  
West Nyack, New York 10994
- Library  
University of Dayton  
Research Institute  
300 College Park Ave.  
Dayton, Ohio 45409

Wright-Patterson AFB, Ohio 45433

- Mr. Y. Telang  
Ford Motor Company  
2000 Rotunda Drive  
P. O. Box 2053  
Dearborn, Mich. 48123
- Mr. L. P. Jahnke, Manager  
Materials Dev. Lab. Oper.  
General Electric Company  
Cincinnati, Ohio 45215
- Mr. M. Levinstein  
General Electric Co.  
Materials Dev. Lab. Oper.  
Adv. Engine & Tech. Dept.  
Cincinnati, Ohio 45215
- Library  
General Electric Company  
R. And D. D.  
Schenectady, N.Y. 12305
- Dr. H. Schadler  
General Electric Company  
R. & D. Center  
P. O. Box 8  
Schenectady, N.Y. 12301
- Mr. D. Hanink, Manager  
Materials Laboratory  
Allison Division  
General Motors Corp.  
Indianapolis, Ind. 46206
- Mr. S. Wolosin  
Howmet Corporation  
Misco Division  
One Misco Drive  
Whitehall, Mich. 49461
- Mr. V. Hill  
I. I. T. Research Inst.  
Technology Center  
Chicago, Ill. 60616
- Mr. J. Wurst  
University of Illinois  
Dept. of Engineering  
Urbana, Ill. 61801
- Mr. J. V. Long,  
Director of Research  
Solar, Int. Harvester  
2200 Pacific Highway  
San Diego, Calif. 92112
- Mr. A. Stetson  
Solar Division  
Int. Harvester Corp.  
2200 Pacific Highway  
San Diego, Calif. 92112
- Dr. J. Berkowitz  
Arthur D. Little, Inc.  
20 Acorn Park  
Cambridge, Mass. 02140
- Mr. R. Perkins  
Lockheed Palo Alto R. Labs  
Mat. and Science Lab.  
251 Hanover Street  
Palo Alto, Calif. 94304
- Mr. D. Goldberg  
Westinghouse Electric  
Astronuclear Lab.  
Pittsburgh, Pa. 15236
- Mr. R. Grekila  
Westinghouse Electric  
Research Labs.  
Beulah Rd., Churchill Bur.  
Pittsburgh, Pa. 15235
- Prof. R. A. Rapp  
Dept. of Metall. Engng.  
Ohio State University  
Columbus, Ohio 43210
- Mr. G. J. Wile  
Polymet Corporation  
11 West Sharon Road  
Cincinnati, Ohio 45246
- Mr. H. D. Kessler  
Reactive Metals, Inc.  
100 Warren Avenue  
Niles, Ohio 44446
- Mr. L. Sama  
Sylvania Electric Prod.  
Sylcor Division  
Cantique Road  
Hicksville, N.Y. 11802
- Mr. Gene Wakefield  
Texas Instruments, Inc.  
M. & C. Division  
P. O. Box 5474  
Dallas, Texas 75222
- Dr. J. Gadd  
TRW, Inc.  
1400 N. Cameron St.  
Harrisburg, Pa. 17105
- Dr. E. Steigerwald  
TRW Electromechanical Div.  
TRW, Inc.  
23555 Euclid Avenue  
Cleveland, Ohio 44117
- Mr. D. Boone  
Adv. Mat. R. & D. Labs.  
Pratt & Whitney Aircraft  
Middletown Plant  
Middletown, Conn. 06158
- Mr. E. F. Bradley  
Pratt & Whitney Aircraft  
United Aircraft Corp.  
400 Main Street  
East Hartford, Conn. 06108
- Dr. J. Wert  
Matis. Engr. Dept.  
Box 1621  
Vanderbilt University  
Nashville, Tenn. 37203
- Dr. J. Mueller  
University of Washington  
Ceramics Department  
Seattle, Wash. 98101
- Mr. D. Maxwell  
Pratt & Whitney Aircraft  
United Aircraft Corp.  
West Palm Beach, Fla. 33402
- Manufacturing Engineering  
Pratt & Whitney Aircraft  
United Aircraft Corp.  
Aircraft Road  
Middletown, Conn. 06457

